UNIVERSITÀ DEGLI STUDI DI GENOVA

POLYTECHNIC SCHOOL

**Department of Electrical, Electronics,
Telecommunication Engineering
and Naval Architecture**

INTELLIGENT ELECTRIC ENERGY SYSTEMS LABORATORY

XXXV Cycle Ph.D in Sciences and Technologies for Electrical Engineering, Naval Engineering, and Complex Systems for Mobility - Curriculum: Electrical Engineering

Flexibility of Electric Power Systems by Network Planning and Service Provision: Challenges for Energy Transition

Bruno Gabriele

Supervisors

Prof. Ing. Stefano Massucco

Prof. Ing. Federico Silvestro

January, 2023

Abstract

In recent years, the electric power system is meeting a radical evolution due to the increasing penetration of Renewable Energy Sources (RESs). These have a relevant impact on most of the applications concerning the electrical network, such as the electricity markets, regulation services provision and the grid management and protection.

However, the deep RESs deployment is the answer that countries all over the world are pursuing to fight climate change according to the Sustainable Development Goals (SDGs) adopted by the United Nations (UN). This evolution requires a great development of the network, that has to host a large quantity of new RESs, and the establishment of new strategies to deal with new challenges.

More and more reserves for regulation services are pursued by units that couldn't provide dispatching services until now, namely small-sized plants and RESs, but also load and storage systems. The demand has become increasingly more active since it has made possible a contribution to instability issues by varying their power profile for a certain amount of time without compromising the final user's comfort, which means being flexible.

As a result, a huge amount of new generation units and load units have started to provide dispatching services by participating to the electricity markets. This condition has led to the need of the improvement of the communication systems among all the actors in the process of power transmission alongside grid balancing, including the Transmission System Operator (TSO), the Distribution System Operators (DSOs), generation, load units and other data aggregators.

The observability of the system is essential to forecast load and generation profiles in order to provide a suitable balancing service and to guarantee the reliability, safety and power quality of the electrical network through state estimation methods which are going to be widely used in modern systems. Observability is also important in making decisions for the planning of the network development by giving access to information about the grid operating conditions. Therefore it suggests how to focus the efforts to improve the

electric power system performance according to the objectives established to reduce the impact of fossil fuels in the climate change.

In sight of this, it can be concluded that the key to deal with climate change is a suitable coordination of such factors: the development of the network, the arrangement of flexibility resources and the communication systems improvement.

During the Doctorate (Ph.D.), the author has worked on several research projects related to the topic of the evolution of the electric system. The project are listed in the Appendices.

This thesis gathers the work done by underlining the importance of the three factors mentioned before in the context of the power system evolution. The developed applications will be presented as particular approaches that can be applied to a general power system and take place in one or more aspects of the ecological transition.

In **Chapter 1**, the UN strategies to deal with climate change are introduced as well as the main consequences they led to and the new needs of the electric system are described. An introduction to regulation services and their purpose is given.

In **Chapter 2** the Italian context, as part of the European and Global plan to reduce emissions, is described. The main tools used by the Italian TSO to plan the network development are introduced and the study case of the network of Sicily is explained in the contest of the project *"Assessments of Battery Energy Storage Systems Potential in Improving the Working Condition of the Grid of Sicily"*.

As a continuation of this work, the method developed in the project *"Optimal Storage Allocation for Transmission Network Development Planning"* is applied to the Sicilian network model and its possible contribution to network infrastructure planning is described.

In **Chapter 3** the impact that the installation of several RESs have on the grid stability is described. The consequent evolution process of the electricity market in order to cope with the increased need of regulation services is

explained. In such context, pilot projects have been established by the TSO to encourage research of flexibility resources with reference to the projects concerning regulation service provision from loads and RESs.

In **Chapter 4**, in project *"Flexibility Evaluation of an Aggregate of Thermal Load Units"*, a definition of flexibility resources is given and a flexibility analysis of aggregates of thermal loads intended for domestic hot water heating, such as domestic electric water heaters or heat pumps, has been carried out during the research activity. A Monte Carlo approach is adopted for the methodology applied to the study case of Italy and Sicily.

Chapter 5 describes and presents the results of the project *"Model Predictive Control for frequency regulation services provision"* where the fast frequency reserve service is explored according to the related pilot project by using Model Predictive Control (MPC) based techniques applied on systems with RESs and Battery Energy Storage Systems (BESSs). Such service is meant to replace the beneficial effect of inertia from the traditional generating units which is progressively decreasing because of the implementation of RESs units in the power system. The decrease of inertia leads to more significant frequency variations after fault events that must be solved within extremely high speed actions, even faster than primary frequency regulation service.

To complete the thesis, the **Conclusions** are presented together with some last comments.

Finally, the publications produced during the Ph.D. and the projects to which contribution was given, collaborations and attended courses are listed, while references cited in this thesis end the dissertation.

Contents

Abstract **iii**

1 New requirements for RES integration **5**
1.1 Development Plans 10
1.2 Scenarios 11
1.3 State of the Italian Network 16
1.4 Electricity Market 19
1.5 Regulation services 24
1.5.1 Scheduling and Dispatch 24
1.5.2 Load Following 25
1.5.3 Operating Reserves 25
1.5.4 Energy Imbalance 25
1.5.5 Real Power Loss Replacement 26
1.5.6 Voltage Control 26

2 Network planning in sight of large RES deployment **27**
2.1 Off-Shore Wind Hosting Capacity in Sicilian Network . . . 27

2.2 Storage allocation for network planning: Study case of Sicily 37

3 New solutions to network support: flexibility by grid services 51
3.1 Deliberation 300/2017 53
3.2 Aggregation 56

4 Flexibility by management of thermal loads 59
4.1 Electrical water heater flexibility 74
4.2 Heat pump flexibility 90
4.3 Final considerations 100

5 Fast frequency reserve needs and proposed solutions 101
5.1 Service provision from BESS 107
5.2 Service provision with WTs contribution 119
5.3 Validation through hardware in the Loop simulations 135
5.4 Study of methods to provide service with Photovoltaics (PVs) 146
5.5 Final considerations 148

6 Conclusions 149

Bibliography 151

List of Publications 163

List of Projects 165

List of Courses 167

Acronyms

BAU Business As Usual

BESS Battery Energy Storage System

BSP Balancing Service Provider

CDF Cumulative Distribution Function

CEN Centralized

CEP Clean Energy Package

CHIL Control Hardware In the Loop

DEC Decentralized

DER Distributed Energy Resource

DG Distributed Generation

DMR Demand Side Response

DSO Distribution System Operator

DSR Demand-Side Response

EHV Extra High Voltage

ENTSO European Network of Transmission System Operators

EU European Union

EWH Electric Water Heater

FPP Flexible Power Point

FRS Fast Reserve Service

FRU Fast Reserve Unit

GME Gestore del Sistema Energetico

HIL Hardware In the Loop

HVDC High Voltage Direct Current

MB Mercato del Bilanciamento

MGP Mercato del Giorno Prima

MI Mercato Infragiornaliero

MILP Mixed Integer Linear Programming

MPC Model Predictive Control

MPP Maximum Power Point

MPPT Maximum Power Point Tracking

MPT Maximum Power Tracking

MSD Mercato per il Servizio di Dispacciamento

NECP National Energy and Climate Plan

NT National Trend

PCHIL Power Control Hardware In the Loop

Ph.D. Doctorate

PNIEC Integrated National Energy and Climate Plan

PUN Prezzo Unico Nazionale

PV Photovoltaic

RES Renewable Energy Source

SDG Sustainable Development Goal

SEDC Smart Energy Demand Coalition

SMP System Marginal Price

SoC State of Charge

TSO Transmission System Operator

TSR Tip Speed Ratio

TYNDP Ten-Years Network Development Plan

UN United Nations

VQU Virtual Qualified Unit

WF Wind Farm

WT Wind Turbine

CHAPTER 1

New requirements for RES integration

This chapter will briefly outline the guidelines that Europe promoted to fight climate change and the political strategies implemented in order to achieve the targets of reduced emissions.

It will also be shown what challenges are introduced in this process and how the three main factors of network development, flexibility resources and communication improvement are strictly connected to each other and are essential to face the power system evolution.

In 2015, the 2030 Agenda for Sustainable Development was adopted by the 193 Member States of the UN [1]. This global agenda for sustainable development consists of 17 SDGs targeting global challenges such as poverty, education, economic growth, innovation, health, peace and climate change, as shown in Figure 1.1.

Figure 1.1: Sustainable Development Goals [2]

Just about this last topic the European Union (EU) ratified the Paris Agreement [3] in 2016. By signing, the EU committed to the target of keeping the global temperature increase below 2 degrees Celsius respect to the pre industrial era and of making efforts to limit the temperature increase below 1.5 degrees. The long-term objective is to achieve climate neutrality before the end of this century in order to mitigate climate change. To aim to this goal, it has been set the sub-target of a 40% reduction of greenhouse gas emissions by 2030.

Moreover, consequently to the Paris Agreement, the EU proposed the Energy Governance Strategy, in the context of the Clean Energy Package (CEP), which leads to the identification of national targets for each European country to be reached by 2030 and strategies in terms of:

- greenhouse gas emissions reduction;
- renewable;
- efficiency;
- safety;

- electricity market;
- research, innovation, competition.

In fact, the Member States of the EU are coordinating to provide new strategies to face the evolution process to satisfy the Agenda 2030 SDGs and to guarantee at the same time the quality and the safety of the power transmission service. In particular, in Italy, the Integrated National Energy and Climate Plan (PNIEC) was adopted [4] in 2019.

Climate change became soon one of the priorities for the new political guidelines through the European Green Deal [5, 6], adopted in 2020.

The European Green Deal consists in a strategy that extends across numerous SDGs including climate objectives (SDG 11, 12 and 13), turned into legislation when the European Climate Law [7, 8] was adopted in 2021.

In this document, the overall objective is to reach climate neutrality by 2050 by pursuing several sub-targets. A 55% reduction of greenhouse gas emissions is forecast by 2030 (compared to 1990s standards) increasing the difficulty of the challenge of innovating the electric power system.

In Italy, the PNIEC represents the reference scenario that expects the requirements for the Italian network to be fulfilled. The main strategy consists of installing a huge amount of power from RES, especially from Photovoltaic (PV) and Wind Turbine (WT), and represents a great challenge for the electric power system in terms of stability and safety of the electric network operating point. In fact, due to the natural characteristics of the renewable sources, such as solar and wind, they are not programmable and are distributed on the territory depending on climate conditions.

This can lead to network congestions, caused by a high concentration of RESs in a specific area. Furthermore, balancing issues arise as their power output is not controllable like traditional generation units. In fact, PV and WT do not contribute to the system inertia and to regulating reserves, thus creating critical conditions which require new strategies to provide regulating services to the grid.

At this point, the need of network development to host the increasing amount of RESs and to reduce congestion and losses is evident. In addition, the research of new reserves for the provision of regulation services to the electric grid found an answer with the Deliberation 300/2017 [9] which included load units and generation plants not already qualified as well as RESs and BESSs to the electricity markets. Obviously, the requirements that these units have to satisfy to be qualified for balancing services provision are specified in this document and will be discussed later in the thesis.

The aim of Deliberation 300/2017 is to increase as much as possible the capability of all qualified units to vary their power consumption for a certain amount of time when requested by the TSO to face imbalance between power generation and demand. In few words, the flexibility of the whole system must be maximized.

The participation to the electricity market of a great number of small units implies the necessity of coordinating them and, as a consequence, the need to improve the communication between these units and the TSO in order to monitor the system and gather the required information about the state of all actors involved in the network balancing process.

Finally, the ecological transition to fight climate change is resulting in a high penetration of RESs in the electric system leading to instability and safety issues. The solution to deal with the challenge that will characterize the next years is identified in a mix of the following factors (Figure 1.2):

- network development;
- flexibility resources;
- communication improvement.

In Italy, the PNIEC [4] identifies the strategies that will be adopted to achieve the committed goals, according to the European strategy and the SDGs [2]. The main targets set in the PNIEC are the complete decarbonization by the end of 2025 and the installation of RESs for a total power of about 60 GW. These ambitious objectives clearly need a great effort of planning since the installation of such a great amount of power to the electrical requires clever decisions on what interventions worth focusing to host the new

plants avoiding congestion and instability issues.

The Development Plans [10] are a series of documents that help the Italian TSO, Terna, in this effort.

This thesis shows the projects the author worked for in the Italian context as possible applications of planning, regulating or protecting of the electric power system underlining every time how each of the three mentioned factor are basically essential to each other.

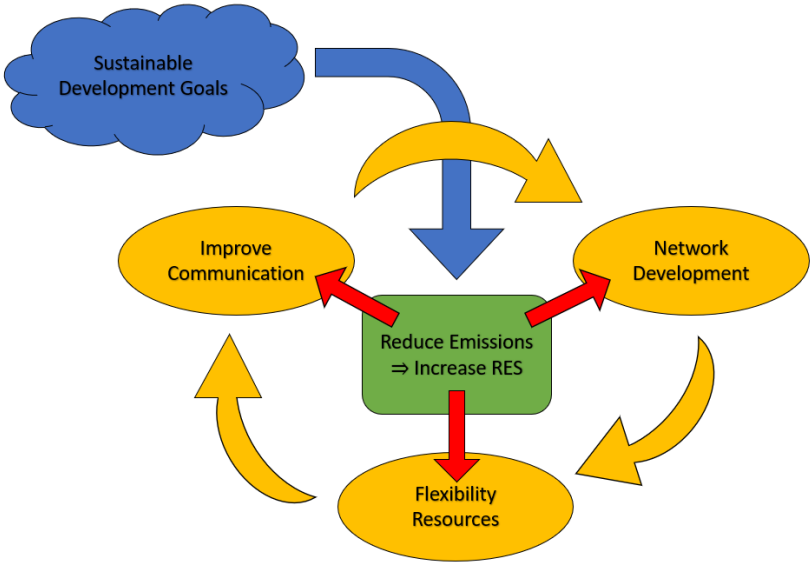

Figure 1.2: The three key factors to the electric power system evolution.

1.1 Development Plans

Development Plans are the planning tool used by the TSO to make the optimal decisions involving the network to achieve the PNIEC targets. In fact, in this decade, the Development Plan of 2021 forecasts interventions for an equivalent expense of 18 billion of euros which will contribute to increase the efficiency of the electric power system and obtain benefits in terms of:

- greater power from RESs (estimated about $40\,\mathrm{GW}$ by 2030);
- disposal of obsolete infrastructures for a total of $60\,\mathrm{km}$;
- reduction of energy losses for about 2000 billions of kWh per year;
- reduction of CO2 emissions in the atmosphere (about 5.6 millions tons per year).

Moreover, the TSO needs to find the best solutions to connect all the RESs to the network and to guarantee at the same time the quality and safety of the service. As an evidence of the great not uniform distribution of the RESs in the territory, in 2020, Sud Italy and the islands of Sicily and Sardinia covered the 87% of the requests of connection to the grid. Given the shape of the Italian network, this high concentration of RESs in South Italy and in the islands results in a considerable impact in terms of congestions and power losses.

As a solution, the Italian TSO has planned to install a new High Voltage Direct Current (HVDC) underwater cable that will connect Sicily, Sardinia and the Italian peninsula with a transmission capacity of $1000\,\mathrm{MW}$, known as Tyrrhenian Link [10].

In order to realize this kind of planning decisions, an analysis of the actual state of the network and the arrangement of development scenarios, such as PNIEC, are needed.

1.2 Scenarios

Planning process for the network development is clearly essential to identify what interventions are to be realized in order to achieve the predetermined targets of decarbonization, energy efficiency and RESs integration.

Definition of prospective scenarios represents a necessary step to perform medium and long-term planning. In fact, they let the TSO track the trajectory toward the national and European targets, test the reliability and safety of the power system and define an appropriate scheduling plan for the infrastructure development.

The Clean Energy Package is the legislative act stipulating that Member States provide on a ten-yearly basis a series of documents which include the strategies and national targets as contribution to the SDGs in terms of energy and climate. In this context, Italy provided, according to the European Commission dispositions, the PNIEC final version in 2019.

At a European level, it is stipulated that European Network of Transmission System Operators (ENTSO) for energy (ENTSO-E) and gas (ENTSO-G) have to publish the Ten-Years Network Development Plan (TYNDP) [11] where the respective networks are analyzed in perspective of several scenario, elaborated every two years, which make up different plausible pathways for the development of the future European power system in order to identify the best investments to make to meet the SDGs.

Among the several considered scenarios, National Trend (NT) scenarios were developed which is based on the National Energy and Climate Plans (NECPs), PNIEC for Italy (Figure 1.3). In fact, in the Italian Development Plan of 2021 [10], the considered scenarios are:

- Business As Usual (BAU) where the system is free of constraints or targets and the technological development is based only on economic thrust (Bottom Up approach);
- PNIEC, which was replaced by the NT in February 2021, where it is expected to meet the predetermined targets (Top Down Approach);

- Centralized (CEN) and Decentralized (DEC) are other two equivalent scenarios based on the TYNDP, where the expected evolution of the system is forecast in case of the achievement of the targets (Top Down Approach).

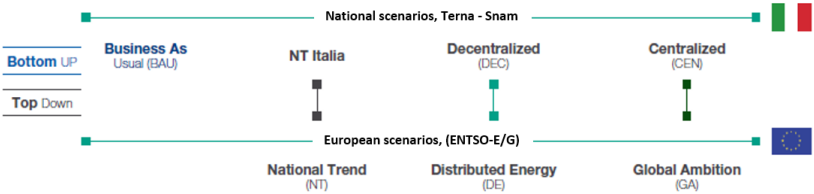

Figure 1.3: Italian scenarios and equivalent European scenarios [10].

The main targets of the NT scenario involves topics concerning the arrest of carbon-based generation units and the promotion of RESs, the increase of the network resilience and flexibility towards extreme climatic phenomenons, the realization of the foreseen interventions on the grid infrastructure and the development of storage systems. Also, a more active role of the demand and the diffusion of electric vehicles are promoted.

The targets set by the NT scenario are considered as minimum requirements to achieve. Scenarios are built considering a short term, a medium term and a long term horizon; in particular, the Development Plan 2021 [10] identifies as reference years the 2025, 2030 and 2040.

Obviously, the complexity of the challenges of the NT scenario comes from the consequent progressive effect that these will have as they are pursued, such as system instability caused by the decreasing inertia, which must be dealt too, leading to an evolution of the electricity market that could appropriately implement new mechanisms to manage the new generation units.

To give an idea of the quantities of wind and solar capacity expected to be implemented in the Italian power system by the NT scenario, the following data are shown in Tables 1.1 and 1.2 and in Figures 1.4 and 1.5

Table 1.1: Expected solar power capacity [MW].

Zone	Installed	Installed+Requested	NT 2030
North	9751	11634	24155
Center North	1992	2609	5139
Center South	3580	9644	8737
South	3466	27947	6671
Calabria	558	1140	1131
Sicily	1486	19408	4111
Sardinia	971	6536	2056

Table 1.2: Expected wind power capacity [MW].

Zone	Installed	Installed+Requested	NT 2030
North	152	1092	218
Center North	162	250	218
Center South	2094	7420	3971
South	4321	23989	6950
Calabria	1172	4425	1986
Sicily	1921	7082	3971
Sardinia	1105	4673	1986

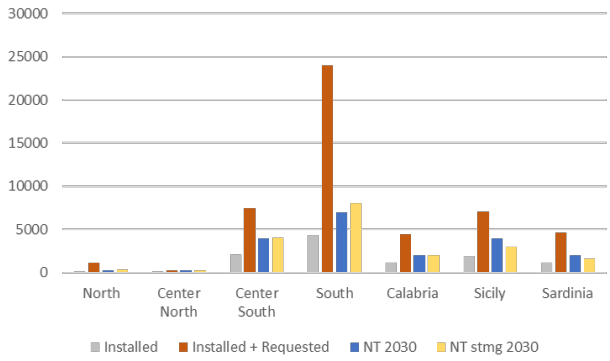

Figure 1.4: Current and expected solar power capacity MW [10].

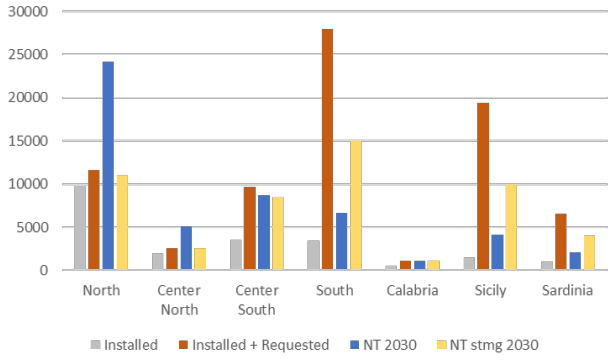

Figure 1.5: Current and expected wind power capacity MW [10].

It can be noted that the NT scenario foresees a distribution of new solar and wind capacity similar with the current one, usually showing higher concentration in South Italy, where climatic conditions are better. Also, data show that the amount of new RESs capacity waiting for authorization exceeds significantly the expected wind capacity.

Of greater interest is the fact that the requested amount of solar capacity is lower than the NT expected solar capacity in North Italy, but definitely higher

in South Italy and Sicily.

Overall the request capacity exceed the expected capacity ($78.9\,\mathrm{GW}$ against $52\,\mathrm{GW}$ for solar and $48.9\,\mathrm{GW}$ against $19.3\,\mathrm{GW}$ for wind), hence giving again evidence of the need to improve the network infrastructure, especially in South regions, to host the expected capacity and implement the new requested capacity as fast as possible to meet the NT 2030 requirements. The information regarding the NT stmg 2030 gives a glimpse on the amount of authorized request, again showing the big efforts foreseen in the Southern Italy.

1.3 State of the Italian Network

The actual state of the electrical network is an essential starting point to infer the network performance in hosting the new generation capacity. The implementation of RESs comes with an investment that must be exploited to prevent the risk of curtailment due to congestions caused by an inadequate network infrastructure. The curtailment risk depends on the capability of the grid interventions, foreseen in the Network Development Plan published by the TSO, to integrate the whole amount of new RES capacity expected.

Risk of curtailment is relevant in critical areas of the grid, where the generation of existing and new expected power plants exceeds the capability of the transmission grid to transport energy. In these areas, curtailment can be expected because the TSO will not be able to dispatch the whole amount of renewable energy, especially at generation peaks of RESs.

The identification of critical areas is performed by the TSO and considers only normal working conditions of the network. Critical areas are defined as portions of the HV network with energy export issues of the new production in the area, as explained in [12]. A given HV network portion is considered critical if the condition below is violated.

$$\left[\sum_i K_f P_{eol}^{STMG} + \sum_i K_f P_{alt}^{STMG} + \sum_i K_f P_{eol}^{INST} + \right. \\ \left. + \sum_i K_f P_{alt}^{INST} - C_{i,min}\right] R_i \geq Lim_{i-j} \qquad (1.1)$$

- P_{eol}^{STMG} and P_{eol}^{INST} are the new and already installed wind production;
- P_{alt}^{STMG} and P_{alt}^{INST} are the new and already installed solar production;
- K_f is the coincidence factor of the production (0.7 for wind, 1 for other RES, solar included);
- $C_{i,min}$ is the minimum power demand;
- R_i is the partition matrix defining power flows towards adjacent areas;

- Lim_{i-j} is the power exchange limits matrix.

After the detection of critical areas in HV network, the new generation arrangement is implemented in the network model and it is checked that it does not lead to the violation of the power exchange limit towards the Extra High Voltage (EHV) network.

If the analysis does not result in a critical area, the analysis on feeders is carried on to gather more detailed information about single power lines. If 80% of transport capacity of feeder A is reached, that feeder is defined as critical.

$$\left[\sum_{A} K_f P_{eol}^{STMG} + \sum_{A} K_f P_{alt}^{STMG} + P_{mean,A}\right] \geq Lim_A \tag{1.2}$$

- A is the power line index;
- P_{eol}^{STMG} is the new wind production;
- P_{alt}^{STMG} is the new solar production;
- K_f is the coincidence factor of the production (0.7 for wind, 1 for other RES, solar included);
- $P_{mean,A}$ is the mean power flow registered in the last year;
- Lim_A is the feeder transport capacity;
- A is the feeder index.

The application of this method for critical areas identification leads to results shown in Figure 1.6 which shows a higher concentration of critical areas in South Italy [13].

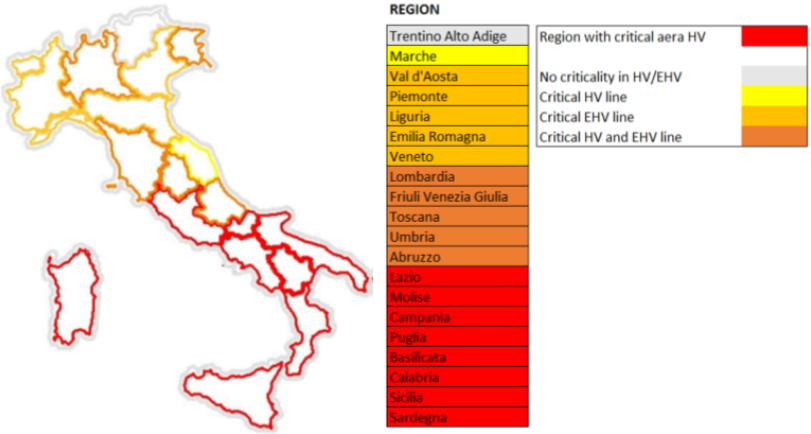

Figure 1.6: Critical areas of Italy [13].

In conclusion, the high amount of requested capacity which comes from the good weather conditions, combined with the critical operating conditions of the electrical network, leads South Italy to be the most interesting study case for the planning of new interventions on the network infrastructure, required to host the expected capacity minimizing the risk of RESs curtailment.

1.4 Electricity Market

In Italy, the electricity market was deregulated following the approval of the Legislative Decree 79/99 [14] as part of a process of transposing the European Directive 96/92/CE [15] on common rules for electricity market. The decree meets the needs, on one hand, to promote competition and, on the other hand, to maximize the transparency and efficiency. According to free market frameworks, power generation, transmission, distribution, and sales activities have been separated into separate corporate entities (process of unbundling).

The electricity market operator in Italy is the Gestore del Sistema Energetico (GME). The principal phases of the electricity market are:

- the Day Ahead Market, or Mercato del Giorno Prima (MGP);
- the Intraday Market, or Mercato Infragiornaliero (MI);
- the Market for Dispatching Service, or Mercato per il Servizio di Dispacciamento (MSD), divided into MSD Ex-Ante and Balancing Market, or Mercato del Bilanciamento (MB).

The MGP is the most relevant phase in terms of quantities of energy exchanged and prices. Producers and consumers can buy and sell energy for each hour of the day ahead submitting offers of sale or purchase during the market sessions. Each offer is given by a quantity of energy and its price.

At this point, the electrical network is represented by few nodes associated to market zones of the power system, typically connected by feeders with limited transmission capacity, defined by the TSO [16].

Market zones of the Italian network, updated in 2021, are reminded, as shown in Figure 1.7:

- North (NORD) comprehends all regions north of Liguria and Emilia Romagna;
- Center North (CNOR) consists of the regions of Toscana and Marche;
- Center South (CSUD) contains Umbria, Abruzzo, Lazio and Campania;

- South (SUD) is made of the southern regions except Calabria and the islands;
- Calabria (CALA);
- Sicily (SICI);
- Sardinia (SARD).

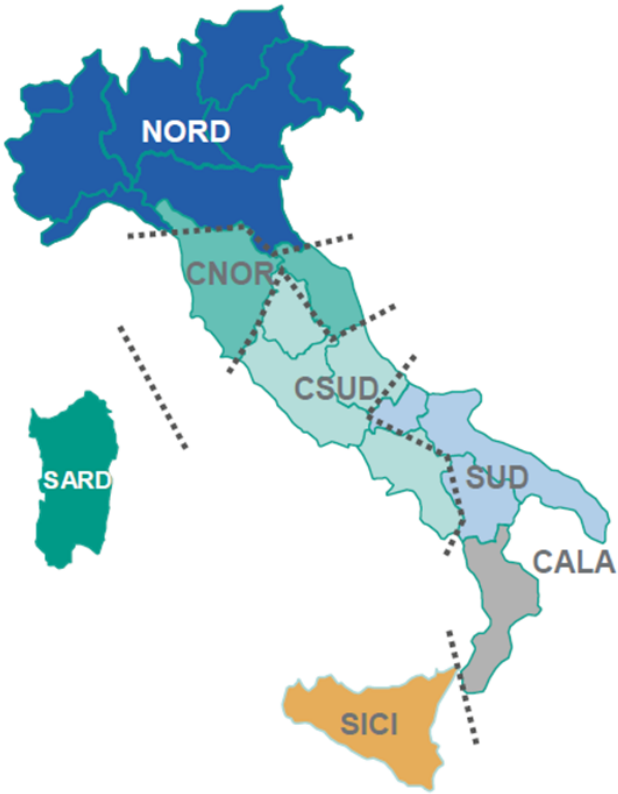

Figure 1.7: Market zones of Italy since 2021 [17].

Energy sale prices are determined through the mechanism of the System Marginal Price (SMP), that is highest price among the accepted offers in each market zone, so a different sale price exists for each zone. On the other hand, the purchase price, namely Prezzo Unico Nazionale (PUN), is the same for all zones and corresponds to the mean value of the zonal sale prices, weighted by demand in each zone. Basically, transmission capacity limits between zones are the reason why a SMP is defined for each zone.

Considering the two-zone example reported in Figure 1.8, if the line transmission capacity is ignored, the generator G1, that is cheaper than G2, is able to satisfy both demands D1 and D2. In this case, the SMP of both zones is equal to $40 €/\mathrm{MWh}$ because it corresponds to the accepted offer with the highest price for a total income of $4000 €$ equally divided among the two zones (Table 1.3).

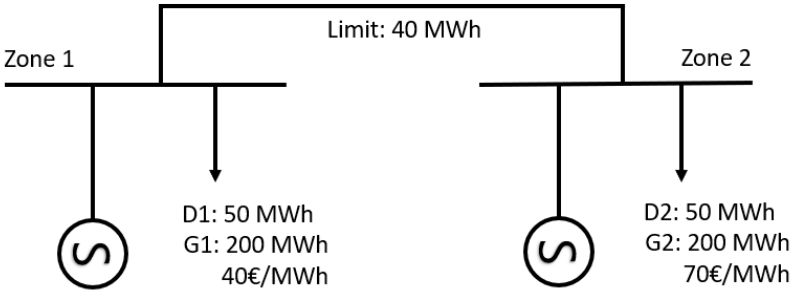

Figure 1.8: Two-zone example of energy price definition.

Table 1.3: Energy cost without considering transmission limit.

Zone	SMP	Producers' income	Consumers' payout
1	$50 €/\mathrm{MWh}$	$100 \times 40 = 4000 €$	$50 \times 40 = 2000 €$
2	$50 €/\mathrm{MWh}$	$0 \times 70 = 0 €$	$50 \times 40 = 2000 €$
total	-	$4000 €$	$4000 €$

Taking into account the transmission limit, generator G1 can't satisfy demand D2 because of system constraints, so it produces $90\,\mathrm{MWh}$, 40 of which are delivered to D2 and the last $10\,\mathrm{MWh}$ are provided by the generator G2 (Table 1.4).

Table 1.4: Energy cost taking into account transmission limit.

Zone	SMP	Producers' income	Consumers' payout
1	$50\,€/\mathrm{MWh}$	$90 \times 40 = 3600\,€$	$50 \times 40 = 2000\,€$
2	$70\,€/\mathrm{MWh}$	$10 \times 70 = 700\,€$	$50 \times 70 = 3500\,€$
total	-	$4300\,€$	$5500\,€$

It happens that the SMP in zone 1 is $40\,€/\mathrm{MWh}$ as before, but in Zone 2 it is $70\,€/\mathrm{MWh}$ since this is the highest price among accepted offers. This lead to a total income of $4300\,€$ for producers, but the energy cost $5500\,€$ for consumers since D2 shall have to pay its whole demand at the SMP.

It results in a difference between the producers' income and the consumers' payout which is intended to be used by the TSO to improve the network infrastructure or to reduce costs. Moreover, in the example it seems that energy costs differently for each zone depending on the system infrastructure, but what really happen is that each consumer pays its demand by the PUN which is, as said before, the weighed mean value of the zonal SMPs. The PUN is introduced because some consumers would be paying extremely high costs otherwise.

During the MI, operators can modify the schedules defined in the MGP by proposing new offers to update the schedule according to more accurate predictions. The mechanism of the offers and of prices definition are equivalent to the one described for MGP.

The MSD is the tool through which the TSO gathers the resources to manage the power system providing the power reserves to support the regulation services. Accepted offers in this phase are paid with the proposed price (pay as bid method).

These resources are fundamental to guarantee instantaneous balance between generation and demand satisfying the operational limits of the power system such as voltage, frequency, flows. In particular, the transmission service needs to respect the voltage profile of all nodes, maintaining the frequency nominal value and respecting transport capacity limits. Auxiliary resources that can be requested by the TSO are divided into exchangeable resources and non exchangeable resources.

To deal with congestions, when the MGP and MI fail to find an operating point that satisfies transmission system constraints, the TSO may request available producing units to vary their scheduled power output.

Operating reserves are established to prevent instability issues of the network that might happen after a relevant unbalance: this would cause the frequency to deviate from its nominal value, thus an immediate action is needed. In light of this, the TSO can request in advance the available generation units to arrange a power reserve to use when necessary to restore the frequency and bring the system back to normal operating conditions as before the event.

This service is offered through the MSD Ex-Ante and consists in a band wherein the generation unit is available to vary its power output. Once that all resources have been set up in the MSD Ex-Ante, the TSO guarantees the real time balancing of the system by changing the setpoints of the pre-selected generation units via the MB.

1.5 Regulation services

To be able to understand their importance to the power system, a definition of ancillary services, or regulation services, should is given. The Federal Energy Regulatory Commission (FERC 1995) defined ancillary services as those services necessary to support areas and transmitting utilities within those control areas to maintain reliable operations of the interconnected transmission system [18].

In this reference, a list of regulation services is given in order to give a quite accurate explanation of what these services are meant for and the logic under the implementation of strategies to let the new categories of generation units, load and BESSs contribute to the power system stability:

- Scheduling and dispatch;
- Load following;
- Reliability;
- Supplemental operating;
- Energy imbalance;
- Real power loss replacement;
- Voltage control;

In the following, a brief explanation of these categories of services is given.

1.5.1 Scheduling and Dispatch

Scheduling takes place before the assignment of generation and transmission resources to meet anticipated load. Dispatch is the real time control of all generation and transmission resources that are currently online and available to meet load and to maintain reliability. This is the traditional mechanism adopted by electricity markets and that will be deeper discussed in the following sections.

1.5.2 Load Following

The basic concept to let a network operating properly is to maintain as instantaneous balance between generation and load. Its worth noting that load can be observed as the sum of three primary components. The first element is the minimum constant base load, the second is the trend during the hour and the third is the random fluctuation in load around the underlying trend. Basically, load following can be referred to as the capability of the network to meet the fast and slow fluctuations of the load. The complexity of this task is given by the uncertainty about loads and system constraints, such as generators ramping requirements, especially for the following of fast fluctuations. Nevertheless, RESs introduce an additional issue since they power output depends on climatic conditions so that also uncertainty about generation from this categories of power plants exists.

1.5.3 Operating Reserves

While the load following service matches generation to load based on the time varying nature of demand, operating reserves balance generation to load in response to unexpected generation to transmission outages. Operating reserves can be split into:

- reliability services, which include spinning reserves and other generating units that can be started quickly (fully available within 10 minutes);
- supplemental operating reserves, which are intended to replace the reliability reserves and stand ready to meet additional contingencies (fully available within 30 minutes).

The deployment of RESs causes again trouble since they are taking the place of dispatchable generation units, thus reducing the available operating reserve. For this reason, new types of flexible resources and new manners to provide regulation services are explored.

1.5.4 Energy Imbalance

Energy imbalance is unavoidable because it is impossible for each control area to exactly match generation to load in an interconnected system. The service is intended to serve primarily as an accounting mechanism to ensure appropriate compensation for the unavoidable small discrepancies between

actual and scheduled flows. It also introduces penalty fees for those customers whose generation is quite different from the scheduled one to discourage imbalances.

1.5.5 Real Power Loss Replacement

Real power losses are the differences between generated real power and the real power delivered to customers. Moving power always results in losses because of the resistance of each element in the transmission system. The losses depend on network configuration, generator locations and outputs, and customer locations and demands. Real power losses must be made up by generators.

1.5.6 Voltage Control

Reactive power management coincides with voltage control, used to maintain nodal voltages within prescribed limits ad to compensate for the reactive requirements of the grid. Injection and absorption of reactive power is also required to maintain system stability, in particular to protect against contingencies that could lead to voltage collapse. Enough reactive power capacity must be available to meet expected demands plus a reserve margin for contingencies. Thus, voltage control is analog to reliability spinning reserve.

Reactive losses are much higher than real losses, in fact voltage drops are predominantly caused by the inductance of the lines and transformers, rather than the resistance, and can be compensated for by supplying reactive power. Conversely, too much reactive compensation can produce excessively high voltages.

Voltage regulation is aimed primarily at maintaining voltage within certain ranges, but is also concerned with minimizing temporal variations in voltage. Finally, most devices are load limited by current rather than by real power, so, if they are carrying significant reactive power, they have less capacity available to transport real power.

CHAPTER 2

Network planning in sight of large RES deployment

2.1 Off-Shore Wind Hosting Capacity in Sicilian Network

In this section an example of analysis of the electrical network in the context of the National Trend (NT) scenario is applied to the Sicilian study case. The analysis has been carried out during the research activity for the implementation of a new floating off-shore wind farm of 2.8 GW.

The study consists in a hosting capacity analysis to understand the maximum power injection from the wind farm that the Sicilian network can dispatch in compliance with safety constraints of the system.

The result will strongly depend on the success of the realization of the other interventions foreseen by the Development Plan in the medium term and long term horizon, 2025 and 2030.

The work included the following steps:

- implementation of the network model based on the NT scenario 2025 and 2030;
- implementation of the one-year power profiles of the generation units and the load, as well as the import/export profile;
- static load flow with normal operating system (N analysis) simulation on hourly basis and one year duration;
- consideration of contingencies (N-1 analysis);
- development of reports of voltage and power flow violations, according to the TSO criterion for N and N-1 analysis.
- optimal siting and sizing of BESSs that could increase the hosting capacity of the Sicilian network.

The grid analysis has been carried out on a model of the Sicilian network [19] including the foreseen interventions to reinforce the power system according to the Development Plan 2021 and the hypothesis of the NT scenario, which corresponds to the case of minimum hosting capacity for the connection of the wind farm which would add to the share of RES generation needed to meet the goals set by the national energy policy.

In Figure 2.1 the HV and EHV ($220\,\mathrm{kV}$ and $380\,\mathrm{kV}$) Sicilian network is shown.

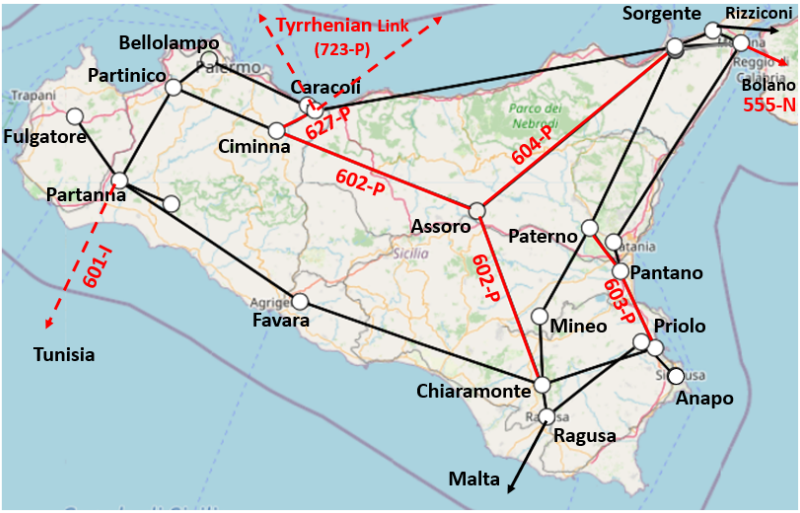

Figure 2.1: Network of Sicily expected by NT scenario 2030.

The main network reinforcements foreseen by the Development Plan 2021 [10] are listed along with their project codes:

- Chiaramonte Gulfi - Ciminna (602-P) is an essential 380 kV connection that will enchance the transmission capacibility between the East and West area of Sicily.
- Paternò - Pantano - Priolo (603-P) connects the South East area of Sicily, where some big power plants are hosted, to the Northern part to facilitate energy export toward the Calabria Region (Italian peninsula).
- Assoro - Sorgente (604-P), coordinated with intervention 602-P, is a direct path from the West Sicily to Sorgente and to Calabria as well.
- Caracoli - Ciminna (627-P) connects the area of Caracoli to Ciminna where the feeder of intervention 602-P starts.
- Bolano - Paradiso (555-N) will improve connection with Calabria and increase the power transmission capacity towards the continent to 2000 MW;

- Tyrrhenian Link (723-P) is a double submarinne HVDC connection between the islands and the region of Campania, thus enhancing interconnections among market zones and addiionally increasing the export capability of Sicily;
- HVDC Tunisia (601-I) will connect Sicily to Tunisia.

The generation and load units have been characterized by associating them with power profiles supplied by MBS through elaboration of historic generation data from the TSO.

Power demand as well as RES generation has been distributed following the current distribution and considering the connection requests still to be authorized. Reference profiles adopted for programmable power units (hydroelectric and thermoelectric units) comes from market scenarios which do not take place in this dissertation.

After implementing the power time characteristics, an annual load flow analysis with normal operating network is conducted (N analysis), giving evidence in Figure 2.2 of the contribution from the different power plant categories.

By zooming the plot, it can be noted in Figure 2.3 the hours of peak generation from photovoltaic during midday, as well as the power consumption, shown as negative generation, of hydro pump storage during night.

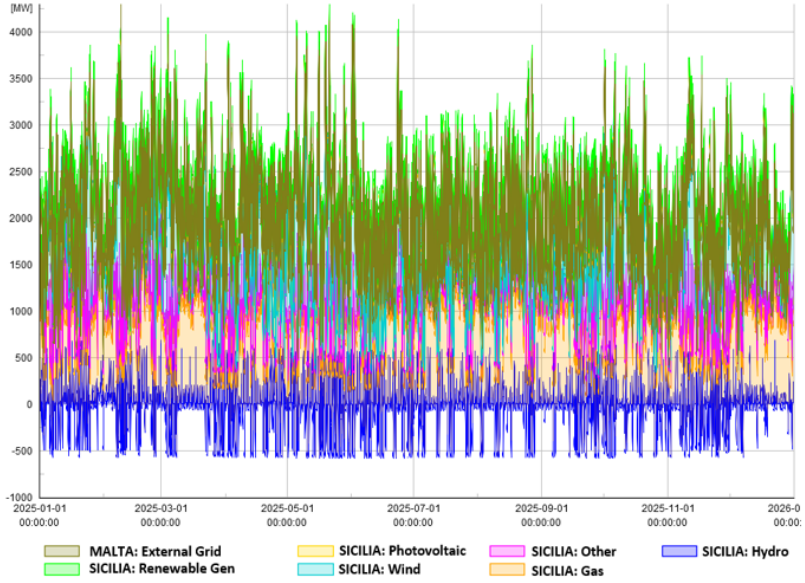

Figure 2.2: Generation output during one-year simulation.

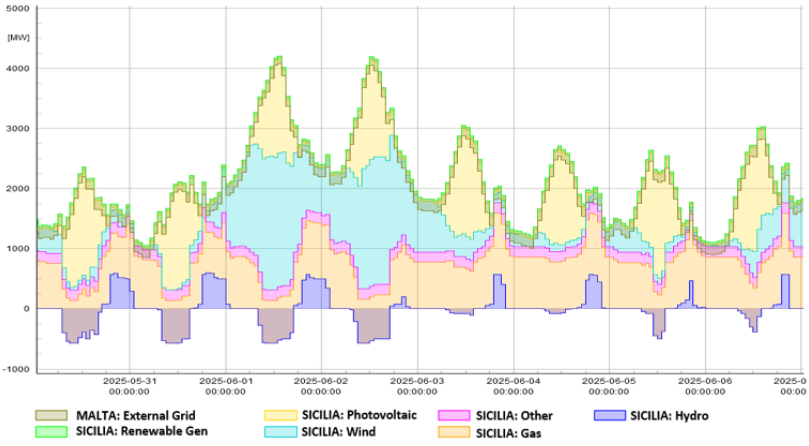

Figure 2.3: Zoom of generation profile.

The N analysis is used to study the hosting capacity of the grid for the offshore wind farm depending on the new RES generation capacity expected and the effective realization of the reinforcement interventions provided for in the Development Plan.

To evaluate the hosting capacity, the validation of the normal operating conditions is checked according to the TSO and ENTSO-E criteria [20]:

- allowed $\pm$ 5% band of nominal voltage of all HV nodes;
- allowed maximum loading of 80% of nominal power of all branches (lines and transformers).

Moreover, contingencies possibility is considered and a N-1 analysis is performed applying it on conditions of peak generation when the system is more stressed. Again, voltage and power flow violations are checked according to the TSO and ENTSO-E criteria during faults:

- allowed $\pm$ 10% band of nominal voltage of all HV nodes;
- allowed maximum loading of 120% of nominal power of all branches (lines and transformers).

In this case, the hypothesis that each HV branch is one by one out of service because of a fault is assumed and a load flow analysis is carried out.

To perform load flow analysis on transmission system of Sicily, DIgSILENT PowerFactory environment is explored to implement the network model; in particular, the Quasi Dynamic simulation tool is used to perform load flow analysis throughout a year by importing generation and load hourly power profiles from external data.

Finally, the report results of the simulation contains the voltage and power flow violations registered during the tests and gives useful information about the maximum power capacity the grid can handle from the wind farm without being over stressed as well as indications of what interventions could help increasing the hosting capacity or if another point of connection would be more effective.

For instance, during the studies it has been assumed to connect the wind plant to the stations of Partanna, in the South West Sicily, or Partinico, in the North West, or both, thus splitting the power capacity between the two nodes. Then the analysis is performed considering the presence or not of the Tyrrhenian Link completed by the 2030 since this is the most important intervention foreseen in the next years concerning Sicily, Sardinia and South Italy and it can have a great impact on the analysis outcome.

In the case without the Tyrrhenian Link, without activating any additional power injection, but only by loading the power profiles of generation and demand in the DIgSILENT network model, results in Table 2.1 already shows critical operating conditions in the interconnections between Sicily and Calabria, thus giving evidence that this intervention is fundamental to export the installed power.

Table 2.1: Overloaded lines in network 2025 without additional injections.

Line	Max Loading	Voltage	NodeA	NodeB
LN06832	117.98 [%]	400 kV	Villafranca	Sorgente 2
LN06481	115.37 [%]	400 kV	App Sicilia 1	Villafranca
LN06478	115.37 [%]	400 kV	App Sicilia 2	Villafranca
LN06476	115.37 [%]	400 kV	App Sicilia 1	App Calabria 1
LN06477	115.37 [%]	400 kV	App Sicilia 2	App Calabria 2
LN02005	103.18 [%]	400 kV	Paradiso	Sorgente
LN01432	103.18 [%]	400 kV	Bolano	Paradiso

At each hour, line loadings are registered. In Figure 2.4, loading profile of interconnections between Sicily and Calabria are given, showing that it exceeds the 80% threshold in less than 100 hours throughout the year. Such information sends a warning about the need of network improvement to enhance the hosting capacity of the Sicily power system.

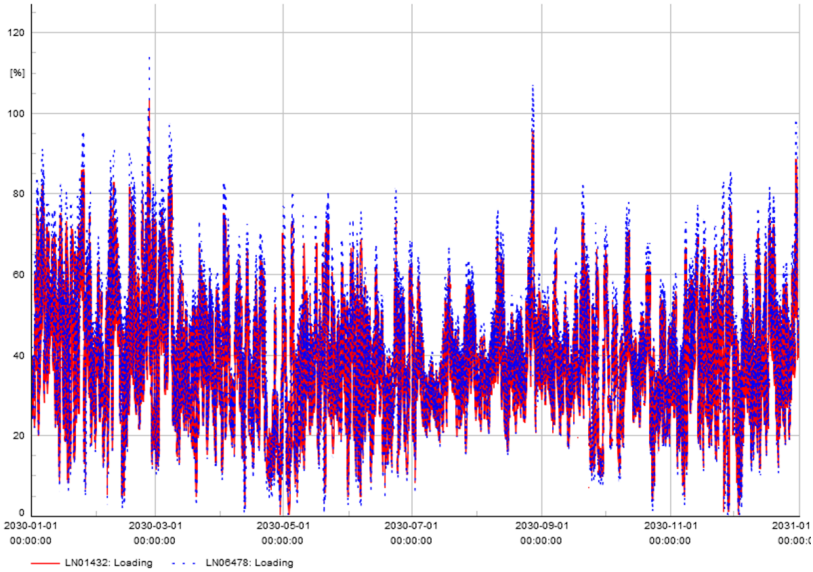

Figure 2.4: Loading profile of lines connecting Sicily and Calabria.

Taking account of activating a power injection of 1000 MW in the node of Partinico, new criticalities are reported in Table 2.2.

Table 2.2: Additional overloaded lines in network 2025 with 1000 MW power injections at Partinico.

Line	Max Loading	Voltage	NodeA	NodeB
LN01455	107.95 [%]	200 kV	Partanna	Partinico
LN01456	107.95 [%]	200 kV	Partanna	Partinico
TR00524	82.15 [%]	400 kV/230 kV	Ciminna	Ciminna

In this case, two 220 kV feeders start working in critical condition, as well as the Ciminna substation transformer. These are local issues that concerns the Sicily power system and can be solved by redirecting the new power generation to Tyrrhenian Link which will be implemented near Ciminna.

Assuming to connect the new plant to the substation of Partanna, no further issues respect to the base case are identified, thus giving evidence that the area of Partanna and South Sicily is less stressed.

In light of this and further analysis, in the case with the Tyrrhenian Link, a production of $1500\,\mathrm{MW}$ at Partinico or Partanna is feasible thanks to the new interconnection. In general, Partinico as point of connection of the wind farm is a better choice than Partanna because it leads to lesser overload condition, especially those at Ciminna substation due to its central position. Bigger power injections still require new interventions to reinforce the West part of Sicily network. A scenario which led to promising results is the case the entire power expected of $2800\,\mathrm{MW}$ is split between Partanna and Partinico and the implementation of a new $380\,\mathrm{kV}$ connection between Partanna and Ciminna is assumed. This condition leads to a good operating point with lesser violation that can be solved through standard curtailment process.

Another option to solve congestions is the siting and sizing of BESSs to support the grid during peak generation hours and increase the hosting capacity. This step is performed by solving an optimization problem that embodies the system model (generators, loads, nodes, branches) and its constraints of voltage and power. The optimal siting appears to be at Partinico and Ciminna as expected because of their central position among the major generation points and the Tyrrhenian Link. The sizing depends on the entity of the overload in terms of number of hours a violation is present in a year.

In conclusion, it can be said that this kind of study gives important information about understanding what could be the optimal siting of new power plants, such as the off-shore wind farm, in terms of feasibility and cost and what interventions might be needed to reinforce the system to keep the network operating without compromising its reliability and safety. Its worth reminding that if interventions are needed to host a new power plant, the TSO might ask the institution who is pursuing the request of connection to provide funds for the actuation of those interventions other than the normal cost of the power plant. For this reason, it is easy to say that this study is of great interest for each institution requesting a connection to the grid, but it is also useful to the TSO to identify the optimal planning strategy.

In light of this, a standardized process is ideal to maximize the possibility and speed of authorization from the TSO thus speeding up the achievements of the targets set by the NT 2030 scenario. To do this, an always updated model of the electric power system is undoubtedly essential to infer reliable information. A huge quantity of data is clearly mandatory for this task, hence, here the interconnection between the network development and the need to improve communication systems can be recognized.

2.2 Storage allocation for network planning: Study case of Sicily

The analysis of network infrastructure can lead to information about optimal sites for new RESs installation. In the case of already over stressed power systems like the Sicily study case, the implementation of new RESs may come with other necessary intervention on the infrastructure to prevent critical network operating conditions.

New interventions usually are the installation of new power lines in the grid to increase hosting capacity and remove transmission system constraints. However, such interventions unavoidably go through strict authorization process and often take a long time for come into operation.

Installation of BESSs is a key intervention for managing the new security and environmental needs brought by the RESs volatility. This is especially important for transmission networks prone to congestion issues, with critical links between portions of the grid and with a very high capacity of renewable generation, such as the transmission network of Sicily.

Literature widely explores the benefits from BESSs. In fact, given unpredictable nature of RESs, many works focus on adopting BESSs to compensate power fluctuation from RESs [21–25].

Moreover, for network planning purposes, BESSs can represent a valid alternative to new power lines that may require facilities and/or authorizations that are not readily available [26]. However, BESS installation comes with high costs, thus tools for optimal BESSs allocation are highly researched [27–31].

The Ph.D. research activity represents the evolution of the works [32–34], wherein an algorithm able to provide voltage regulation and to perform optimal sizing and siting of BESSs has been developed. In this work, the methodology adopted is applied to the transmission network of Sicily.

It is worth reminding that Sicily has become a relevant study case in the Italian scenario, especially in terms of new generation from BESSs. In addition, the Sicilian transmission network will undergo several interventions

of great importance for congestion relief, as planned in [35]. In fact, the Sicilian network indeed suffers from congestion problems, due to its peculiar geographical location and its high concentration of RESs favoured by ideal climate conditions.

The algorithm validated in [32] is recalled in this section. The optimal formulation uses Mixed Integer Linear Programming (MILP) computation, implemented in GAMS environment [36].

Given a network of N bus and B branches, voltages are computed linearly as a function of nodal injections adapting power flow equations in per unit.

$$\begin{cases} \begin{pmatrix} I_S \\ I_N \end{pmatrix} = \begin{pmatrix} Y_{SS} & Y_{SN} \\ Y_{NS} & Y_{NN} \end{pmatrix} \cdot \begin{pmatrix} V_S \\ V_N \end{pmatrix} \\ I_k = S^*_{Pk}(2 - V^*_k) + S^*_{Ik} + S^*_{Zk} V_k \end{cases} \tag{2.1}$$

Current injection have a constant impedance (S_{ZN}), a constant current (S_{IN}) and a constant contribution (S_{PN}), while:

- V_S is the slack nodal voltage;
- I_S is the slack nodal injection;
- V_N is the non-slack nodal voltage;
- I_N is the non-slack nodal injection;

To perform voltage regulation, equation 2.1 are derived isolating the constant current injection at each node (S^{re}_{Ik}, S^{im}_{Ik}) so that they can be used as variables in the optimization, obtaining the following equations:

$$\begin{cases} A_{re} = (-B_{re} - C_{re})V^{re}_N + (C_{im} - B_{im})V^{im}_N + \\ \qquad\qquad + S^{re}_{IN} - D_{re}V_s \\ A_{re} = (-B_{im} - C_{im})V^{re}_N + (B_{re} - C_{re})V^{im}_N + \\ \qquad\qquad - S^{re}_{IN} - D_{im}V_s \end{cases} \tag{2.2}$$

where:

$$\begin{cases} A = -2S^*_{PN} \\ B = diag(S^*_{PN}) \\ C = Y_{NN} - 1 - diag(S^*_{ZN}) \\ D = Y_{NS} \end{cases} \tag{2.3}$$

Assuming slack voltage $V_S = 1e^{j0}$ and a reasonable range of phases, voltage limits can be derived for Cartesian components in order to keep voltage magnitude between 0.9 and 1.1 per unit:

$$\begin{cases} 0.9 \leq V^{re}_k \leq 1.1 & k = 1, \ldots, N \\ -0.5 \leq V^{im}_k \leq 0.5 & k = 1, \ldots, N \end{cases} \tag{2.4}$$

Branch current going from node h to node k is computed in Cartesian components as well, both lines and transformers are described by a π-model with longitudinal parameters (resistance R_b and reactance X_b):

$$\begin{cases} V^{re}_h - V_k re = R_b I^{re}_b - X_b I^{im} & b = 1, \ldots, B \\ V^{im}_h - V_k im = X_b I^{re}_b + R_b I^{im} & b = 1, \ldots, B \end{cases} \tag{2.5}$$

Maximum current constraints are approximated as proposed in [32]:

$$\begin{cases} -I^{max}_b \leq I^{re}_b \leq I^{max}_b \\ -I^{max}_b \leq I^{im}_b \leq I^{max}_b \\ -\sqrt{2} I^{max}_b \leq I^{re}_b \pm I^{im}_b \leq \sqrt{2} I^{max}_b \end{cases} \tag{2.6}$$

For clarity, voltage and branch current limits are graphically represented in Figure 2.5.

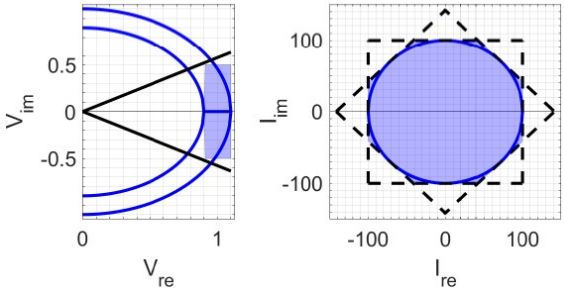

Figure 2.5: Voltage and branch current limits in terms of Cartesian components [32].

As said before, current injections are used as optimization variables: Distributed Generations (DGs) reactive injections and BESSs contributions are indeed modelled as current-controlled sources.

The DGs reactive power contribution, required to supply reactive compensation within operational limits, i.e. keeping a power factor higher than 0.9:

$$-P_{g,t}tan(\phi_{min}) \leq Q_{g,t} \leq P_{g,t}tan(\phi_{min}) \tag{2.7}$$

Moreover, BESSs can be installed in the grid to help guaranteeing power flow feasibility, though it is to be penalized in the objective function.

The optimization problem minimizes the overall number of storage modules located at each node $N_{BESS}(k)$:

$$ObjFun = \min \sum_{k=1}^{N} (N_{BESS}(k)) \tag{2.8}$$

$$s.t. \begin{cases} SOC_{k,t} = SOC_{k,t-1} + (S_{Ik,t}^{C,re}\eta_C - S_{Ik,t}^{D,re}/\eta_C)\Delta T \\ -P_{max}(k) \leq P_{b,t} \leq P_{max}(k) \\ -Q_{max}(k) \leq Q_{b,t} \leq Q_{max}(k) \\ P_{max} = Q_{max} = C_{rate}N_{BESS}(k)E_{BESS} \\ 0 \leq SOC(k,t) \leq N_{BESS}(k)E_{BESS} \end{cases} \tag{2.9}$$

where:

- State of Charge (SoC) is the state variable of the BESS;
- η_C and η_D are charge and discharge efficiencies;
- ΔT is the granularity [s];
- C_{rate} is the rate of charge;
- E_{BESS} is the energy capacity [MW].

BESS modules are considered equal in capacity and in the other parameters, as reported in Table 2.5, so that for sizing only the number of modules is to be decided for each node with an allocated BESS.

Finally, in order to achieve a sustainable configuration, an energy management strategy for BESSs is implemented; specifically, BESSs are requested to keep the same SoC at the end of each day ($t = T$), hence initialising it to the value of 50% at $t = 0$ s.

$$\begin{cases} SOC_{k,t=0} = 50\% \\ SOC_{k,t=T} = N_{BESS}(k) \cdot SOC(k, t = 0) \end{cases} \tag{2.10}$$

To apply the algorithm to the study case of Sicily, the network model has been implemented, along with the operational conditions, on DIgSILENT PowerFactory environment to perform load flow analysis. The load flow outcome has been used to create a model within the Matpower format [37], thus including the power injection to each node, necessary to exploit the algorithm. In addition, the Matpower tool can be used to validate the algorithm results. The model of the HV transmission network of Sicily has been reduced in a 37 bus system, described in Table 2.3, whose power demand is expressed as the sum of load and small size generators located at lower voltage level network, included in the equivalent power flow of the substation transformers.

Table 2.3: Nodes of Sicilian network model.

Zone	380 kV	220 kV	Zone	380 kV	220 kV
Sorgente	1 (slack)	14	S.F. del Mela 2	–	17
Villafranca	2	–	Misterbianco	–	18
Sorgente 2	3	20	Caracoli	–	21
Paterno	4	–	Termini 1	–	22
Pantano	5	19	Termini 2	–	23
Priolo	6	36	Bellolampo	–	24
ERG Nord	7	–	Partinico	–	26
ISAB Sud	8	–	Partanna	–	27
Melilli	9	35	Fulgatore	–	28
Mineo	10	–	Sambuca	–	29
Chiaramonte	11	32	Catt. C. LE	–	30
Assoro	12	–	Favara	–	31
Ciminna	13	25	Ragusa	–	33
Ferdofin	–	15	Versalis	–	34
S.F. del Mela	–	16	Anapo	–	37

In particular, the interface between TSO and DSOs is a key point to correctly model the contribution from Distributed Energy Resource (DER) [38]. In this study each HV node connected to lower voltage levels has been represented as shown in Figure 2.6 where transformers are replaced with an equivalent aggregation of distributed units, such as PVs, WTs and loads [39].

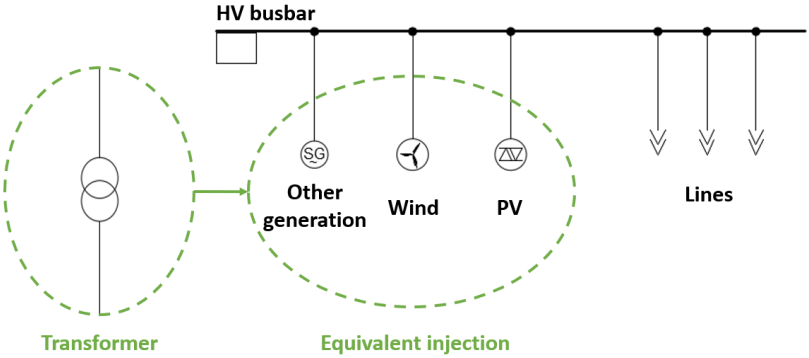

Figure 2.6: Representation of HV node with equivalent distributed units (PV, WT and load).

Generators in Table 2.4, meant for the voltage regulation control, are identified in the power plants of largest installed power since they are the most suitable to supply the network with reactive power.

Table 2.4: Relevant generation units.

Name	Node	Zone	Size [MVA]
Rizziconi	2	Calabria	1500
ERG Nord	7	Priolo	600
ISAB Sud	8	Priolo	700
Termini	22-23	Termini	900
Anapo	37	Anapo	500

Furthermore, in order to apply the algorithm for future scenarios, the power setpoints of generation and load in the Matpower model have been updated at each cycle, as illustrated in the flowchart in Figure 2.7, untl the final cycle at day_{end} is reached.

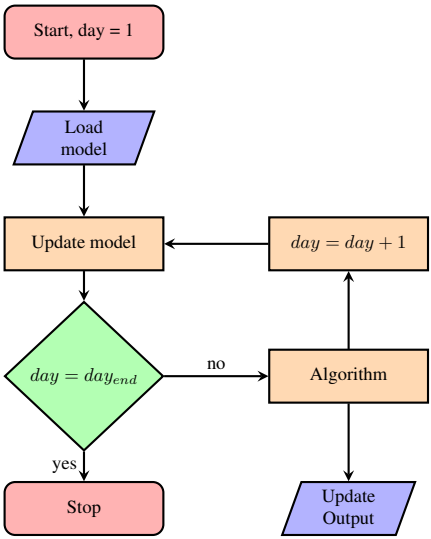

Figure 2.7: Method flowchart.

In particular, to perform a one year simulation with a hourly sampling, the algorithm is run with a daily horizon, resulting in 365 cycles ($day_{end} = 365$). At each cycle, the model power setpoints of load and generators are updated

each time. The power profiles that would feed the setpoints of generation and load are built starting from annual profiles with a hourly granularity. The profiles are first split according to their distribution in the four geographical areas of the island.

In each area, then, uniform distribution is assumed among the HV nodes. Wind generation is also augmented with generation data estimated via the distribution of wind speed in the selected areas of the region. Wind speed and other data are gathered in [40]:

- North-East (NE);
- North-West (NO);
- South-East (SE);
- South-West (SO);

Then, power profile from each plant category (load, PV, wind, etc.), a typical daily profile is estimated, together with its variance, in a similar fashion to the Montecarlo methodology presented in [32]. Such typical profiles are computed for the four seasons of the year.

In Figure 2.7, the block "Algorithm" of the flowchart includes the process wherein the Matpower model is loaded and then given as an input to the optimization problem in GAMS environment, described by Equations 2.1 – 2.10. After that, the output is stored, the model is updated and the algorithm is run again.

The proposed methodology also lets implement the hypothesis of new generators by defining the installed power and the node of connection in the Matpower model to infer conclusions about the possible impacts on the network by the insertion of the new units, In case of RESs, such process can give an idea about the risk of curtailment due to over generation issues and what could be the necessary actions to perform on the system, such as the installation of new feeders or BESSs, to prevent any portion of the network from working in critical conditions.

To give evidence of the contribution of the proposed methodology, an example of application of one day duration is described in the following section.

Considering the network operating in a summer day, when there is a large power generation from RESs, the algorithm only performs one cycle. During each hour of the considered day, system constraints (2.4) and (2.6) are checked and a solution of reactive power injections from generators is given to provide voltage regulation. If there is no solution that does not violate the system constraints, the algorithm performs an optimal BESS allocation. The sizing of BESSs is achieved by the definition of a module so that the algorithm finds out the minimum number of modules at each node required to satisfy system constraints. BESS module parameters are given in Table 2.5.

Table 2.5: BESS module parameters.

Quantity	Value	Unit
Battery size	100	MWh
Initial SoC	50	%
Charge efficiency	0.95	–
Discharge efficiency	0.9	–
C-rate	4	–

After simulation, optimized reactive power setpoints from generators in Table 2.4 are computed as shown in Figure 2.8. Nodal voltages are reported in Figure 2.9 where voltage levels before optimization, drawn in blue, present a violation that is cleared after optimization (voltages drawn in red).

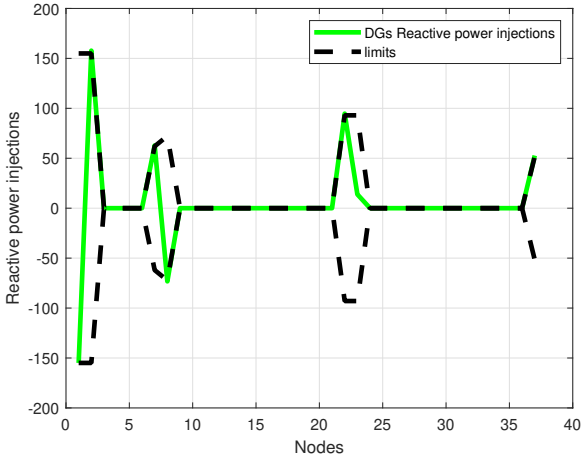

Figure 2.8: Optimized reactive power injection.

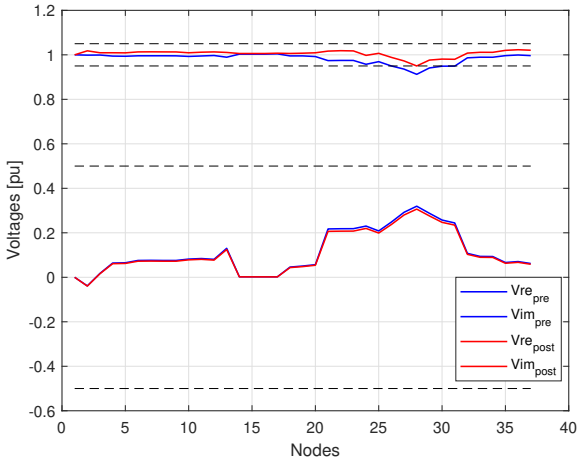

Figure 2.9: Nodal real and imaginary voltage at hour 19 before optimization, in blue, and after optimization, in red.

In this section, results of the simulation of one year duration are shown; with respect to the DIgSILENT model it is assumed the implementation of an additional Wind park rated $2000\,\mathrm{MW}$ at Partinico. Simulation results show that, to keep system constraints satisfied, a certain number of BESS modules are required, despite the generators contribution. At each cycle, one per day, the algorithm establishes that from 1 to 4 BESS modules are to be installed at node of Ciminna, adjacent to Partinico. Such result suggests that, to absolutely prevent any voltage or current violation, the worst case scenario shall be selected, thus 4 modules would be installed.

Introducing cost considerations and possibility to apply curtailment strategies, the best solution can be different as a trade off between network operating conditions and implementation cost of new units and associated BESSs, as shown in Table 2.6.

Table 2.6: Significant quantiles of injections from BESS among all scenarios.

	P_b	Q_b	$\sum_{k=1}^{N} N_{BESS}(k)$
Quantile	[MW]	[MVar]	n.
1.00 (Max)	1600	1600	4
0.99	1003	1250	4
0.95	392	877	3
0.9	216	826	3

In Table 2.6, it can be observe that while a total of $1600\,\mathrm{MW}$ and MVar injection can cover all the needed active and reactive power regulation of the BESS unit, $1003\,\mathrm{MW}$ (resp. $1250\,\mathrm{MVar}$) are needed in just 1% of the time (less than 4 days). Similarly, with $392\,\mathrm{MW}$ (resp. $877\,\mathrm{MVar}$), and just 3 modules, the BESS unit can can satisfy the 95% of the hours; with $216\,\mathrm{MW}$ (resp. $826\,\mathrm{MVar}$) given by 3 modules, 90% of the hours satisfies all the constraints.

A sizing for each percentage can be derived in this way, by looking at the Cumulative Distribution Functions (CDFs) of the absolute value of the active power injection (Figure 2.10), and reactive power injection (Figure 2.11). The vertical portions of the CDFs are the ones in which a little increase of size in

the BESS unit can result in significant gains in the frequency of hours covered by the allocated storage.

Conversely, the horizontal portions are the ones for which a big increase in the size of the storage unit is needed for a little advantage in terms of hours covered. For active power (Figure 2.10) the CDF becomes horizontal more quickly, meaning, than the marginal usefulness of increasing the BESS unit size decreases rapidly. On the other hand, the reactive power CDF (Figure 2.11) is more regular in its increase, meaning that an optimal size is harder to spot. However, in both cases, one can see that most of the needed rated power will be used very rarely, with consequent unnecessary higher costs.

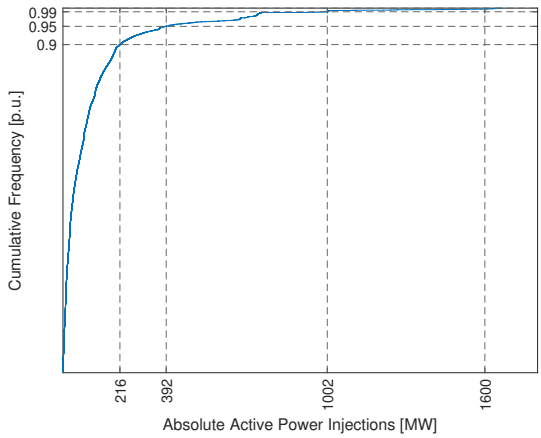

Figure 2.10: Cumulative Distribution Function of Active Power Injections (in absolute value), with significant frequencies.

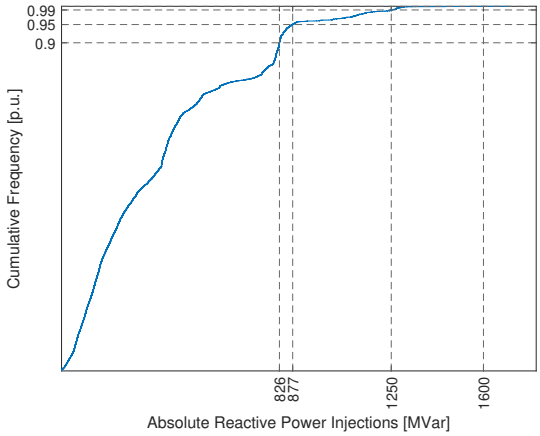

Figure 2.11: Cumulative Distribution Function of Reactive Power Injections (in absolute value), with significant frequencies.

CHAPTER 3

New solutions to network support: flexibility by grid services

The strong promotion of RESs is evident in Italy, as shown in Chapter 2, but in other countries the trend is not different according to the SDGs concerning climate set by the 2030 Agenda. The great involvement of RESs generation units, such as PV and WT, has introduced some critical issues in the scheduling of the power generation and in the operation of the power system in safety conditions.

For instance, relevant modifications affected the residual demand, which is total power consumption profile after deduction of the power injections from RESs [41]. Such profile has significantly decreased such that it can be negative during hours of maximum production from PVs. Also, the difference between the peak value during evening and the minimum value at noon has increased, thus increasing the residual demand profile variability which leads to new umbalance issues for the electric power system.

Also, the increase of power injection from RES units takes place at the expense of programmable units. Nevertheless, programmable units have the characteristic of quickly varying their power injection towards the grid while they are active, hence they are suitable to provide regulation services because of the upward and downward reserve they make available.

Regulation services are used by the TSO to carry out balancing and congestion resolution functions, thereby ensuring the safety and quality of electricity supply.

Therefore, the reduction of programmable units leads to the effect of decreasing the power reserve for service provision. Also, since RESs are less predictable, their implementation results in an increase in power reserve requirements. In fact, the need of power reserves that are quick to activate when needed (just in time), is recently highlighted by the TSO to address the new constraints for additional flexibility performance [42].

Thus, the need of the power system for new flexibility resources, that are available from units ready to change their baseline power injection or consumption to allow balancing of the electrical system, is evident.

At a distribution level, RESs penetration has led to the recent phenomenon of reverse power flows towards the transmission network, emphasizing issues of limited hosting capacity, congestions and voltage instability that can bring to the service interruption (curtailment of generation and/or load).

The solution can be found in the use of flexible resources directly localized in the distribution system, provided from distributed generation, load units or BESSs. Such resources can contribute to increase the distribution network capacity, change the demand profile providing peak shaving and load shifting services, reduce power losses and increase the service quality and the system reliability.

These are the main reason why the electricity market is evolving in order to include to the service provision units considered unable to provide balancing services. Clearly, the introduction of flexibility services requires to update the market rules and the responsibilities of all parts involved [43, 44].

3.1 Deliberation 300/2017

Only qualified units can take part of in the MSD to provide regulation services. Qualified units have to meet the minimum operative requirements specified by the TSO.

Before the recent changes in the electricity market framework introduced with the Deliberation 300/2017 [9] of the Italian Regulatory Authority for Energy, Networks and Environment [45], such requirements prevented small generation units, with nominal power lower than $10\,\mathrm{MVA}$, and RES, which have non dispatchable resources (wind, photovoltaic, etc.), from participating the MSD.

Moreover, following [46] and [47], where the European Commission defines the guidelines to allow aggregates to be involved in the dispatching and balancing markets, deliberation [9] led the TSO to write the codes of pilot projects for the enlargement of the dispatching resources.

Functional requirement were set too, such as the capability to vary the power output for a given time extension depending on the requested regulation service, as designed in [48].

With the great technological development of RES, which could not contribute to the MSD, a strong reduction of the maximum qualified power for ancillary services has been registered, originating critical issues concerning the network stability due to the higher risk power reserve that might be insufficient to overcome relevant disturbances to the system. Nevertheless, the increase of RESs, whose power generation is not purely predictable since it depends on climatic conditions, brings even more the need of a greater power reserve that might assure the balance between generation and load.

In fact, the effect of the employment of RESs can be seen in residual demand profile, that is the difference between the demand and the generation from RESs; this represents the share of load that must be satisfied by traditional dispatchable power plants. RESs are having a so relevant impact that such profile can reach negative values, especially during midday when photovoltaic production is at its maximum and meets alone the power demand.

In addition, a faster increase of residual demand is registered respect to the total load profile due to the typical increase of load during evening hours and the loss of power generation from photovoltaic.

In light of these problems, an evolution of the MSD criteria started with the attempt to find a way to gather new regulation resources from RESs, DG (with nominal power lower than $10\,\mathrm{MVA}$) and demand, namely Demand Side Response (DMR) [49].

This innovation requires also the redesign of some ancillary services and the definition of new ones through documents called pilot projects which define the minimum operational requirements for a generation unit to provide a given regulation service.

It can be said that the MSD reform started with Deliberation 300/2017/R/eel [9] which defines the criteria to let demand and not already qualified generation units participate the MSD; also BESSs are considered. In particular, given the reduced regulation capacity and the higher need of power reserve, the system requires flexible services defined as operating downward and upward reserve services that can be provided by units characterized by high flexibility in their operation, that is a great capability in rapidly varying their production or consumption.

The use of such flexible resources supports the ability of the power system to respond to imbalances between generation and load at all times. As said before, resources that are present in the network, but not included in the MSD until now, may provide flexible service such as:

- RESs, independently from the nominal power;
- DG, that has nominal power lower than $10\,\mathrm{MVA}$;
- BESSs;
- load.

Regarding those programmable power generation units excluded from MSD because of their low nominal power, lower than 10 MVA, thermoelectric and

hydroelectric power plants would be already technically suitable for the flexibility service provision. If the nominal power requirement for the participation to the MSD would be removed these categories of generation units would be able to contribute to the system flexibility with similar manners as already qualified big power plants already do.

On the other hand, RESs use a random and high variable resource (solar and wind), so they would be able in the service provision only when the primary resource is available. Moreover, they usually work at the maximum operating point for priority reasons, hence, even if required by the TSO, they can't increase they power generation any further. In this case, new methods must be developed to have RESs provide flexible resources.

BESSs can be used to deal with network congestions during peak generation hours from RESs by storing the overgeneration that couldn't be safely evacuated and releasing it back when the generation is at a tolerable level. The benefit of adopting BESSs comes from the minimization of the curtailment of RESs necessary to keep the power system safely working.

In light of this, BESSs can provide invaluable services for the integration of RESs considering the short times of installation; in other words, they can be deployed in specific locations where the grid operating conditions are critical to deal with issues that currently exists or is expected to occur already in the short term, in anticipation or replacement of structural network reinforcements that have a greater environmental impact and require much longer time for authorization and implementation.

The capability of load units to vary their power consumption depends on several factors which define its flexibility, hence the ability to provide Demand-Side Response (DSR) service [49]. Generally, a flexible load is able to vary its power consumption respecting the technical and performance constraints given the by the TSO without relevant consequences for the end user.

Basically, flexibility of power consumption is related to the possibility to store energy in general. In Italy, the usage of electrical energy for thermal purposes is lower respect to other European states. Such condition leads to an increased difficulty in finding new flexibility resources in industrial process

and tertiary and domestic sectors.

The limited power consumption of domestic users is found in [50] that reports a mean power demand per family of $2777\,\mathrm{kWh}$ per year in Italy, compared with $3512\,\mathrm{kWh}$ in Germany and $6343\,\mathrm{kWh}$ in France.

The importance in the definition of the roles of the operators involved in the electricity market is highlighted in an analysis from the Smart Energy Demand Coalition (SEDC) association [51–56]. The study proves that proper regulation would encourage the definition of new business models and the participation of demand to the market.

3.2 Aggregation

Briefly, the evolution of the electricity market is motivated by the increasing need to arrange power reserve to handle the strong penetration of RESs. and let to the increase of qualified units, both generation and load, able to participate to the MSD.

At this point, however, the aggregation of such resources becomes important since the involvement of the DG and end users connected to the distribution network allows on the one hand to increase flexibility, but on the other introduces complexities of managing large quanities of small units (generation and load) by TSO and DSOs, especially with regard to aspects of metering and verification of the provision of the services themselves (monitoring activities).

The aggregator, or Balancing Service Provider (BSP) is the responsible for the provision of regulatory services to the TSO by end customers and will work as interface towards TSO and DSO for the provision of flexibility services by small power units, both generation and load. The aggregator shall have the possibility to monitor all resources under its area of responsibility, to impose the injections and withdrawals of all its clients and to know all technical constraints.

However Virtual Qualified Units (VQUs) must meet some requirements in terms of performance and metering and communication to provide full observability of the system and of the potential power reserve in the context of pilot projects. Aggregation is a first example of how the ecological transition requires improved communication systems because of the electrical network becoming more and more complex.

Pilot projects are identified by the TSO and can involve any aspect that the TSO deems useful to test such as:

- MSD participation by load and not enabled generation units;
- service provision by BESSs;
- aggregation and remuneration systems.

Within this framework, research projects have been carried out to test the potential flexibility services that RESs and load can provide.

The rest of the dissertation explores the theme of flexibility resource that can be provided by:

- loads;
- BESSs;
- WTs paired with BESSs;
- PVs.

Demand side service contribution is explored through analysis of aggregated thermal loads flexibility capability in Chapter 4. Study of service provision from RESs and BESSs has been realized as well, according to the TSO pilot project about Fast Reserve Service (FRS) [57], discussed in Chapter 5.

CHAPTER 4

Flexibility by management of thermal loads

As already said, the Deliberation 300/2017 defines the requirements to let loads and RES participate to the MSD in the context of pilot projects stipulated by the TSO. Small power generation and load units are requested to participate to the MSD as aggregated entities, namely VQUs, which can composed by loads [58], generating units, or by a mix of them [48] that cooperate and interface, as a unique entity, with services and energy markets.

As a consequence, load became an active part in service provision by deliberately reducing the power consumption according to the user's needs. Literature provides many examples of load aggregate management strategies with the aim of providing regulation services [59–64].

A flexibility analysis of aggregates of thermal loads intended for domestic hot water heating, such as domestic electric water heaters or heat pumps, has been carried out during the research activity. Aggregates are modeled as equivalent of the VQUs defined by the TSO as group of provinces, the Italian

territory is divided into 15 VQUs, according to [65].

The aggregate flexibility is determined by taking into account all external factors that have an impact on the water heater thermal dynamic such as the external temperature, the water temperature and the baseline demand profile. Given and elaborated such quantities, flexibility is defined by the power variation and the time duration of such variation that the system is able to sustain.

Installed power in each VQU is estimated by assuming an overall uniform distribution of thermal units. Moreover, 5 climatic zones can be identified throughout Italy, as shown in Figure 4.1.

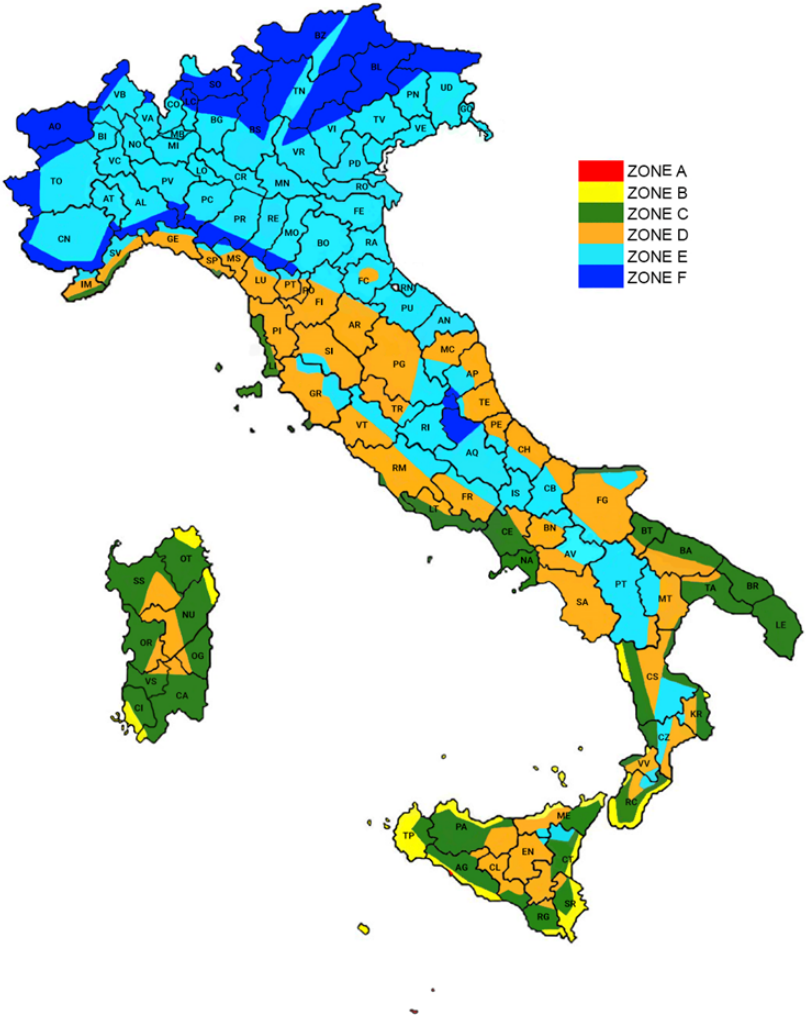

Figure 4.1: Climatic zones in Italy [66].

Climatic zones are defined in [67] depending on the sum of positive difference between conventional temperature (20 °C) and mean air temperature of

each day, expressed in degree-days, as follows:

- Zone A: degree-days lower than 600;
- Zone B: degree-days between 600 and 900;
- Zone C: degree-days between 900 and 1400;
- Zone D: degree-days between 1400 and 2100;
- Zone E: degree-days between 2100 and 3000;
- Zone F: degree-days larger than 3000.

Definition of degree-days comes from [68], according to which low values of degree-days identify zones with temperatures close to the conventional temperature, meanwhile large values identify zones with colder temperatures.

Finally, predictive data about installed power of each VQU and percentage of territory inside each climatic zone are given in Table 4.1.

Table 4.1: Installed power and distribution of VQUs in climatic zones.

	Power [MW]	Zone B [%]	Zone C [%]	Zone D [%]	Zone E [%]	Zone F [%]
VQU 1	209.06	0	0	0	100	0
VQU 2	170.73	0	8	48	23	21
VQU 3	108.4	0	0	0	100	0
VQU 4	287.07	0	0	0	100	0
VQU 5	174.07	0	0	13	84	3
VQU 6	88.78	0	0	0	100	0
VQU 7	334.64	23	53	12	12	0
VQU 8	236.08	0	75	19	6	0
VQU 9	934.76	85	6	5	3	0
VQU 10	727.32	0	10	82	8	0
VQU 11	534.54	0	86	7	8	0
VQU 12	26.71	0	0	100	0	0
VQU 13	75.28	0	0	70	30	0
VQU 14	193.67	0	0	91	9	0
VQU 15	407.76	0	88	12	0	0
Italy	4508.87	19.3%	29.2%	26.1%	24.4%	0.9%

The daily profile of water withdrawal for each unit is assumed to be the same in the whole Italian territory and expressed as percentage $w_h^{\%}$ of the overall demand per hour as shown in Figure 4.2.

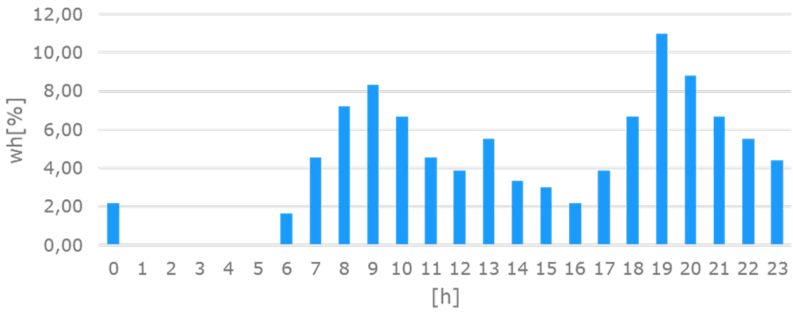

Figure 4.2: Daily profile of domestic hot water withdrawal [69].

The overall hot water demand is computed by considering the daily quantity of water demanded for a housing depending on the dwelling floor space, according to normative UNI TS 11300-2 [70] which states that it is given by the following equation:

$$V = a \cdot S + b \tag{4.1}$$

where:

- V is the water volume daily requested [$\mathrm{l/day}$];
- S is the dwelling floor space [$\mathrm{m^2}$];
- a and b are parameters given in Table 4.2, expressed in [$\mathrm{m^2\,day}$] and [$\mathrm{m^2/day}$].

Table 4.2: Characteristic parameters

Floor space	$S \leq 35$	$35 \leq S \leq 50$	$50 \leq S \leq 200$	$S > 200$
a	0	2.667	1.067	0
b	50	-43.33	36.67	250

For a better representation, the relation is given in Figure 4.3.

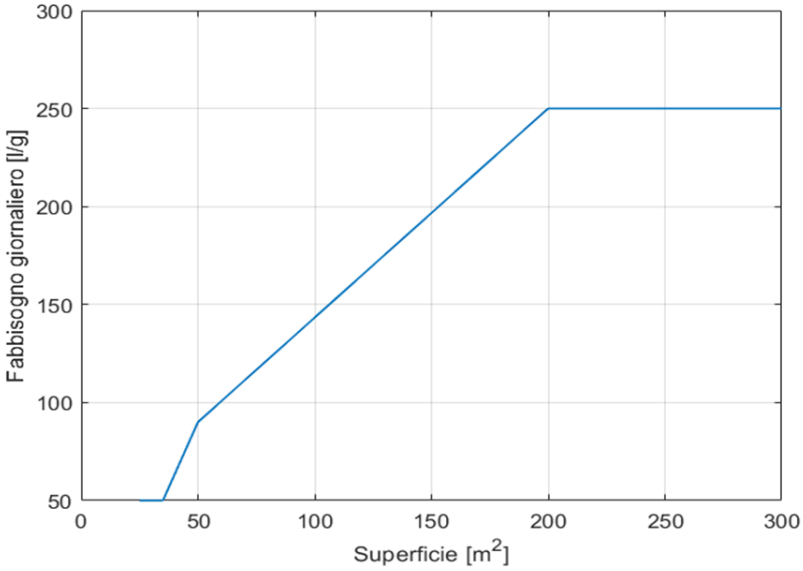

Figure 4.3: Relation between water demand and floor space according to [70].

The dwelling floor space distribution in Italy has been gathered by ISTAT data [71] and elaborated, resulting in the following Table 4.3.

Table 4.3: Number of houses classified by floor space

Floor space $[m^2]$	Housing number -
20	0
24.5	32'343
34.5	459'987
44.5	1'121'167
54.5	1'618'318
69.5	4'993'602
89.5	6'081'472
109.5	4'192'549
129.5	2'897'122
175	2'738'625
200	0

Assuming a Gaussian distribution of the dwelling floor space, a mean value of 98 m^2 has been computed, which corresponds to a daily mean hot water demand equal to $w_{tot} = 142\,\mathrm{l/day}$ from Equation 4.1. Finally, the daily hot water withdrawal profile can be properly characterized.

To model the dynamic of a single unit of the aggregate, some assumptions have been made to perform a stochastic generation of the consumption profile.

The single use of hot water is assumed to have a duration that goes from 1 to 10 minutes with a uniform distribution and with a water flow rate uniformly distributed between $4\,\mathrm{l/min}$ to $12\,\mathrm{l/min}$. The mean number of usages of hot water per each hour is given by:

$$n_h(j) = w_h^{\%} \frac{w_{tot}}{100} \cdot \frac{4}{(\tau_{short} + \tau_{long})(w_{min} + w_{max})} \tag{4.2}$$

The effective number of usages in an hour is generated from a Poisson distribution with mean value equal to $n_h(j)$.

Water flow rates are scaled to represent the mix between hot and cold water set b the user. Hence, a desired temperature $T_d = 40\,^{\circ}\mathrm{C}$ is defined and

assumed not to be changed during the usage. In light of this, the flow rate is scaled as follows:

$$w = w' \frac{T_o - T_d}{T_o - T_o^u} \tag{4.3}$$

where:

- w [l/min] is effective flow rate;
- T_o [°C] is cold water temperature;
- T_o^u [°C] is the boiler water temperature at the beginning of the usage.

Such equation implies that a lower temperature of the water in the boiler leads to a bigger flow rate. As a result, some withdrawal profiles are given in Figure 4.4.

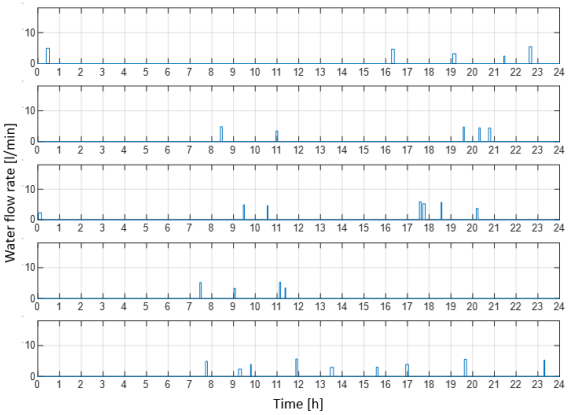

Figure 4.4: Example of withdrawal profiles.

Summing the profiles of the units of a sufficiently large aggregate shall result in the following of the daily baseline profile, shown in Figure 4.2, to validate the model; evidence of this is given in Figure 4.5 where the baseline aggregate profile and the generated profiles of 50000 units are compared.

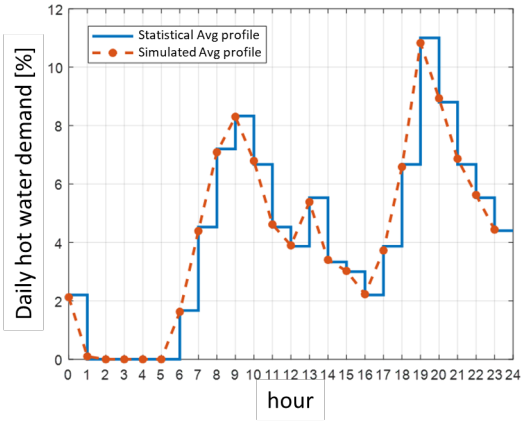

Figure 4.5: Aggregate profile.

Energy demand of a boiler depends on cold water temperature T_o and on environmental temperature T_e, other than water withdrawals, and their impact has been discussed. For each climatic zone, the cold water temperature profile is obtained by an application tool developed by RSE. Data didn't show any relevant variation during the day so, to characterize a one day simulation in a given month, the mean value of cold water temperature is computed for each month and for each climatic zone.

In Figure 4.6 the yearly profiles of cold water temperature for each climatic zone are proposed as well as their monthly average values, also reported in Table 4.4. Such profiles have been computed using the application TgCalc, developed by RSE and University of Padova [72].

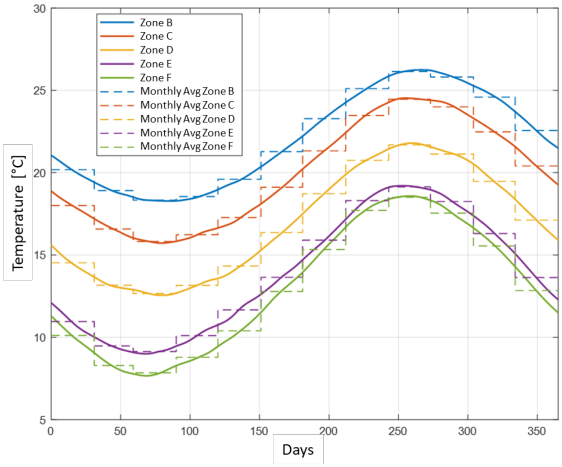

Figure 4.6: Cold water temperature profile of each climatic zone.

Table 4.4: Mean monthly average cold water temperature.

T_o [°C]	Zone B	Zone C	Zone D	Zone E	Zone F
January	20.2	18.0	14.5	11.0	10.1
February	20.2	16.6	13.2	9.5	8.3
March	18.3	15.8	12.7	9.1	7.8
April	18.6	16.2	13.2	10.1	8.8
May	19.6	17.3	14.3	11.7	10.4
June	21.3	19.1	16.4	13.6	12.8
July	23.3	21.3	18.7	15.9	15.3
August	25.1	23.5	20.7	18.3	17.7
September	26.1	24.5	21.7	19.1	18.5
October	25.8	24.0	21.1	18.2	17.5
November	24.6	22.5	19.5	16.3	15.5
December	22.6	20.4	17.1	13.6	12.8

Regarding environmental temperature, data for one year for each climatic zone are gathered. Moreover, through a stochastic study, three day categories have been developed to identify hot, medium and cold temperature days. However, only intermediary case has been considered since the impact of the three scenarios is negligible in the flexibility definition. In Figures 4.7–4.11 the external temperature for each scenario and each climatic zone are shown. Such profiles are obtained by data registered in the five climate zones, for twenty years, collected in database [73].

To correctly model the external temperature impact on the temperature dynamic of the boiler, is crucial considering that the temperature inside the building can be different from the temperature outside due to heating and cooling systems that can be active respectively in Winter and Summer. To deal with this aspect, minimum and maximum temperature random thresholds from 18 to 20 and from 24 to 26 respectively with uniform distribution are assumed. If the temperature outside the building is lower than the minimum threshold, the environmental temperature T_e is set to the threshold. On the other hand, if the temperature outside the building is higher than the maximum threshold, only for a percentage of simulated boilers T_e is set to the threshold, otherwise such threshold is ignore and T_e coincides with the temperature outside the building. The percentage is implemented to represent the portion of building without cooling system and is set equal to 40%.

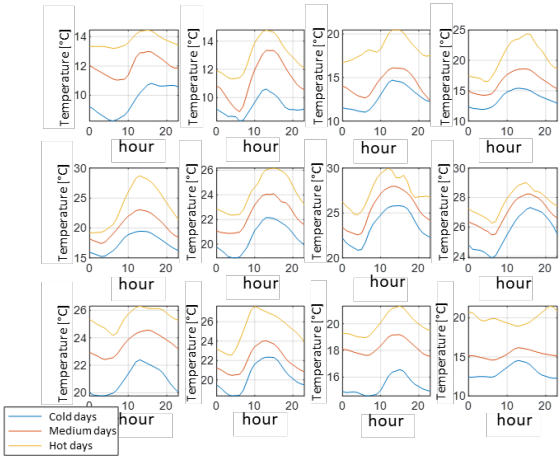

Figure 4.7: Average external temperature for cold, medium and hot days – Zone B

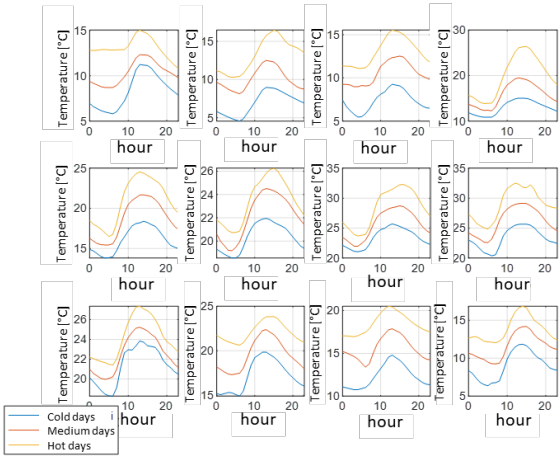

Figure 4.8: Average external temperature for cold, medium and hot days – Zone C.

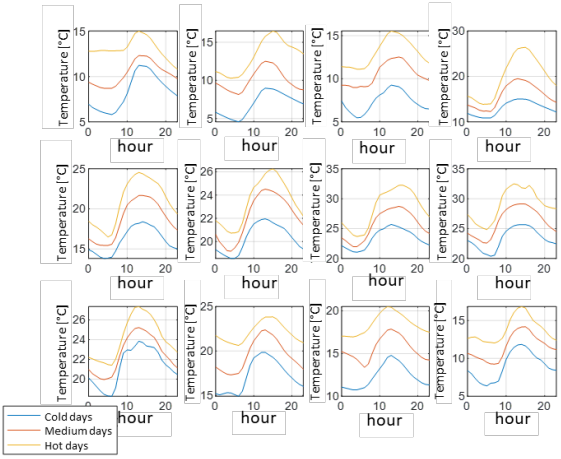

Figure 4.9: Average external temperature for cold, medium and hot days – Zone D.

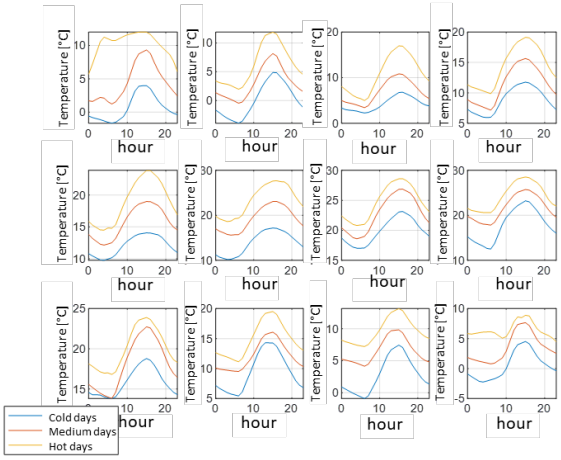

Figure 4.10: Average external temperature for cold, medium and hot days – Zone E.

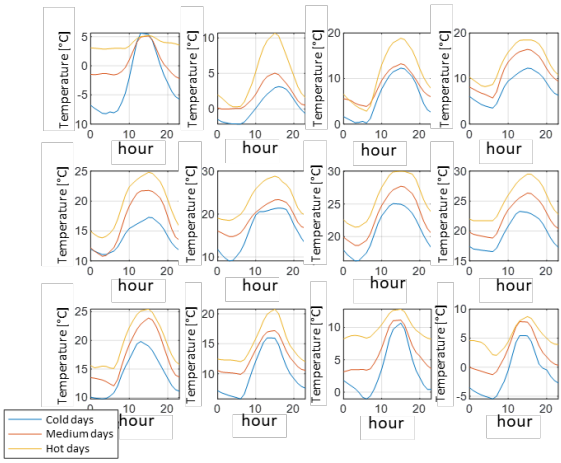

Figure 4.11: Average external temperature for cold, medium and hot days – Zone F.

4.1 Electrical water heater flexibility

The proposed method is applied to Electric Water Heaters (EWHs) considering three different technologies, shown in Table 4.5.

Table 4.5: EWHs operational parameters.

Model	R50 V/3	R80 V/3	R100 V/3
Capacity [l]	50	80	100
Power [kW]	1.2	1.2	1.5
Voltage [V]	230	230	230
Heating time [h,min]	2,17	3,40	3,40
Maximum Temperature [°C]	75	75	75
Heat loss [kWh/day]	0.99	1.35	1.56
Maximum Pressure [bar]	8	8	8
Weight [kW]	16	21	24
Spread percentage [%]	22	60	18

The adopted boiler model is the following [74]:

$$\dot{T} = -\frac{1}{RS_wV\rho}(T - T_e) - \frac{w}{60 \cdot V}(T - T_o) + \frac{1}{S_wV\rho}qP^{nom} \tag{4.4}$$

where:

- T [°C] is the boiler water temperature;
- T_e [°C] is the environmental temperature;
- T_o [°C] is the cold water temperature entering the boiler;
- w [$\mathrm{m}^3/\mathrm{min}$] is the water flow rate;
- R [°C/W] is the heat transfer resistance;
- S_w [$\mathrm{J}/(\mathrm{kg}\,°\mathrm{C})$] is the specific thermal capacity;
- V [m^3]] is the boiler capacity;

- ρ [kg/m^3] is the water density;
- P^{nom} [W] is the boiler nominal power;
- q is the thermostat state (1 if on; 0 if off).

Thermostat turns on and off according to boiler water temperature T; in particular, given a temperature set-point T_{sp} [°C]:

$$q = \begin{cases} 1, & \text{if } T > T_{sp} + \Delta \\ 0, & \text{if } T < T_{sp} - \Delta \end{cases} \tag{4.5}$$

2Δ is the thermostat dead-band and as long as the temperature is close enough to T_{sp} the thermostat state will not change.

The algorithm framework is developed in Matlab & Simulink and is shown in Figure 4.12.

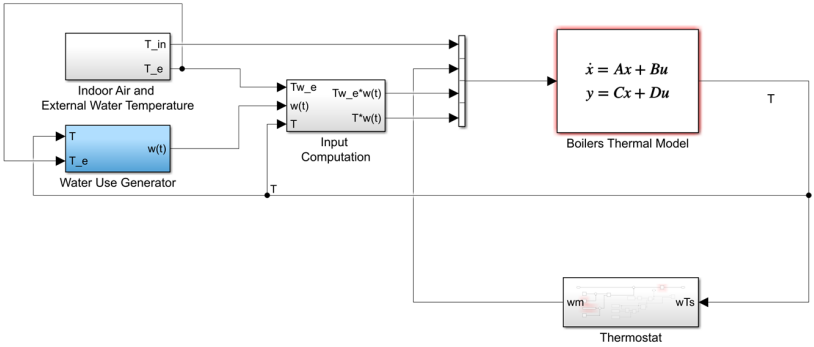

Figure 4.12: Boiler model implemented in Simulink.

- The block "Boilers Thermal Model" implements the dynamic equation 4.4;
- the block "Thermostat" includes the thermostat logic;
- the block "Indoor Air and External Water Temperature" imports environmental and the cold water temperature profiles;
- the block "Water Use Generator" imports the stochastic hot water withdrawals;

- the block ”Input Computation” elaborates the quantities that are the inputs of the boiler model.

The Matlab & Simulink model is able to perform a simulation computing the dynamic of an aggregate of N boilers, optionally characterized by different parameters and different set-point temperatures. Simulation results include temperature profile and thermostat state of the N boilers; hence, by multiplying each thermostat state for the respective device nominal power, the power consumption can be derived. Finally, the sum of power consumption from each boiler leads to the total aggregate load.

As example, a one boiler simulation is performed and shown in Figure 4.13. Such example is referred to a 100 litres boiler with a set-point temperature of 65 °C in August and climate zone D.

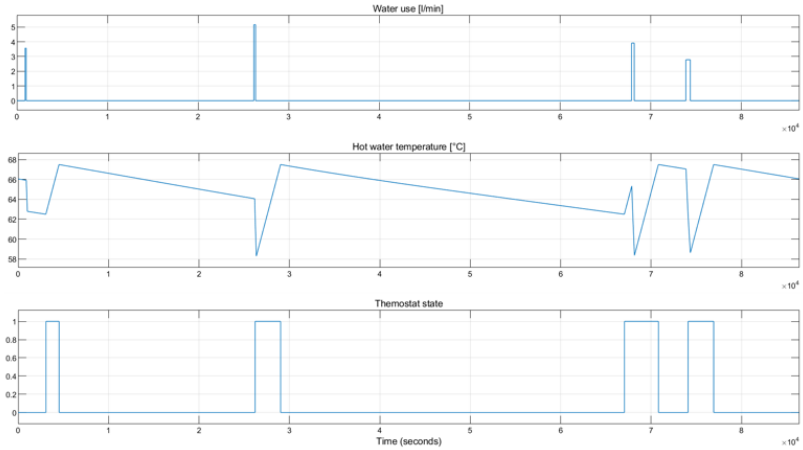

Figure 4.13: Simulation of dynamic behaviour of a single boiler.

A computation problem arises when the aggregate to simulate becomes equivalent to the VQUs defined by the TSO, since the number of devices is such high that is impossible simulate every single unit; Hence, a Monte Carlo approach is used.

Given the boiler technologies (parameters), the simulation scenario (external inputs defined by the month and the climatic zone) and the working conditions (set-point temperature), a one day simulation of N sample boiler is carried out using the Matlab & Simulink model from which the N thermostat states are gathered and the total power consumed is computed:

$$P = P_{tot}^{nom} \sum_{i=1}^{N} \frac{q_i}{N} \tag{4.6}$$

where P_{tot}^{nom} is the nominal power of the considered aggregate. To do this, the number of devices N has to be large enough to return a statistically valid result and small enough to reach acceptable simulation time.

To obtain the power consumption of one of the 15 VQUs defined by the TSO it is requested to simulate the dynamic of sub-aggregates, one for each boiler technologies and for each climatic zone present in the considered VQU. For instance, territory of VQU 10 is divided among 3 climatic zones and each of the 3 technologies has to be considered, thus simulation a total of 9 sub-aggregates is performed and respectively power profiles are summed.

Once that the simulation environment has been validated, a method to evaluate the flexibility of an aggregate has to be developed. As already said, the flexibility of a load represents the ability to vary its power profile, when requested by the TSO with the aim to provide ancillary services, respect to the baseline profile defined as the one realized if the load does not provide any service. Flexibility can be upward if the power generation increases, or if the power consumption decreases for loads, and downward otherwise (load demand increases). It is basically identified by the power variation ΔP that is achievable for the time duration Δt.

The flexibility evaluation method involves the simulation of the same considered aggregate with three different working conditions. In particular,the three scenarios are:

- the baseline working condition is defined by the standard set-point temperature which determine the baseline profile;
- the maximum set-point working condition in which the maximum threshold of the thermostat coincides with the boiler maximum temperature;

- the minimum set-point working condition, with the minimum threshold of the thermostat equal to T_m^0 that is the minimum temperature such that prevent the hot water temperature from being lower than the user desired temperature.

In Table 4.6, the three working conditions are resumed, reminding the standard set-point of $65\,^{\circ}\mathrm{C}$, the boiler parameters and the thermostat dead-band of $\pm\ 2.5\,^{\circ}\mathrm{C}$.

Table 4.6: Operating condition temperature set-points.

Operating condition	T_{max} [°C]	T_{min} [°C]	T_{sp} [°C]
Maximum	75	70	72.5
Baseline	67.5	62.5	65
Minimum	T_m^0+5	T_m^0	T_m^0+2.5

To compute T_m^0, a set of M hot water withdrawal profiles is statistically generated starting from the withdrawal profile already described in Figure 4.2 with a sampling time of a quarter hour. For each quarter hour of the simulation day, distribution of litres of water used is studied and the value of litres of water such that the water consumption is lower than that value with a probability P_d is identified. Assuming the starting condition of boiler temperature equal to T_o^u and applying Equation 4.2 and Equation 4.3 to model the mix of cold and hot water and the boiler dynamic, temperature $T_m^0(q)$ can be computed. Finally, to guarantee the boiler temperature condition, the maximum value of $T_m^0(q)$ is selected. Since T_m^0 depends on boiler parameters and on external temperatures which are related to the month and climatic zone; for this reason T_m^0 has been computed for each month, climatic zone and boiler technology, results are shown in Figure 4.14.

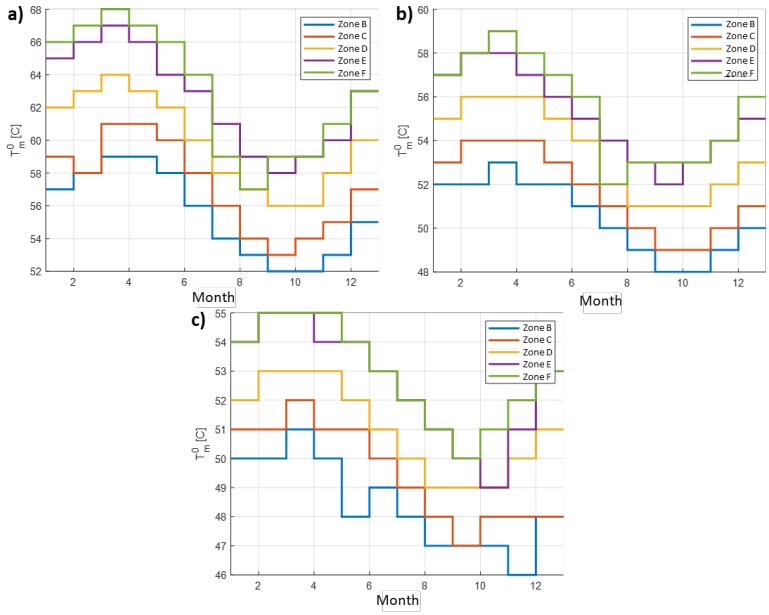

Figure 4.14: Minimum hot water temperature of boilers of a) 50 l, b) 80 l, c) 100 l capacity.

At the end of the three simulations, the three power profiles are gathered and compared: it is easy to say that the operating condition with the maximum set-point will be the one with the largest power consumption as well as the minimum set-point is associated to the lowest power usage. Generally, it is assumed that the boiler can be remotely controlled and the temperature set-point can be changed between the minimum value T_m^0 and the boiler maximum temperature. Hence, the aggregate is able to vary its power demand from the baseline profile towards the maximum profile to provide downward reserve service (increase of load) or towards the minimum profile to provide upward reserve service (decrease of load). In other words, the upward and downward reserves are represented by the difference between the maximum and the minimum profile respect to the baseline profile. For a better representation, power profiles corresponding to the three operating conditions for the VQU 9, related to the area of Sicily during August, are proposed in Figure

4.15, along with the upward and downward reserves in Figure 4.16, computed from the differences between such profiles. In particular, upward reserve is computed from the difference between the baseline profile and the minimum set-point profile and downward reserve is computed from the difference between the maximum set-point profile and baseline profile.

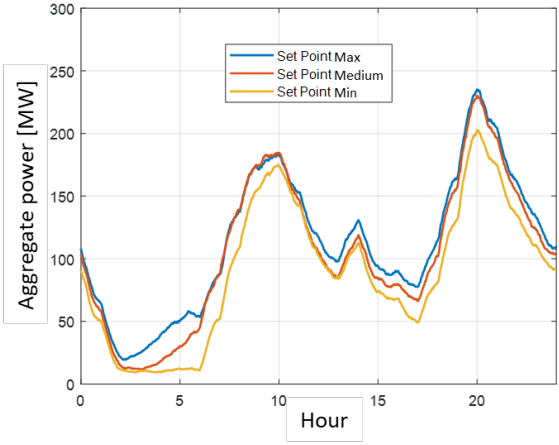

Figure 4.15: Power demand of VQU 9 for each operating condition.

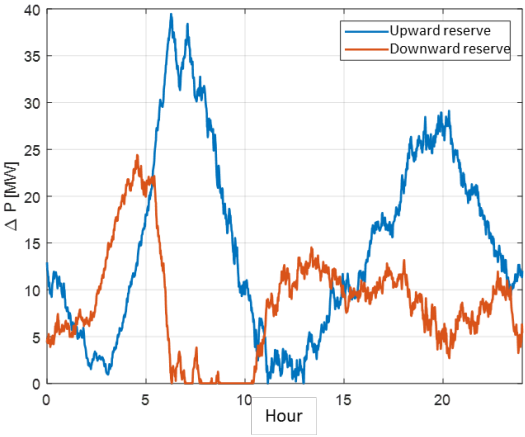

Figure 4.16: Upward and downward power reserve of VQU 9.

Since power reserves depend on time, to identify flexibility, the considered power reserve profile evolution must be analyzed within a time interval Δt to gather the minimum reserve value in such time window to determine the power variation ΔP the aggregate can provide. Flexibility results are collected starting from each quarter hour $q = 1...96$ in the simulation day and considering time windows Δt of $m = 5, 10, 15, 30, 45, 60$ minutes. In general, the quarter hour q and the time duration Δt determine the power variation $\Delta P(q, \Delta t)$. Referring again to VQU 9 during August, example of how upward flexibility results are shown in Figure 4.17 and in Table 4.7.

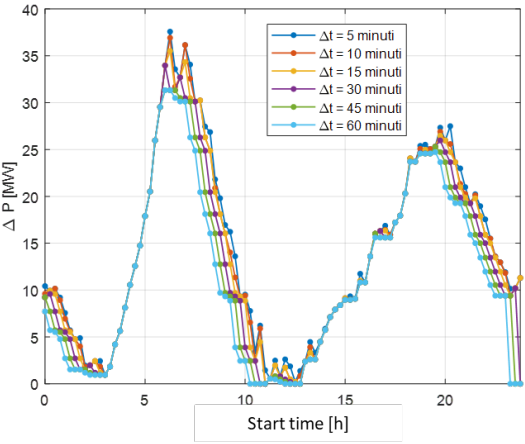

Figure 4.17: Upward flexibility of VQU 9 during August.

Table 4.7: Values of upward flexibility of VQU 9 in August, expressed in MW.

Hour	$\Delta P(:,5)$	$\Delta P(:,10)$	$\Delta P(:,15)$	$\Delta P(:,30)$	$\Delta P(:,45)$	$\Delta P(:,60)$
00:00	10.43	9.61	9.23	9.23	9.23	7.72
00:15	9.93	9.93	9.93	9.58	7.72	5.71
00:30	10.15	10.15	9.58	7.72	5.71	5.52
00:45	9.21	8.92	7.72	5.71	5.52	4.76
...	...	...	...	...	...	...

Now full results of VQU 9 are shown; VQU 9 corresponds to the area of Sicily and have a nominal power of $934.76\,\mathrm{MW}$ (Table 4.1). Power profiles related to the three operating conditions and the consequent power upward and downward power reserve are shown in Figures 4.18 and 4.19, while upward and downward flexibility are given in Figures 4.20 and in Figures 4.21 respectively. Results are given from daily simulation referring to the months of February, May, August and November, one month for each season.

It can be observed that the main factor determining differences between months is the cold water temperature which reaches its peak values between

August and November and the minimum values between February and May (Figure 4.6). This explains why the highest power demand is registered between February and May, with peak values of $300\,\mathrm{MW}$, respect August and November, where the peak value reaches almost $250\,\mathrm{MW}$. Also, the dependency of such profiles with the daily hot water withdrawal distribution is evident, in fact, peak values occur in the morning and in the evening and minimum values occur during the night, when the request is low.

Generally, upward power reserve is larger than downward power reserve and in all months reserves are higher when the load is low, associated to the hours with low hot water demand. On the other hand, when load is high, reserves decrease. Since it is assumed that the end user always requests the hot water desired temperature T_d, the minimum boiler temperature T_m^0 required to achieve the desired hot water temperature T_d increases in cold months, when the external water temperature is low. This results in the decrease of the differences between power profiles, especially in February. Such effect is less evident in August, when external water temperature is higher.

Regarding upward flexibility, power variation profiles are similar with the upward power reserves and reach larger values in August and minimum values in February. Its interesting noting that the shorter is the time window Δt, the larger is the achievable power variation ΔP. Differences by changing the service time duration are relevant during stages of decrease of profiles. On the other hand, during stages of increasing profiles, flexibility does not depend on time duration.

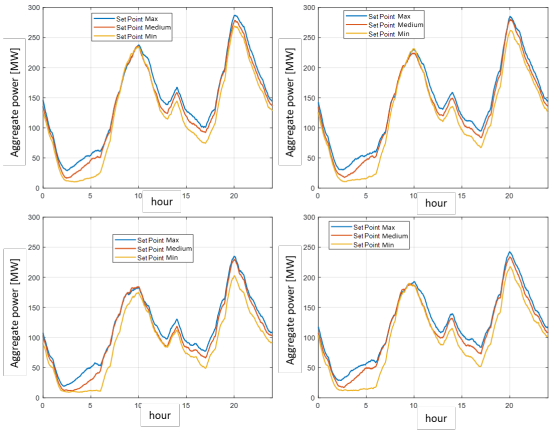

Figure 4.18: Power demand of VQU 9 during February, May, August and November.

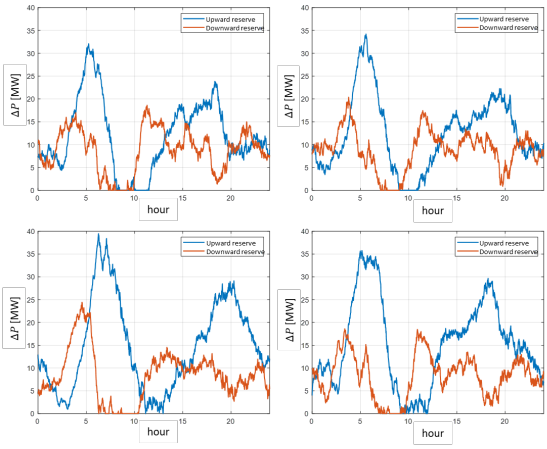

Figure 4.19: Power reserve of VQU 9 during February, May, August and November.

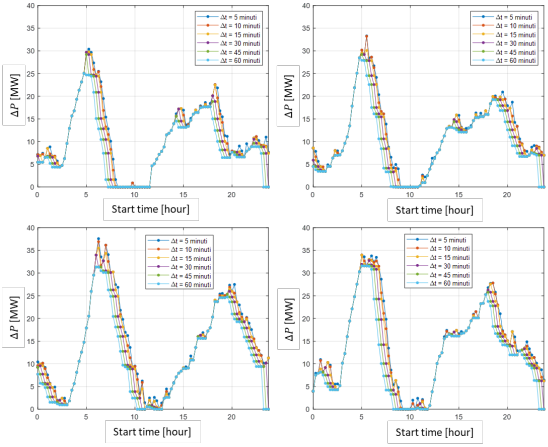

Figure 4.20: Upward flexibility of VQU 9 during February, May, August and November.

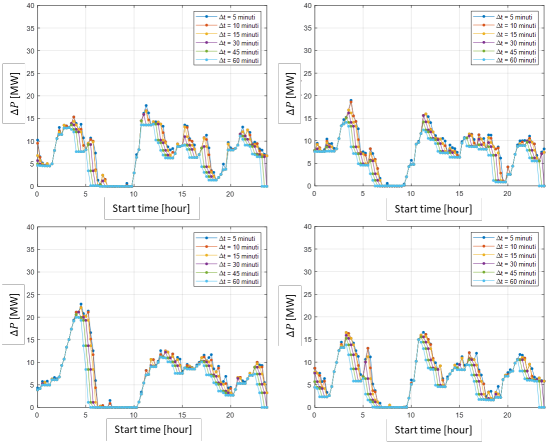

Figure 4.21: Downward flexibility of VQU 9 during February, May, August and November.

Upward flexibility is larger in the early morning (from 5 a.m. to 7 a.m.) and in the late afternoon (from 5 p.m. to 7 p.m.). This happens because from 5 a.m. the hot water demand starts increasing from zero to the morning peak at 9 a.m.. During the first two hours, many EWHs are switched on and become ready to be temporarily deactivated. Such an availability is lowered at the morning demand peak time, since, even if lots of EWHs are switched on, they cannot be easily deactivated because of the high requirement of hot water. A similar behavior occurs when, at 4 p.m., the hot water demand start increasing toward the evening peak at 7 p.m.

Downward flexibility is larger during deep night (from 3 a.m. to 5 a.m.) and during the central daytime hours (around noon). This happens because, from 1 a.m., hot water demand is zero. Thus, after a couple of hours, most of EWHs are switched off and, consequently, they become ready to be activated. A similar scenario occurs around noon: after the morning peak of the hot water demand (9 a.m.), many EWHs recover the temperature set-point and switch off, becoming ready to be activated.

Maximal values of upward flexibility are reached in August with about 35 MW in the morning and about 27 MW in the afternoon. May and November are similar, with peaks of about 33 MW, whereas February is the month with the lower flexibility, especially in the late afternoon. Except for August, in all months, upward flexibility is zero during a time interval from 7 a.m. and 11 a.m..

The maximal value of the downward flexibility is reached in August with about 25 MW in the night, whereas, in the other months, the night and daytime peaks are all at about 20 MW. In all the months, downward flexibility is zero during a time interval from 5 a.m. to 10 a.m.. Excepting for peak values, there are no significant differences among the downward flexibility computed in the four months.

Similar behaviour can be observed in downward flexibility profiles. It is usually lower than upward flexibility and shows lesser differences in the four simulated months.

Same considerations have been carried out for all the VQUs to determine the potential flexibility of all thermal units in Italy. The set of VQUs described in Table 4.1 has a total installed power of $4508.87\,\mathrm{MW}$. Power profiles related to the three operating condition are shown in Figure 4.22, power reserves in Figure 4.23 and upward and downward flexibility in Figures 4.24 and 4.25.

Once again, similar behaviour can be noted:

- power profiles follows the same distribution of the daily hot water withdrawal demand;
- upward power reserve is usually higher than the downward power reserve;
- power reserves are higher during hours with low demand;
- regarding flexibility, the maximum feasible power variation depends on the time duration established for the service, the shorter is Δt, the larger is ΔP: bigger differences are registered during stages of decrease of profiles.

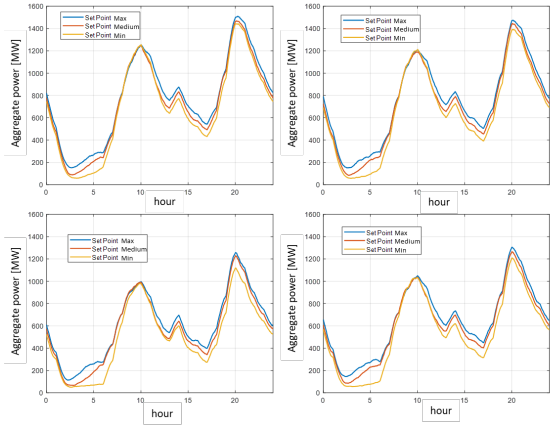

Figure 4.22: Power demand of all VQUs during February, May, August and November.

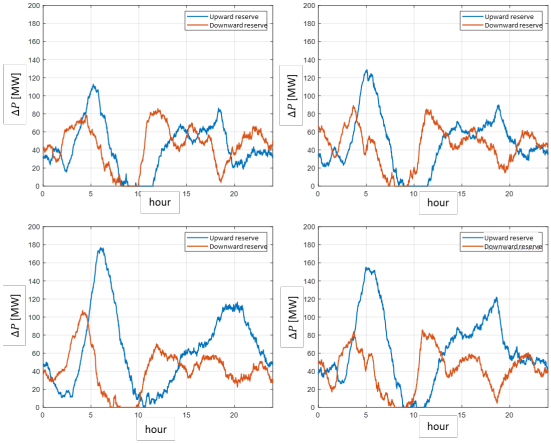

Figure 4.23: Power reserve of all VQUs during February, May, August and November.

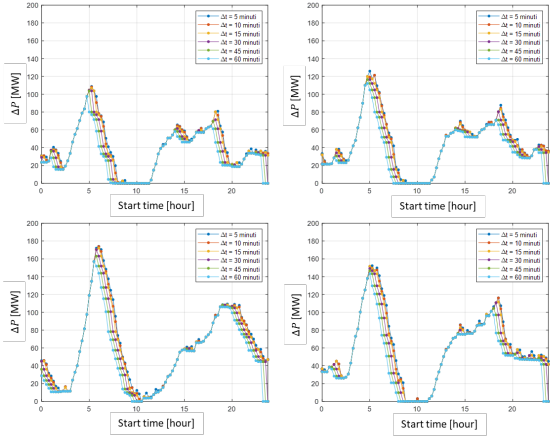

Figure 4.24: Upward flexibility of all VQUs during February, May, August and November.

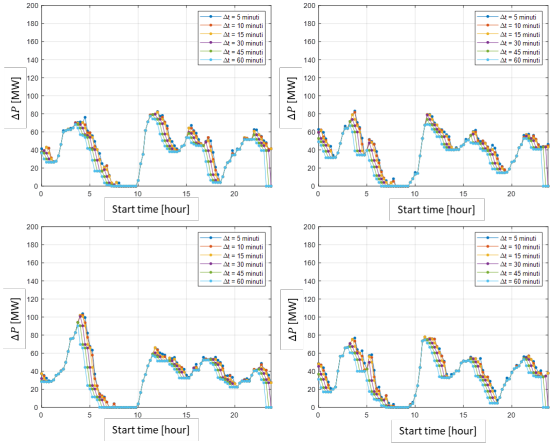

Figure 4.25: Downward flexibility of all VQUs during February, May, August and November.

As for Sicily, except for August, the amount of the downward flexibility is similar in all the considered months, with night and daytime peaks around 80 MW.

The upward flexibility of May and February are similar, with a morning peak of about 100-120 MW and a late afternoon peak of about 80 MW. Differently from Sicily, November flexibility is similar to the one of August, except for the peak value, which in November is lower, about 150 MW against the 170 MW of August.

4.2 Heat pump flexibility

The proposed flexibility evaluation method can be repeated for other thermal units technologies. During the research activity, flexibility capability of heat pump water heaters has been discussed. All the external inputs such as, the environmental temperature and the cold water temperature remain unchanged along with the assumptions made for the distribution of the hot water withdrawal demand. The same VQUs definition by the TSO is applied and their nominal power and territory distribution among the climatic zones is reported in Table 4.8. New predictive data about installed power in each VQU is assumed.

Table 4.8: VQUs power and distribution among climatic zones.

	Power [MW]	Zone B [%]	Zone C [%]	Zone D [%]	Zone E [%]	Zone F [%]
VQU 1	144	0	0	0	100	0
VQU 2	135	0	8	48	23	21
VQU 3	252	0	0	0	100	0
VQU 4	572	0	0	0	100	0
VQU 5	874	0	0	13	84	3
VQU 6	580	0	0	0	100	0
VQU 7	262	23	53	12	12	0
VQU 8	321	0	75	19	6	0
VQU 9	542	85	6	5	3	0
VQU 10	345	0	10	82	8	0
VQU 11	437	0	86	7	8	0
VQU 12	39	0	0	100	0	0
VQU 13	107	0	0	70	30	0
VQU 14	238	0	0	91	9	0
VQU 15	252	0	88	12	0	0
Italy	5100	19.3%	29.2%	26.1%	24.4%	0.9%

The considered heat pump water heater parameters are reported in Table 4.9.

Table 4.9: Heat pump parameters.

Model parameter	Value
Capacity [l]	200
Power [kW]	0.9
Voltage [V]	220-240
Maximum Temperature [°C]	62
Heat loss [kWh/day]	1.2
Maximum Pressure [MPa]	0.6
Weight [kW]	90
Set-point temperature [°C]	55

Moreover, coefficient of performance COP must be defined for heat pump technology and it is reported in Figure 4.26 according to the device data sheet. COP is expressed as a function of the temperature outside the building T_a, hence it is not affected by the heating or cooling systems which affect only the temperature inside the building T_e.

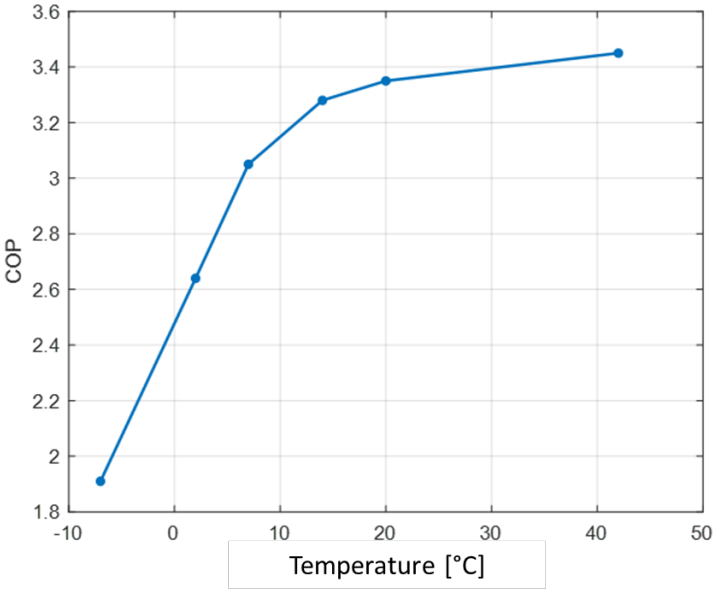

Figure 4.26: Heat pump coefficient of performance.

Also the water heater model must be modified respect to the one adopter for boiler technology.

$$\dot{T} = -\frac{1}{RS_wV\rho}(T-T_e) - \frac{w}{60 \cdot V}(T-T_o) + \frac{1}{S_wV\rho}qP^{nom} \cdot COP(T_a) \quad (4.7)$$

For the flexibility evaluation, the three operating conditions are identified in Table 4.10, according to the technology.parameter.

Table 4.10: Heat pump operating conditions.

Operating condition	T_{max} [°C]	T_{min} [°C]	T_{sp} [°C]
Maximum	62	59.5	57
Baseline	57.5	52.5	55
Minimum	T_m^0+5	T_m^0	T_m^0+2.5

The minimum set-point temperature T_m^0 computation process is the same explained before for the first set of simulations and reaches values included between 43 °C and 48 °C which are significantly lower than the case with boilers (Figure 4.27). Its worth reminding that this technology has a capacity of 200 l, way higher than the capacity of the considered boiler technologies.

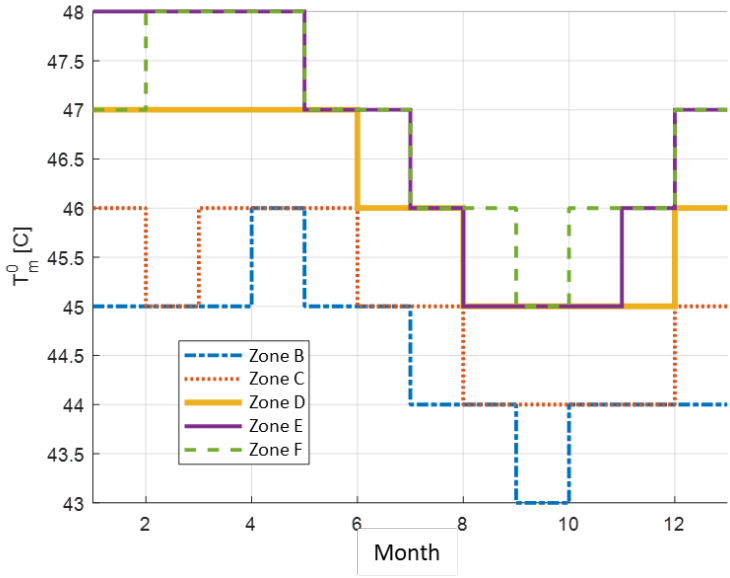

Figure 4.27: Withdrawal profiles example.

Results, again regarding VQU 9 and the whole Italy, are proposed and compared to the outcome of the simulations with boilers. It is reminded that VQU 9 corresponds to the area of Sicily with and a total installed power of $542\,\mathrm{MW}$ (Table 4.8). Power profiles of VQU 9 related to the three identified operating conditions are shown in Figures 4.28.

It can be observed that the peak power demand occurs during February with a maximum value of $80\,\mathrm{MW}$ and the minimum value is registered in August with $60\,\mathrm{MW}$. Such phenomenon can be explained by the different cold water temperature and the different environmental temperature which have impact on the COP. It can be said again that the profiles have the same distribution of the daily hot water withdrawal profile, with peaks during the morning and the evening and minimum values during night. Comparing the two technologies, similar behaviour can be highlighted. Larger values respect to the VQU nominal power can be noted for boilers ($300\,\mathrm{MW} = 32\%P_{nom}$) respect to heat pumps ($80\,\mathrm{MW} = 15\%P_{nom}$) because of the higher efficiency of the devices with COP. Upward and downward power reserves are shown in Figures 4.29.

In February and May, upward and downward reserves have averagely the same magnitude, but different distribution; in August and September upward reserve is usually larger than the downward reserve. However, heat pumps reserves magnitude is significantly lower than boilers reserves. Such reduction is determined by the reduced distance between operating conditions set-points in heat pumps which have a nominal temperature of $62\,^{\circ}\mathrm{C}$ against the $75\,^{\circ}\mathrm{C}$ of boilers. Also, due the high capacity in heat pumps, the standard set-point temperature is equal to $55\,^{\circ}\mathrm{C}$ against the $65\,^{\circ}\mathrm{C}$ of the boilers. Such aspect can be improved by the activation of boost resistance that let reach higher temperatures than the nominal value up to a $75\,^{\circ}\mathrm{C}$ for heat pumps too. Their application would lead to an increase of the downward flexibility, but at the cost of a higher power consumption.

In Figures 4.30 and 4.31 upward and downward flexibility are given. As for boilers, the dependency of power variation and time duration is evident during stages of decrease of profiles, on the contrary, it is negligible during stages of increase of profiles. Also, higher power variations can be provided within shorter time windows.

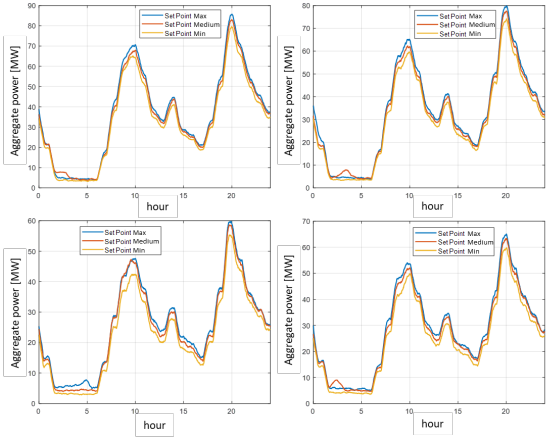

Figure 4.28: Power demand of VQU 9 during February, May, August, November.

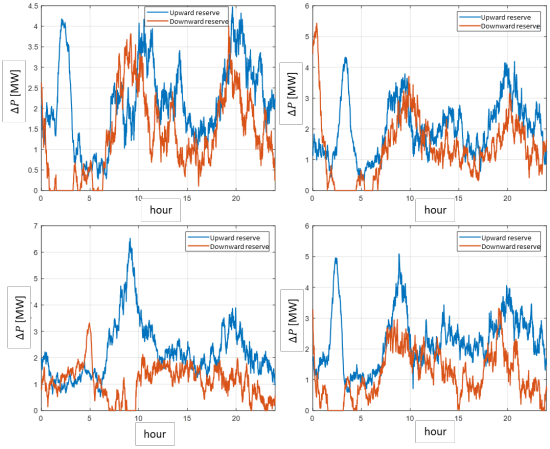

Figure 4.29: Upward and downward power reserves of VQU 9 during February, May, August and November.

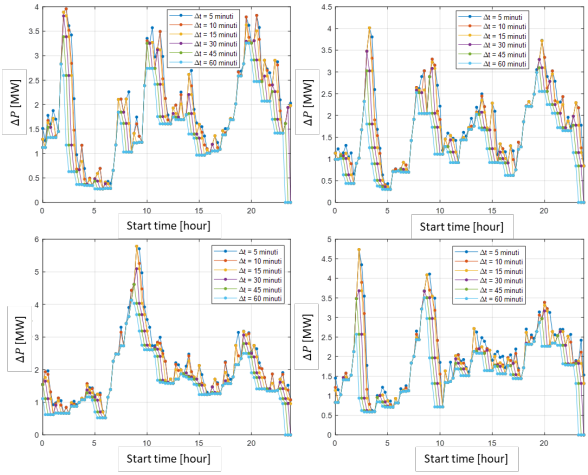

Figure 4.30: Upward flexibility of VQU 9 during February, May, August and November.

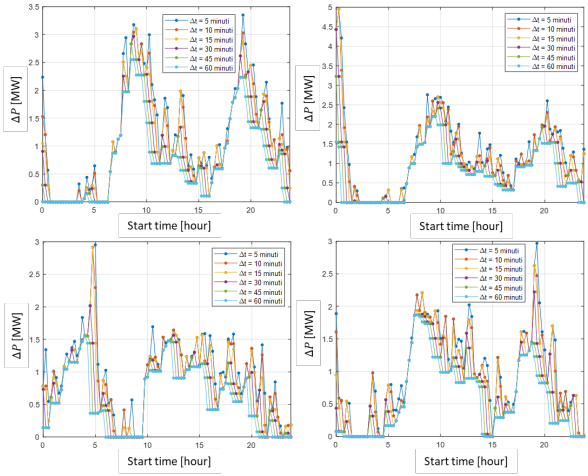

Figure 4.31: Downward flexibility of VQU 9 during February, May, August and November.

Upward flexibility is larger in the early morning (around 3 a.m. and from 8 a.m. to 10 a.m.) and in the evening (around 8 p.m.). This happens because from 5 a.m. the hot water demand starts increasing from zero to the morning peak at 9 a.m. In August the dynamic is quite different with respect to the other months, since of the external air and cold water temperatures are significantly higher.

Downward flexibility is larger during the morning (from 7 a.m. to 10 a.m.) and during the evening (around 20 p.m.). In all months except August there is an interval during night when downward flexibility is low.

Maximal values of upward flexibility are reached in August with almost 6 MW in the morning and about 3 MW in the afternoon. February, May and November are similar, with peaks of about 4 MW.

The maximal value of the downward flexibility is reached in May with about 5 MW in the midnight, whereas, in the other months, the night and daytime peaks are all at about 3 MW. In all the months, except for August, downward flexibility is zero between midnight and 5 a.m.

Finally, the same set of simulations is repeated for the aggregate of all VQUs to represent Italy, with a total power of $5100\,\mathrm{MW}$ (Table 4.8):

- in Figure 4.32 the power profiles related to the three operating conditions are given;
- Figure 4.33 shows the upward and downward power reserves;
- upward flexibility is shown in Figures 4.34;
- downward flexibility is shown in Figures 4.35.

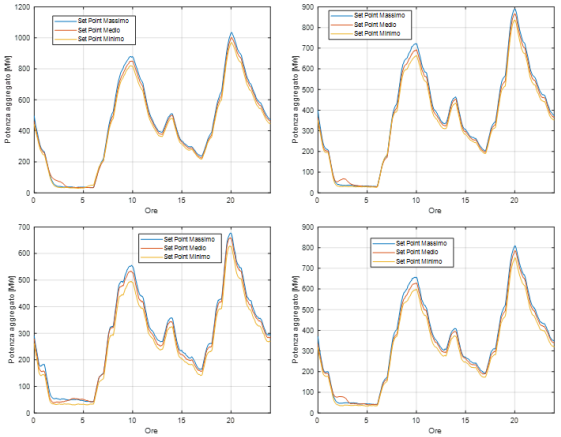

Figure 4.32: Power demand in all three operating conditions of all VQUs during February, May, August and November.

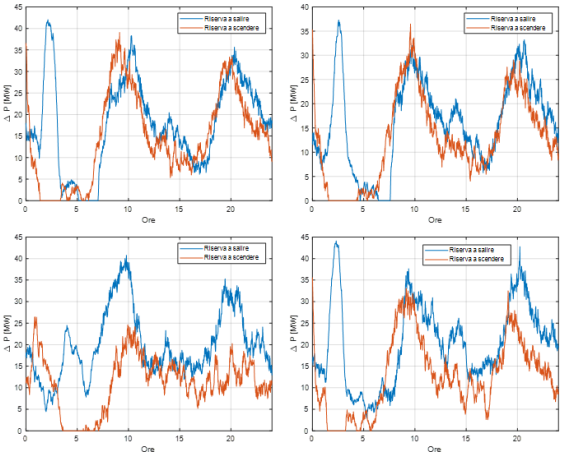

Figure 4.33: Power reserve of all VQUs during February, May, August and November.

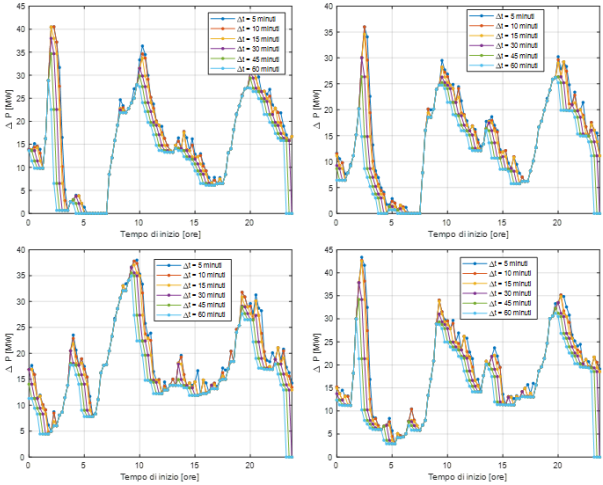

Figure 4.34: Upward flexibility of all VQUs during February, May, August and November.

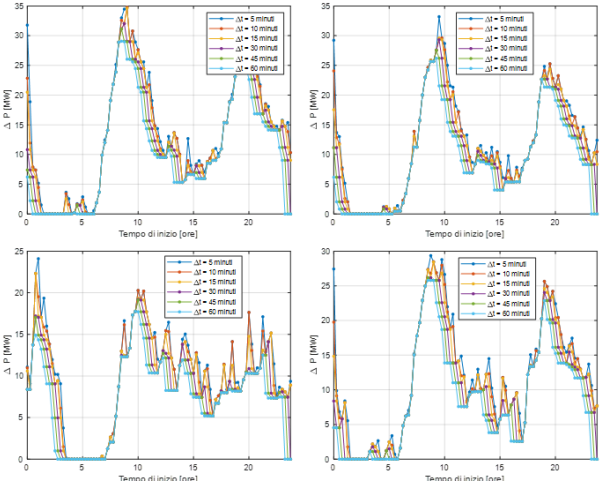

Figure 4.35: Downward flexibility of all VQUs during February, May, August and November.

As for Sicily, the amount of the downward flexibility is similar in all the considered months, except for August, with night and daytime peaks of about 25 MW and the shifting of the interval with low flexibility. The upward flexibility of February, May and November are similar, with a morning peak of about 40 MW and a late afternoon peak of about 30 MW. Differently from Sicily, the peak value is not reached in August, but in November and the flexibility profiles of the considered months are more similar to each other.

4.3 Final considerations

Overall, the flexibility achievable by heat pumps is small compared to the installed capacity, and quite smaller than the flexibility achievable by EWHs due to the lower operating temperatures. In fact, for both, Sicily and all Italy peak values of upward and downward flexibility from EWHs are 4% and 2% of installed power, respectively, while they are lower than 1% in the case of heat pumps.

The developed methodology manages to identify the potential capability of an aggregate of thermal loads to vary its power consumption from a baseline profile, for a given time extension. This process gives information about how load can support the grid through service provision.

CHAPTER 5

Fast frequency reserve needs and proposed solutions

In the context of pilot projects promoted by the TSO, the research activity includes studies about service provision from RESs and BESSs.

Studies focus on RESs providing the Fast Reserve Service (FRS), defined in [57], introduced by the TSOs in many countries, especially in North America and Europe [75]. The FRS shall contribute improving the dynamic response of the system in the time instants immediately after events that lead to frequency transients.

Such service is meant to replace the beneficial effect of inertia from the traditional generating units which is progressively decreasing because of the implementation of RESs units in the power system. The decrease of inertia leads to more significant frequency variations after fault events that must be solved within extremely high speed actions, even faster than primary frequency regulation service.

Many review papers state that inertia and FRS can be provided from WTs [75–78]. As far as upward regulation is concerned, a fast contribution can be provided for a short duration just relying on the kinetic energy of the rotor [79–81]. TO meet the duration requirements of FRS (typically 15 minutes [82, 83]), WTs need to operate not generating the maximum power. This approach is adopted in [84–87] by controlling the rotor speed, in [88, 89] by controlling the pitch angle and in [90, 91] by combining the two control methods.

Therefore, many papers such as [86, 92–94], proposes control strategies to coordinate the response of different WTs in a Wind Farm (WF) which may have different size and different wind conditions.

Also, the WF can be coupled with a BESS that takes charge of the regulation service provision. BESSs are particular suited for FRS provision [95–97] and can meet the duration requirement of the service. Many approaches to schedule the operation of BESSs integrated with a WF to deliver FRS are provided [98–100].

The FRS is characterized by full activation time such that it can be implemented to overcome this issue and can operate coordinately with primary frequency regulation to guarantee the system safety. Units that can provide FRS can be stand-alone units or aggregates of devices, namely Fast Reserve Units (FRUs), and must meet the requirements stated in the following, according o the pilot project framework [57]:

- Qualified power between $5\,\mathrm{MW}$ and $25\,\mathrm{MW}$;
- possibility to provide continuously power proportional to the frequency deviation from the nominal value with activation within one second from the event that activated the service;
- without additional frequency errors, ability to keep the power signal as described in the previous point for 30 seconds; after that time the FRU must decrease the power output until the power variation for the FRS is zero in a time interval of 300 seconds;
- possibility to provide power variation equal to the qualified power, upward or downward, for at least 15 minutes every two hours;

- ability to keep connection with the power grid independently from the operating condition, even in case of emergency, if voltage level at the point of connection is:

$$\begin{cases} 85\%V_n < V < 115\%V_n & \text{if } V_n \leq 150kV \\ 85\%V_n < V < 110\%V_n & \text{if } V_n > 150kV \end{cases}$$

  and if frequency value is between $47.5\,\text{Hz} \leq f \leq 51.5\,\text{Hz}$;

- tolerance of 1% of qualified power of the power output realized respect to the expected one after 1 second from the event that led to the service activation.

In Figure 5.1, the expected power output as defined in [57] is shown.

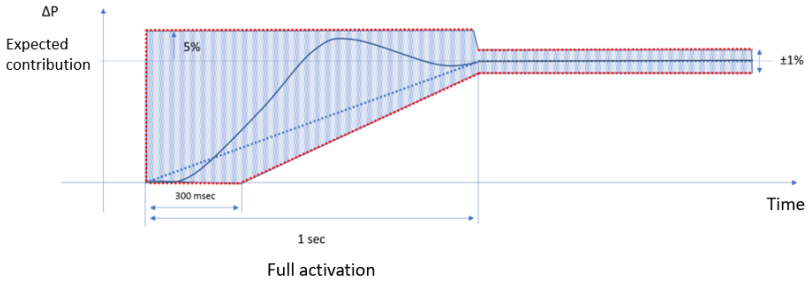

Figure 5.1: Definition of FRS tolerance.

Moreover, it is necessary that FRUs with limited energy capacity devices, such as BESSs, include energy management strategies to help the FRU satisfy the technical constraints.

The FRU power output basically depends on the frequency deviation from the nominal value. To define the service activation conditions, two frequency error thresholds, equal to $0.05\,\text{Hz}$ and $0.2\,\text{Hz}$, are set up. Below the first threshold the frequency is within a tolerable band and the service is not activated, hence the FRU only manages capacity of BESSs if present.

Once the frequency error exceeds the first threshold, the service is activated and the FRU is requested to provide a power output proportional to the frequency error within 1 second. In this stage, a clock of 30 seconds begins and after that the FRU will decrease the power variation linearly as already specified. If not completed, the clock shall interrupt if the frequency error exceeds the second threshold. In such condition, the FRU must provide the qualified power for a maximum time interval of 15 minutes or until the frequency error falls below the second threshold; after that the 30 seconds clock starts again.

Once the emergency has been solved, the FRU has a timeout interval of 200 seconds to replenish the power reserve before the FRS is activated again. Only in the case where the frequency error subsequent the new event is inverted respect to the previous error, the timeout interval is not provided and the service can be immediately activated again. For a better representation, the service activation is expressed in Figure 5.2.

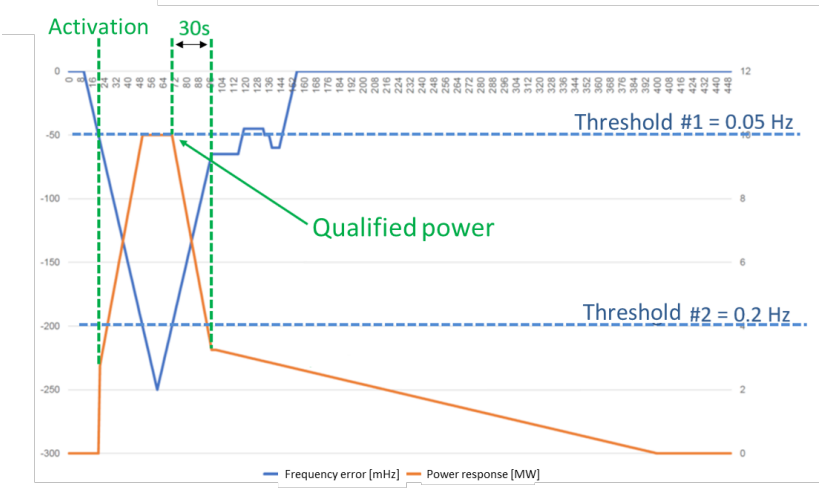

Figure 5.2: Definition of FRS activation.

The method adopted to have the simulated FRU perform the power output with such specifications is based on MPC [101]. It consist of solving an optimization problem to compute optimal values of controllable variables to

pursue the desired trajectory of the system model. The cost function to be minimized is associated to the error between the desired value of the model output and the real one (Figure 5.3).

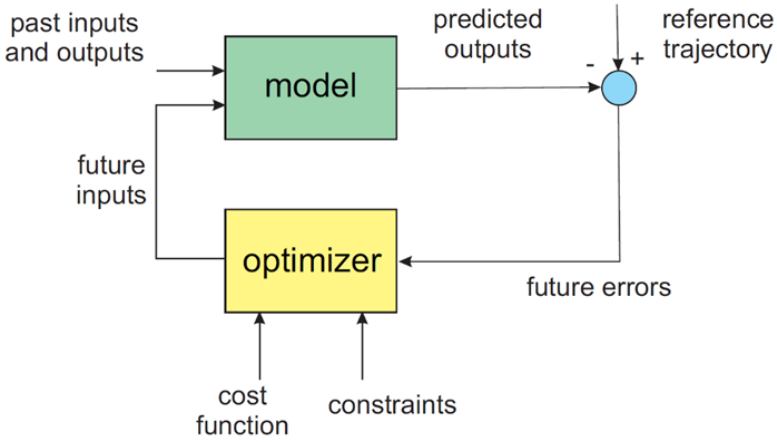

Figure 5.3: Withdrawal profiles example.

Benefits of adopting a MPC-based approach is its versatility and the possibility of dealing with non linear models, however, it requires a strong computation effort for solving the optimization problem and a complex model to have accurate results, since the MPC approach can lead to wrong conclusions if the model disagrees with the real process. In light of this, the model must be appropriately complete to avoid errors, but also sufficiently simple to solve the optimization problem within feasible computation time.

Usually, models are non-linear and continuous and, for such reason, they are difficult to understand. It is convenient to approximate the model in order to treat the model as linear in a limited range of state variables. Also, the model typically has technical constraints regarding controllable variables, that just need to be kept within the tolerable limits, and output variables, which must meet with the constraints for safety reasons. A linear and discrete time model, along with constraints, is expressed as:

$$\begin{cases} \dot{x}(t+1) = Ax(t) + Bu(t) \\ y(t) = Cx(t) + Dx(t) \end{cases} \tag{5.1}$$

$$s.t. \begin{cases} u_{min} < u(t) < u_{max} \\ y_{min} < y(t) < y_{max} \end{cases} \tag{5.2}$$

where:

- $x \in \Re^n$ is the state vector;
- $u \in \Re^m$ is the controllable variables vector;
- $y \in \Re^p$ is the output variables vector;
- t identifies the time instant;
- $A \in \Re^{n \times n}$, $B \in \Re^{n \times m}$, $C \in \Re^{p \times n}$, $D \in \Re^{p \times m}$ are matrices the describe the model; u_{min} and u_{max} are minimum and maximum controllable variables values; y_{min} and $y_{min}$are minimum and maximum controllable variables values.

Such limitations must be considered while minimizing the cost function, which is expressed considering only the time window of N time instants, namely the horizon, following the actual time instant as a function of the input, output and state variables.

$$\min_{u_t,\ldots,u_{t+N-1}} \sum_{k=0}^{N-1} h(x_{t+K}, u_{t+K}, y_{t+K}) \tag{5.3}$$

The MPC approach consist in solving the described optimization problem within the selected horizon to compute the optimal values for the input variables in the following N instants. After that, only the control action related to the first time instant is applied. Successively, at time instant $t+1$ the model output is measured and the optimization problem is repeated within a shifted time window, always including N time instants.

Several MPC-based approaches have been developed to provide ancillary services with not traditional generating units such as load frequency control [102], frequency regulation [60, 81] and synthetic inertia [103].

5.1 Service provision from BESS

The objective of the study is to develop a process for the FRS provision, as described by the pilot project [57], through a FRU made of a group of BESS. The dynamic of the SoC of the i-th battery is given by:

$$S\dot{O}C = -\frac{\eta_i}{E_{b,i} \cdot 36} P_{b,i} \tag{5.4}$$

where

- i is the BESS index;
- $P_{b,i}$ is power exchanged with the BESS (if positive, the battery is discharging, if negative, the battery is charging) [MW];
- E_b represent the BESS capacity [MWh];
- η_i is the charging (η_i^{ch}) or discharging (η_i^{dsc}) efficiency, defined as:

$$\eta_i = \begin{cases} \eta_i^{ch} & \text{if } P_{b,i} \leq 0 \\ \eta_i^{dsc} & \text{if } P_{b,i} \geq 0 \end{cases} \tag{5.5}$$

By making the dynamic equation 5.4 discrete time and taking account of equation 5.5, we obtain that:

$$SOC_i(t+1) = SOC_i(t) - \frac{\Delta}{36 \cdot E_{b,i}} \left(\eta_i^{ch} P_{b,i}^{ch}(t) + \eta_i^{dsc} P_{b,i}^{dsc}(t) \right) \tag{5.6}$$

with Δ, expressed in seconds, being the sampling time and $P_{b,i}^{ch}$ and $P_{b,i}^{dsc}$ the power exchanged during the charging and discharging of the BESS.

Through the MPC-based approach, given the BESS model and an assumption of the initial state of the system, an optimization problem is solved at each time instant to achieve the desired power output from the FRU. The cost function is defined depending on which of the stages, defined as reported below, of the service is active.

- Stage 1: the frequency error is below the first threshold of $0.05\,\mathrm{Hz}$, hence the system is only requested to reach the ideal conditions to face

the next event; in this case, the optimal condition of BESSs to provide both upward and downward service is to keep the SoC equal to 50% of nominal capacity.

- Stage 2: the frequency error exceeds the first threshold, the FRS activates; the FRU has to provide power proportional to the frequency error if it is below the second threshold of $0.2\,\mathrm{Hz}$ or equal to the qualified power otherwise;
- Stage 3: at the end of the service, the FRU is requested to linearly decrease the power output to the set-point it had before the activation event in a selected time interval as already specified.

Its worth noting that the MPC approach appears useless if the FRU would be made of only one BESS, but it becomes convenient when there are more devices to manage.

In light of this, for each Stage the function cost and the system constraints need to be defined.

During Stage 1 the FRS is not active and the FRU has only the task to manage the N BESSs energy capacity; thus, the quantity to minimize is the SoC deviation from the optimal value of 50%.

$$\min_{P_{b,i}(j)} \sum_{i=1}^{N} \left[\left(\sum_{j=k}^{k+T-1} w_{s,i}(SOC_i(j) - SOC_i^*)^2 + w_{p,i}(\Delta P_{b,i}(j))^2) \right) + \right.$$
$$\left. + \; w_{f,i}(SOC_i(k+T) - SOC_i^*)^2 \right] \tag{5.7}$$

where:

- SOC_i^* is the desired SoC, that is 50%;
- $\Delta P_{b,i}(j) = P_{b,i}(j) - P_{b,i}(j-1)$
- T is the number of sampling times that represent the horizon;
- $w_{s,i}$, $w_{p,i}$ and $w_{f,i}$ are weights used to give priority to the quantities included in the cost function: since the main goal in Stage 1 refers to SoC, $w_{s,i}$ and $w_{f,i}$ will be higher than $w_{p,i}$.

To understand better, the terms included in the cost function are explained. All elements are quantities to be minimized during the optimization problem. The first element is the distance of SoC from the desired value and represent the main target of the optimization; the second is the power variation between two consequent time instants and is introduced to reduce stress on BESSs; the last element refers to SoC again, but only concern the time instant at the end of the horizon of duration T.

Along with the cost function, constraints are defined. First of all, the BESS dynamic equation 5.6 must be satisfied. Other constraints of the BESSs are reported below and include power limits, SoC limits and power variation limits.

$$s.t. \begin{cases} -P_{b,i}^{max} \leq P_{b,i}(j) \leq P_{b,i}^{max} & \forall i = 1:N, j = k:k+T-1 \\ SOC_i^{min} \leq SOC_i(j) \leq SOC_i^{max} & \forall i = 1:N, j = k:k+T-1 \\ |\Delta P_{b,i}(j) - P_{b,i}(j-1)| \leq \Delta P_{b,i}^{max} & \forall i = 1:N, j = k:k+T-1 \end{cases} \tag{5.8}$$

Also constraints of the whole system, concerning the total FRU power output and power variation, are considered.

$$s.t. \begin{cases} P_{FRU}(j) = \sum_{i=1}^{N} P_{b,i}(j) & \forall j = k:k+T-1 \\ -P_{FRU}^{max} \leq P_{FRU}(j) \leq P_{FRU}^{max} & \forall j = k:k+T-1 \\ |\Delta P_{FRU}(j) - P_{FRU}(j-1)| \leq \Delta P_{FRU}^{max} & \forall j = k:k+T-1 \end{cases} \tag{5.9}$$

In Table 5.1, all parameters defined in Stage 1 are collected. MPC optimization has been implemented using the AMPL [104] language and solved by IBM CPLEX solver.

Table 5.1: Stage 1 MPC parameters.

Quantity	Parameter	Value
General		
Sampling time	$\Delta[s]$	60
Horizon	T [-]	10
Single BESS		
SoC weight	$w_{s,i}$	$\frac{10^3}{100^2}$
power variation weight	$w_{p,i}$	$\frac{1}{P_{b,i}^{max}}^2$
final SoC weight	$w_{f,i}$	$\frac{10^3}{100^2}$
desired SoC	SOC_i^* [%]	50
max power	$P_{b,i}^{max}$	$P_{b,i}^{nom}$
max power variation	$\Delta P_{b,i}^{max}$	$2P_{b,i}^{max}$
FRU		
max power	P_{FRU}^{max}	$\min(P_{FRU}^{nom} - P_Q, 0.25P_Q)$
max power variation	ΔP_{FRU}^{max}	$2P_{FRU}^{max}$

The parameter P_{FRU}^{nom} is defined as the maximum power that the BESSs can provide; usually $P_{FRU}^{nom} = \sum P_{b,i}^{nom}$. The value of the parameter P_{FRU}^{max}, with P_Q being the qualified power, is given by the FRS specifications. In fact, the FRU is requested to vary its power profile by a maximum power of P_Q and to perform the SoC management keeping a power variation not larger than 25% of P_Q from the baseline profile.

In Stage 2, when the FRS is activated by an event that led to frequency error beyond the fixed threshold, the FRU is requested to provide an addition power contribution proportional to that frequency error. Hence, the FRU desired power output is computed according to the FRS specifications as follows:

$$P_{FRU}^* = P_{FRU}^{pre.act} + \begin{cases} -P_Q \frac{\Delta f(k) - th_1}{th_2 - th_1} & \text{if } |\Delta f(k)| < th_2 \\ -P_Q \cdot sign(\Delta f(k)) & \text{if } |\Delta f(k)| > th_2 \end{cases} \tag{5.10}$$

$P_{FRU}^{pre.act}$ is the power exchanged by the FRU at the instant of FRS activation, in the transition from Stage 1 to Stage 2. The desired power profile

P^*_{FRU} can't be computed at the beginning of the event since the frequency error is not available to be measured expect for the actua time instant. Thus, it is assumed that such profile is constant for the duration of the horizon.

$$P^*_{FRU}(j) = P^*_{FRU}(k) \forall j = k : k + T - 1 \tag{5.11}$$

This hypothesis introduces a computation error that can be corrected by the MPC closed loop; in fact, the desired power output profile is updated at each time step.

The cost function is here defined:

$$\min_{\alpha_i(j)} \sum_{i=1}^{N} \left[\left(\sum_{j=k}^{k+T-1} w_{s,i}(SOC_i(j) - SOC^*_i)^2 + w_{p,i}(\Delta P_{b,i}(j))^2) \right) + \right.$$
$$\left. + \; w_{f,i}(SOC_i(k+T) - SOC^*_i)^2 \right] \tag{5.12}$$

In this case, optimal values of the service contribution allocation coefficient $\alpha_i(k)$ are sought. During researches, this method showed better performances respect to directly computing the BESSs power set-points 5.7. Once, again, constraints are given by the BESS dynamic equation 5.6, BESSs limits (Equation 5.8) and FRU limits (Equation 5.9) to which should be added the following:

$$s.t. \begin{cases} P_{b,i}(j) = \alpha_i(j) P^*_{FRU}(j) & \forall i = 1 : N, j = k : k + T - 1 \\ -1 \leq \alpha_i(j) \leq 1 & \forall i = 1 : N, j = k : k + T - 1 \\ 1 - \frac{tol}{100} \leq \sum_{i=1}^{N} \alpha_i(j) \leq 1 + \frac{tol}{100} & \forall i = 1 : N, j = k : k + T - 1 \end{cases} \tag{5.13}$$

The last constraint introduces the required tolerance during the following of the desired power profile.

In Table 5.2, all parameters defined in Stage 2 are collected.

Table 5.2: Stage 2 MPC parameters.

Quantity	Parameter	Value
General		
Sampling time	$\Delta[s]$	1
Horizon	T [-]	30
Single BESS		
SoC weight	$w_{s,i}$	$\frac{1}{100^2}$
power variation weight	$w_{p,i}$	$\frac{1}{P_{b,i}^{max}}^2$
final SoC weight	$w_{f,i}$	$\frac{1}{100^2}$
desired SoC	SOC_i^* [%]	50
max power	$P_{b,i}^{max}$	$P_{b,i}^{nom}$
max power variation	$\Delta P_{b,i}^{max}$	$2P_{b,i}^{max}$
FRU		
max power	P_{FRU}^{max}	$\sum_{i=1}^{N} P_{b,i}^{max}$
max power variation	ΔP_{FRU}^{max}	$2P_{FRU}^{max}$
tolerance	$tol[\%]$	0.5

In Stage 3, when the FRU is to be brought back to the value before the service activation ($P_{FRU}^{pre.act}$), cost function and constraints are the same used in Stage 2, but with a different definition of the desired power profile P_{FRU}^*.

$$P_{FRU}^*(k) = P_{FRU}^*(k-1) + \alpha^* \quad \forall t = k : k+T-1 \tag{5.14}$$

where:

- $\alpha^* = -\frac{P_{FRU}^*(k_d) - P_{FRU}^{pre.act}}{T_{der}}$
- k_d is the time instant of the transition from Stage 2 to Stage 3;
- T_{der} is the fixed duration of Stage 3.

Now that the profile P^*_{FRU} does not depend on the frequency error any more, it can be computed in advance. Parameter values remain unchanged from Stage 2 and are those reported in Table 5.2. To validate the proposed method, a FRU made of two batteries whose parameters are reported in Table 5.3 has been tested.

Table 5.3: BESSs parameters.

Quantity	Parameter	BESS 1	BESS 2
Capacity	$E_{b,i}$ [MWh]	2	2
Nominal power	$P^{max}_{b,i}$ [MW]	3	3
Charging performance	η^{ch}_i	0.9116	0.9207
Discharging performance	η^{dsc}_i	0.9582	0.9582
Maximum SoC	$SOC^{max}_i[\%]$	90	90
Minimum SoC	$SOC^{min}_i[\%]$	10	10

As a result, the whole system has a total energy capacity of $E^{tot}_b = 4\,\mathrm{MWh}$ and a nominal power P^{max}_{FRU} $6\,\mathrm{MW}$ while the qualified power P_Q has been set equal to $5\,\mathrm{MW}$. Consequently, the FRU may modify the power profile to manage the BESSs energy capacity during Stage 1 within a $\pm\,1\,\mathrm{MW}$ band.

Assuming that the FRU service contribution is negligible respect to the installed power in the network where the FRU is connected, a test profile (Figure 5.4) and a plausible profile (Figure 5.5) for frequency error are given as an input to the MPC-based approach.

In both Figure 5.4 and Figure 5.5, the control mode is shown to give evidence of the successfully definition of Stages 1, 2 and 3. This is clearly visible in the test frequency error profile where the service is activated when the first event occurs and, after 30 seconds, Stage 3 begins and lasts 300 seconds; the second event is ignored because it occurs by the end of the timeout interval and has the same direction of the former event. Finally, the service activates again when the frequency error changes sign; in this case, Stage 2 is kept for more than 30 seconds because the frequency error exceeds the second threshold and only when the frequency falls below that threshold, the FRU enters in Stage 3.

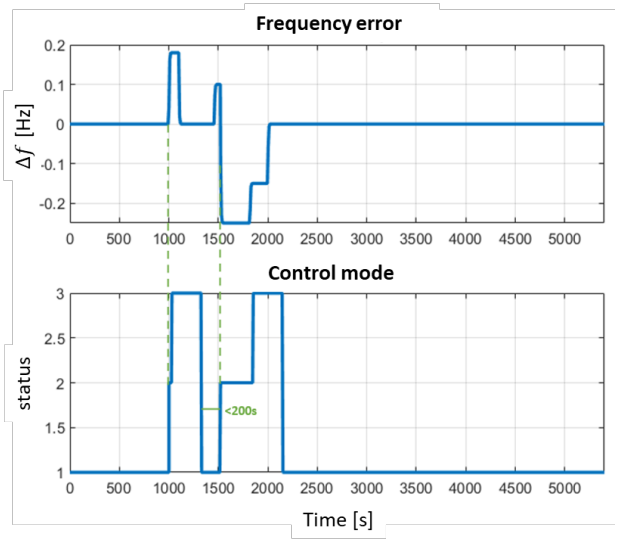

Figure 5.4: Test frequency profile.

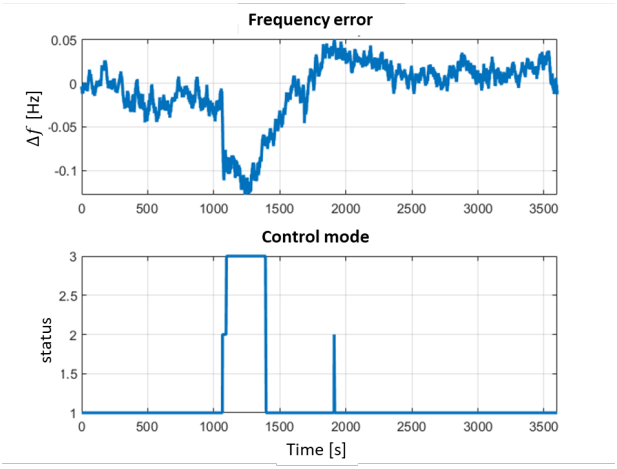

Figure 5.5: Real frequency profile.

During simulations, the FRU power profile, along with the desired power profile P^*_{FRU}, and the SoCs of the two batteries are gathered; moreover, the initial conditions of SoCs are set equal to 40% and 60 % to give evidence of the energy capacity managing process. Figure 5.6 and Figure 5.7 show results of the simulation carried out with the test profile.

During Stage 1, at the beginning of the simulation and after the event that causes the FRS activation, power set-points far from zero are sent to the BESSs to manage their SoC. As expected, in fact, the two batteries are brought to the ideal condition of SoC equal to 50% independently from their initial condition. After the event, both of them enter in charging mode to restore the SoC without changing the power profile of more than $1\,\mathrm{MW}$ from the baseline profile, plotted in red in 5.6. During Stages 2 and 3, the desired power profile is computed and successfully followed by the real power exchanged by the FRU.

Equivalent results regarding the plausible frequency error profile are shown in Figure 5.8 and Figure 5.9 and the same conclusion can be stated.

After simulation tests, it has been proved that the research of optimal service contribution allocation coefficients $\alpha_i(k)$ (Version 2) leads to better performances than the direct computation of BESSs power set-points (Version 1); evidence of this is given in Figures 5.10 and 5.11.

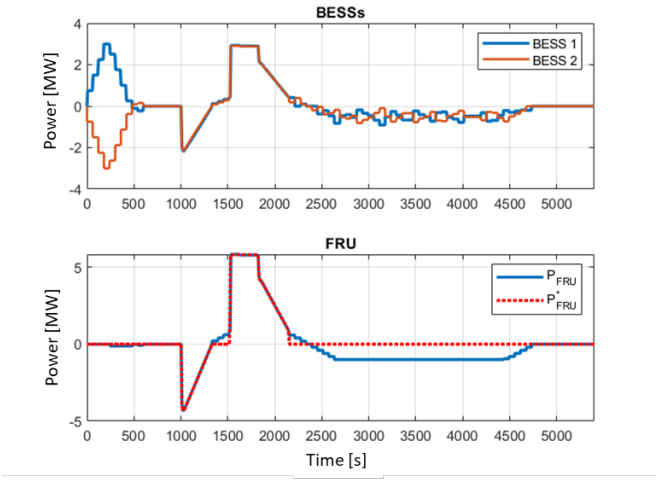

Figure 5.6: FRU power profile.

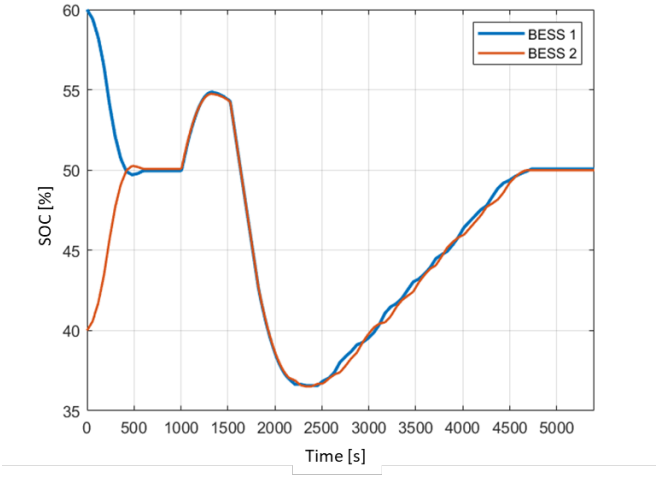

Figure 5.7: BESS state of charge.

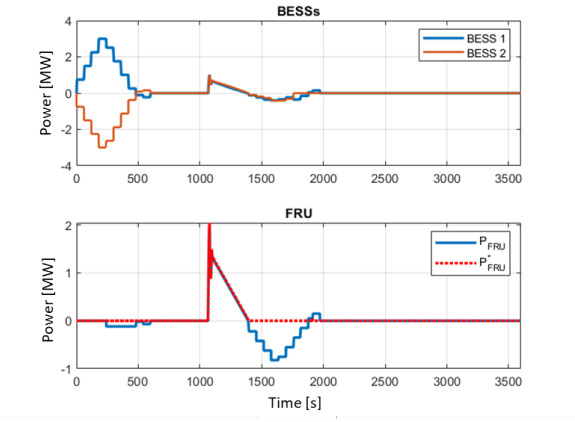

Figure 5.8: FRU power profile.

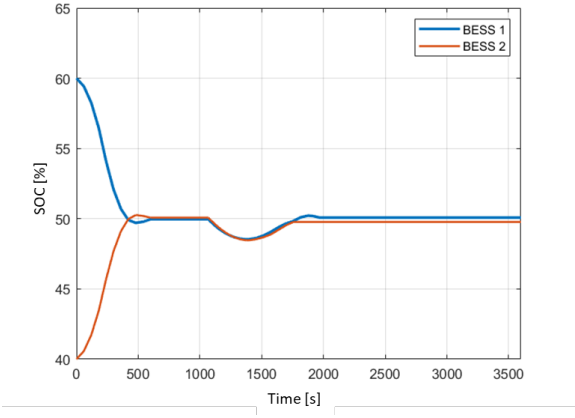

Figure 5.9: BESS state of charge.

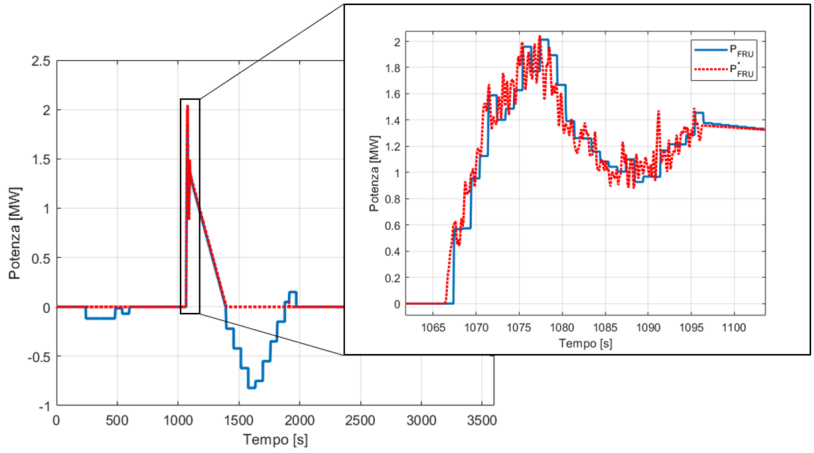

Figure 5.10: Performance detail of Version 1 during Stage 2.

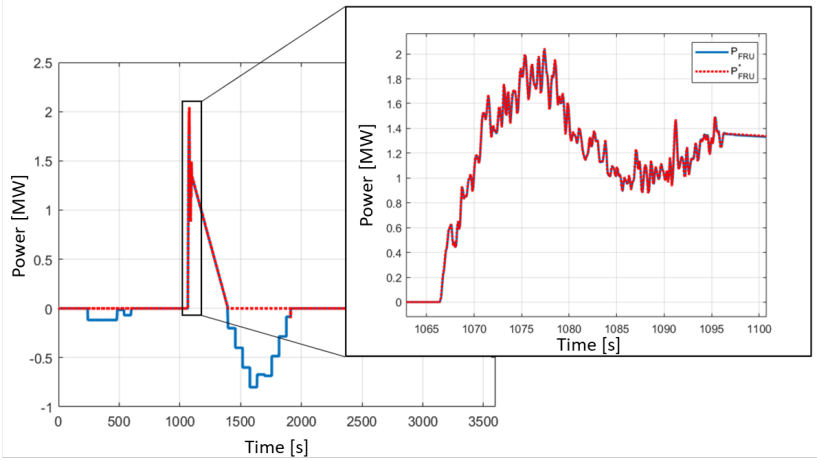

Figure 5.11: Performance detail of Version 2 during Stage 2.

5.2 Service provision with WTs contribution

The same MPC-based method has been applied to a FRU including N BESSs and a wind farm made of M wind turbines that can work together to provide the service. First of all, the MPC approach require to develop an appropriate model of the wind farm. The dynamic equation of the single wind turbine is given by:

$$\begin{cases} \dot{\omega}_i = \frac{1}{J_i}\left(\frac{P_{a,i}}{w_i} - \frac{P_{g,i}}{\eta_i \omega_i}\right) \\ P_{a,i} = \frac{1}{2}\rho A_i C_{p,i}\left(\beta_i, \lambda_i\right) v_i^3 \end{cases} \tag{5.15}$$

where:

- J_i is the turbine inertia [$\mathrm{kg\,m^2}$];
- $P_{a,i}$ is the aerodynamic power [W];
- ω_i is the rotational speed [$\mathrm{rad/s}$];
- η_i is the generator efficiency;
- ρ is the air density [$\mathrm{kg/m^3}$];
- $A_i = \pi R_i^2$ is the area covered by the wind turbine blades [$\mathrm{m^2}$];
- $C_{p,i}$ is the aerodynamic efficiency;
- β_i is the pitch angle [rad];
- $\lambda_i = \omega R_i / v_i$ is the Tip Speed Ratio (TSR);
- v_i is the wind speed [$\mathrm{m/s}$];
- i is the turbine index.

The aerodynamic efficiency $C_{p,i}\left(\beta_i, \lambda_i\right)$ is a non-linear function identified through experimental studies. The pitch angle β_i is defined respect to the blades inclination corresponding the maximum aerodynamic efficiency. The definition used in an example from Matlab guide [105] is here reported:

$$\begin{cases} C_p\left(\lambda, \beta\right) = c_1\left(\frac{c_2}{\theta} - c_3\beta - c_4\right) e^{-\frac{c_5}{\theta}} + c_6\lambda \\ \frac{1}{\theta} = \frac{1}{\lambda + 0.08\beta} - \frac{0.035}{\beta^3 + 1} \end{cases} \tag{5.16}$$

By assigning to the coefficients of Equation 5.16 the values reported in Table 5.4, the maximum value of the aerodynamic efficiency $C_p^{max} = 0.48$ is achieved, obtained when $\beta = 0\,\mathrm{rad}$ and the TSR is $\lambda^* = 8.1$, as shown in Figure 5.12.

Table 5.4: Aerodynamic efficiency coefficients.

c_1	c_2	c_3	c_4	c_5	c_6
0.51763	116	0.4	5	21	0.006795

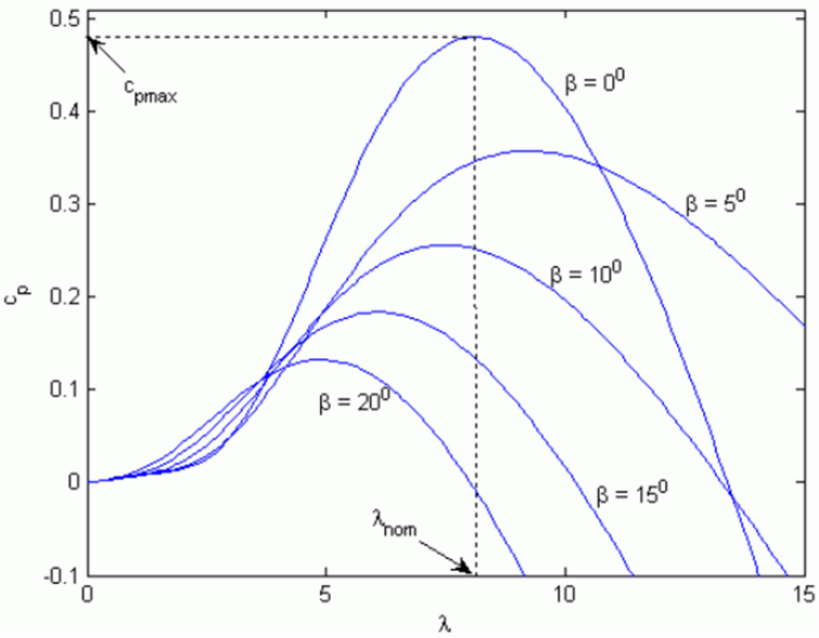

Figure 5.12: Withdrawal profiles example.

For a better understanding of the model, quantities have been converted in per unit, in particular:

$$\begin{cases} \bar{P}_{a,i} = \frac{P_{a,i}}{P_{w,i}^{nom}} \\ \bar{w}_i = \frac{w_i}{w^{nom}} \\ \bar{v}_i = \frac{v_i}{v_{b,i}} \\ \bar{C}_{p,i} = \frac{C_{p,i}(\lambda_i, \beta_i)}{C_{p,i}^{max}} \end{cases} \tag{5.17}$$

where:

- $P_{w,i}^{nom}$ is the nominal power of the wind turbine [W];
- w^{nom} is the nominal rotational speed [rad/s];
- $v_{b,i}$ is the base wind speed, fixed equal to $12\,\mathrm{m/s}$;
- $C_{p,i}^{max} = C_p\left(\lambda_i^*, 0\right)$.

Applying the per unit conversion to the model expressed in Equation 5.15:

$$\begin{cases} \dot{\bar{\omega}}_i = \frac{1}{2H_i}\left(\frac{\bar{P}_{a,i}}{\bar{w}_i} - \frac{\bar{P}_{g,i}}{\eta_i \bar{\omega}_i}\right) \\ \bar{P}_{a,i} = K_{p,i}\bar{C}_{p,i}\left(\beta_i, \lambda_i\right)\bar{v}_i^3 \end{cases} \tag{5.18}$$

where:

- $2H_i = J_i\left(\omega^{nom}\right)^2 / P_{w,i}^{nom}$ is the inertia constant [s];
- $K_{p,i} = \frac{1}{2}\rho A_i$ [kg/m].

Moreover, the TSR can be expressed as:

$$\lambda_i = \frac{\lambda_i^*}{\bar{\omega}_{b,i}}\frac{\bar{\omega}_i}{\bar{v}_i} \tag{5.19}$$

being $\omega_{b,i}$ the rotational speed of the wind turbine blades ($\bar{\omega}_{b,i}$ if converted in per units) when the wind speed is equal to $v_{b,i}$ to obtain the optimal value of the TSR:

$$\lambda_i^* = \omega_{b,i} R / v_{b,i} = \left(\bar{\omega}_{b,i} \cdot \omega^{nom}\right) R / v_{b,i} \tag{5.20}$$

In other words, Equation 5.19 is obtained by applying the definition of $\omega_{b,i}$ expressed in Equation 5.20 to the definition of the TSR.

To provide the FRS through the wind farm, the generation power set-point shall be moved from the optimal profile corresponding to the maximum power generation from wind kinetic energy. Such optimal power profile is realized through the Maximum Power Tracking (MPT) system and is obtained when the TSR is equal to the optimal value λ_i^*. Hence, applying this condition to Equation 5.19, optimal rotational speed is:

$$\bar{\omega}_i^* = \bar{\omega}_{b,i}\bar{v}_i \tag{5.21}$$

Such optimal condition leads to have $\bar{C}_{p,i} = 1[p.u.]$ and by applying the Equation 5.21 to Equation 5.18, the aerodynamic power can be expressed as:

$$\bar{P}_{a,i}^*(\bar{\omega}_i^*) = K_{p,i}\left(\frac{\bar{\omega}_i^*}{\bar{\omega}_{b,i}}\right)^3 \tag{5.22}$$

In light of this, the MPT technique uses Equation 5.21 to identify the optimal power set-point after computing the optimal rotational speed $\bar{\omega}_i^*$ using Equation 5.22. However, such rotational speed is limited within a range between a maximal value, namely the cut-in speed $\bar{\omega}_i^{cut-in}$, and a minimal value, namely the cut-off speed $\bar{\omega}_i^{cut-off}$. Always by referring to the Matlab & Simulink example provided in [105], the MPT curve which defines the optimal power set-point as a function of the turbine speed is defined in Figure5.13 where the limit speeds are $\bar{\omega}_i^{cut-in} = 0.7\,\mathrm{p.u.}$ and $\bar{\omega}_i^{cut-off} = 1.2\,\mathrm{p.u.}$.

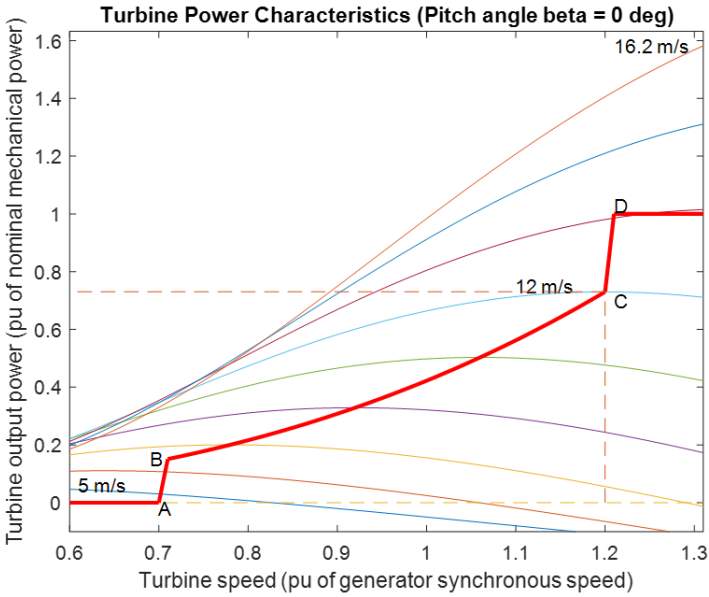

Figure 5.13: Withdrawal profiles example.

The curve is identified by the points A, B, C and D, which are defined as follows:

- A: $\bar{P}_A^* = 0, \bar{\omega}_A = \bar{\omega}_i^{cut-in}$;
- B: $\bar{P}_B^* = K_{p,i} l \left(\bar{\omega}_B^* / \bar{\omega}_{b,i}\right)^3, \bar{\omega}_B = \bar{\omega}_i^{cut-in} + 0.01$;
- C: $\bar{P}_C^* = K_{p,i} l \left(\bar{\omega}_C^* / \bar{\omega}_{b,i}\right)^3, \bar{\omega}_C = \bar{\omega}_i^{cut-in} + 0.01$;
- D: $\bar{P}_D^* = 1, \bar{\omega}_D = \bar{\omega}_i^{cut-off}$;

The operating range of turbine speed shall be between points B and C where the MPT curve is given by Equation 5.22.

The model given by Equation 5.18 is not linear and time continuous and it requires to be linear and converted in discrete time to be applied to the MPC

algorithm.

Once modelled the wind farm, the MPC is applied to provide the FRS with BESSs and the wind farm operating coordinately. The control strategies are similar to those used for the stand-alone BESSs case and are here reminded:

- Stage 1: the frequency error is below the first threshold of $0.05\,\mathrm{Hz}$, hence the system is only requested to reach the ideal conditions to face the next event; in this case, the optimal condition of BESSs to provide both upward and downward service is to keep the SoC equal to 50% of nominal capacity.
- Stage 2: the frequency error exceeds the first threshold, the FRS activates; the FRU has to provide power proportional to the frequency error if it is below the second threshold of $0.2\,\mathrm{Hz}$ or equal to the qualified power otherwise;
- Stage 3: at the end of the service, the FRU is requested to linearly decrease the power output to the set-point it had before the activation event in a selected time interval as already specified.

In this case, the contribution of the wind farm is requested too. thus, the cost functions require to be defined taking account of the participation of the wind farm to the service provision. Also, new constraints regarding the wind turbines must be introduces to the optimization problem.

In Stage 1, while the FRS is not active, BESSs must restore their SoC and the wind farm is not involved in the problem, hence, the function cost and the batteries constraints are the same of the stand-alone BESS case (Equations 5.7-5.8) with a difference for the FRU constraints. In fact, let the FRU expressed in Equation 5.9 be replaced by the following:

$$s.t. \begin{cases} -P_{b,tot}^{max} \leq \sum_{i=1}^{N} P_{b,i}(j) \leq P_{b,tot}^{max} & \forall j = k : k+T-1 \\ |\sum_{i=1}^{N} P_{b,i}(j) - \sum_{i=1}^{N} P_{b,i}(j-1)| \leq \Delta P_{b,tot}^{max} & \forall j = k : k+T-1 \end{cases} \tag{5.23}$$

being:

$$\begin{cases} P_{b,tot}^{max} = \min\left(\sum_{i=1}^{N} P_{b,i}^{nom} - P_Q, 0.25P_Q\right) \\ \Delta P_{b,tot}^{max} = 2P_{b,tot}^{max} \end{cases} \tag{5.24}$$

Parameters of MPC problem are unchanged respect to Table 5.1.

During Stage 2, the service is active and the FRU is requested to follow the desired power profile, proportional to the frequency error up to the qualified power, defined by Equation 5.10. The cost function is defined as follow:

$$\begin{aligned} \min_{[\alpha_{b,i}(j),\alpha_{g,i}(j)]} \sum_{i=1}^{N} \Bigg[\Bigg(\sum_{j=k}^{k+T-1} w_{s,i}(SOC_i(j) - SOC_i^*)^2 + \\ + w_{p,i}(\Delta P_{b,i}(j))^2) \Bigg) + w_{f,i}(SOC_i(k+T) - SOC_i^*)^2 \Bigg] + \\ + \sum_{i=1}^{M} \Bigg[\Bigg(\sum_{j=k}^{k+T-1} w_{\omega,i}(\bar{\omega}_i(j) - \bar{\omega}_i^*(k))^2 + w_{g,i}(\Delta P_{g,i}(j))^2) \Bigg) + \\ + w_{f\omega,i}(\bar{\omega}_i(k+T) - \bar{\omega}_i^*(k))^2 \Bigg] \end{aligned} \tag{5.25}$$

$$s.t. \quad SOC_i(t+1) = SOC_i(t) - \frac{\Delta}{36 \cdot E_{b,i}} \left(\eta_i^{ch} P_{b,i}^{ch}(t) + \eta_i^{dsc} P_{b,i}^{dsc}(t)\right) \tag{5.26}$$

$$s.t. \begin{cases} -P_{b,i}^{max} \leq P_{b,i}(j) \leq P_{b,i}^{max} & \forall i = 1:N, j = k:k+T-1 \\ SOC_i^{min} \leq SOC_i(j) \leq SOC_i^{max} & \forall i = 1:N, j = k:k+T-1 \\ |\Delta P_{b,i}(j) - P_{b,i}(j-1)| \leq \Delta P_{b,i}^{max} & \forall i = 1:N, j = k:k+T-1 \end{cases} \tag{5.27}$$

$$s.t. \begin{cases} \Delta\bar{\omega}_i(j+1) = a_i \Delta\bar{\omega}_i(j) + b_j \Delta\bar{P}_{g,i}(j) + f_i \\ \bar{\omega}_i(j) = \bar{\omega}_i(k) + \Delta\bar{\omega}_i(j) \\ \bar{\omega}_i^{cut-in} \leq \bar{\omega}_i(j) \leq \bar{\omega}_i^{cut-off} \\ \Delta\bar{\omega}_i(k) = 0 \end{cases} \tag{5.28}$$

$$s.t. \begin{cases} P_{g,i}^{min} \leq P_{g,i}(j) \leq P_{g,i}^{max} \\ -\Delta P_{g,i}^{max} \leq \Delta P_{g,i}(j) \leq \Delta P_{g,i}^{max} \\ P_{g,i}(j) = \bar{P}_{g,i}(j) \cdot P_{w,i}^{nom} \\ \bar{P}_{g,i}(j) = \bar{P}_{g,i}(k) + \Delta \bar{P}_{g,i}(j) \end{cases} \tag{5.29}$$

$$s.t. \begin{cases} P_{FRU}(j) = \left(\sum_{i=1}^{N} P_{b,i}(j)\right) + \left(\sum_{i=1}^{M} P_{g,i}(j)\right) \\ -P_{FRU}^{max} \leq P_{FRU}(j) \leq P_{FRU}^{max} \\ -P_{b,tot}^{max} \leq \sum_{i=1}^{N} P_{b,i}(j) \leq P_{b,tot}^{max} \\ |P_{FRU}^{*}(j) - P_{FRU}(j)| \leq \frac{tol}{100} P_Q \end{cases} \tag{5.30}$$

The MPC optimization problem parameters value are given in Table 5.5.

Table 5.5: MPC problem parameters in Stage 2.

Quantity	Parameter	Value
General		
Sampling time	$\Delta[s]$	1
Horizon	T [-]	30
Single BESS		
desired SoC	SOC_i^* [%]	50
max power	$P_{b,i}^{max}$	$P_{b,i}^{nom}$
max power variation	$\Delta P_{b,i}^{max}$	$2P_{b,i}^{max}$
Wind turbine		
min power	$P_{g,i}^{min}$	$P_{w,i}^{nom}$
max power	$P_{g,i}^{min}$	$\bar{P}_C^* \cdot P_{w,i}^{nom}$
max power variation	$\Delta P_{g,i}^{max}$	$P_{w,i}^{nom}$
FRU		
max power from BESSs	$P_{b,tot}^{max}$	$\sum_{i=1}^{N} P_{b,i}^{max}$
max power	P_{FRU}^{max}	$P_{b,tot}^{max} + \sum_{i=1}^{M} P_{w,i}^{nom}$
tolerance	$tol[\%]$	0.5
Weights		
SoC weight	$w_{s,i}$	$\frac{1}{100^2}$
BESS power variation weight	$w_{p,i}$	$\frac{1}{P_{b,i}^{max2}}$
final SoC weight	$w_{fs,i}$	$\frac{1}{100^2}$
turbine speed weight	$w_{\omega,i}$	0.01
turbine power variation weight	$w_{g,i}$	$\frac{0.02}{P_{b,i}^{max2}}$
final turbine speed weight	$w_{f\omega,i}$	0.01

In Stage 3, the desired power profile is again computed using Equation 5.14 to linearly reduce the FRU power deviation from the baseline profile in a fixed time interval. The cost function is defined as follow:

$$\min_{[\alpha_{b,i}(j),\alpha_{g,i}(j)]} \sum_{i=1}^{N} \Bigg[\Bigg(\sum_{j=k}^{k+T-1} w_{s,i}(SOC_i(j) - SOC_i^*)^2 + \\ + w_{p,i}(\Delta P_{b,i}(j))^2) \Bigg) + w_{f,i}(SOC_i(k+T) - SOC_i^*)^2 \Bigg] + \\ + \sum_{i=1}^{M} \Bigg[\Bigg(\sum_{j=k}^{k+T-1} w_{\omega,i}(\bar{\omega}_i(j) - \bar{\omega}_i^*(k))^2 + w_{g,i}(\Delta P_{g,i}(j))^2) \Bigg) + \\ + \sum_{j=k}^{k+T} w_{r,i}(r_{g,i}(j))^2 + w_{f\omega,i}(\bar{\omega}_i(k+T) - \bar{\omega}_i^*(k))^2 \Bigg] \quad (5.31)$$

Same constraints of Stage 2, expressed in Equations 5.26-5.30, are maintained, in addition to the constraint related to the integral contribute.

$$s.t. \quad r_{g,i}(j+1) = r_{g,i}(j) + (\bar{\omega}_i(j) - \bar{\omega}_i^*(k)) \quad (5.32)$$

Parameters values are reported in Table 5.6.

Table 5.6: MPC problem parameters during Stage 3.

Quantity	Parameter	Value
General		
Sampling time	$\Delta[s]$	1
Horizon	T [-]	30
Single BESS		
desired SoC	SOC_i^* [%]	50
max power	$P_{b,i}^{max}$	$P_{b,i}^{nom}$
max power variation	$\Delta P_{b,i}^{max}$	$2P_{b,i}^{max}$
Wind turbine		
min power	$P_{g,i}^{min}$	$P_{w,i}^{nom}$
max power	$P_{g,i}^{min}$	$\bar{P}_C^* \cdot P_{w,i}^{nom}$
max power variation	$\Delta P_{g,i}^{max}$	$P_{w,i}^{nom}$
FRU		
max power from BESSs	$P_{b,tot}^{max}$	$\sum_{i=1}^{N} P_{b,i}^{max}$
max power	P_{FRU}^{max}	$P_{b,tot}^{max} + \sum_{i=1}^{M} P_{w,i}^{nom}$
tolerance	$tol[\%]$	0.5
Weights		
SoC weight	$w_{s,i}$	$\frac{1}{100^2}$
BESS power variation weight	$w_{p,i}$	$\frac{1}{P_{b,i}^{max2}}$
final SoC weight	$w_{fs,i}$	$\frac{1}{100^2}$
turbine speed weight	$w_{\omega,i}$	0.01
turbine power variation weight	$w_{g,i}$	$\frac{0.02}{P_{b,i}^{max2}}$
final turbine speed weight	$w_{f\omega,i}$	0.01
integral control weight	$w_{r,i}$	0.03

The tested FRU is characterized by two batteries and a wind farm made of 20 turbines divided into 4 groups to model 4 different wind speed profiles.

BESSs and wind farm parameters are reported in Table 5.7 and Table 5.8 respectively.

Table 5.7: BESSs parameters.

Quantity	Parameter	BESS 1	BESS 2
Capacity	$E_{b,i}$ [MWh]	3	3
Nominal power	$P_{b,i}^{max}$ [MW]	6	6
Charging performance	η_i^{ch}	0.9116	0.9207
Discharging performance	η_i^{dsc}	0.9582	0.9582
Maximum SoC	$SOC_i^{max}[\%]$	90	90
Minimum SoC	$SOC_i^{min}[\%]$	10	10

Table 5.8: Wind farm parameters.

Quantity	Parameter	Value
Nominal power	$P_{w,i}^{nom}$ [MW]	10
Inertia constant	H_i [s]	5
Efficiency	η_i	1
max turbine speed	$\bar{\omega}_i^{cut-off}$ [p.u.]	1.2
min turbine speed	$\bar{\omega}_i^{cut-in}$[p.u.]	0.7

The BESS system has a qualified power equal to $P_Q = 4\,\mathrm{MW}$, hence, during Stage 1 batteries can modify the power they exchange with the network within a band of $\pm\ 1\,\mathrm{MW}$ to restore the SoC, accordingly to the limit specification 25% of P_Q from the baseline profile. The wind turbines are identical, so the total nominal power of the wind farm is equal to $40\,\mathrm{MW}$. The FRU has been tested simulating the test and plausible frequency profiles already shown in Figure 5.4 and Figure 5.5. It is reminded that the 4 groups of wind turbines are affected by four different plausible wind speed profiles.

Within real frequency scenario, power exchanged by the BESS system, by the wind farm and by the whole FRU are shown in Figure 5.14 while the batteries SoC and wind turbines speed are given in Figure 5.15.

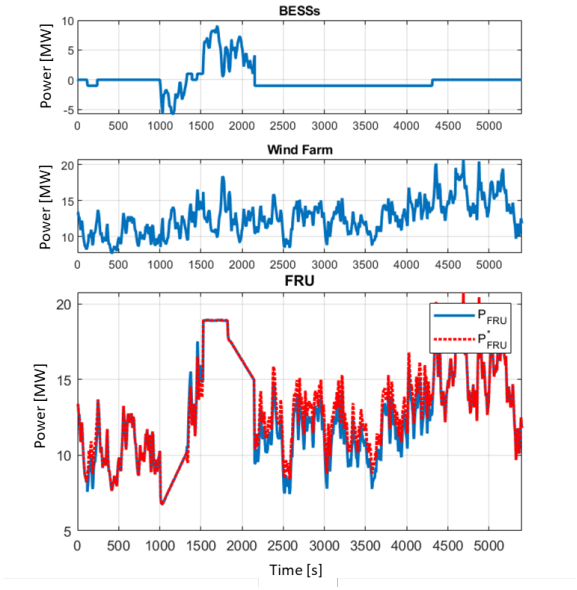

Figure 5.14: Withdrawal profiles example.

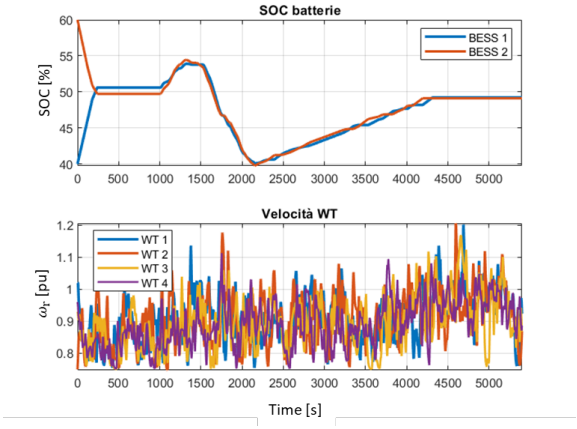

Figure 5.15: Withdrawal profiles example.

The desired power P^*_{FRU} profile is considered as the the reference profile of the whole FRU. With the BESS system alone, the P^*_{FRU} profile was considered as the sum of the power baseline profile and the service power contribution; when the service was not active, the BESSs were not intended to exchange power and the reference profile was zero.

Similarly, with the wind farm active in the FRU, P^*_{FRU} profile shall be considered starting from the FRU baseline profile, which is the power exchanged by the wind turbines. For this reason, in Figure 5.14, P^*_{FRU} is equal to the power actually generated by the wind farm during Stage 1, except when the BESS system requires to restore the SoC after the event. Also, the typical desired power profile described by the TSO pilot project [57] is evident during Stage 2 and Stage 3, when the FRS is active, and successfully realized by the FRU.

To realize such regular power profile when the FRS is active, the BESSs provide the difference between the wind farm power generation and P^*_{FRU}. As stated in the cost functions of Stage 2 and Stage 3, though, also the wind farm attempts to change its power production away from the baseline profile that would be realized without the service activation. Evidence of this is given in Figure 5.16 where small difference between the two profiles can be observed.

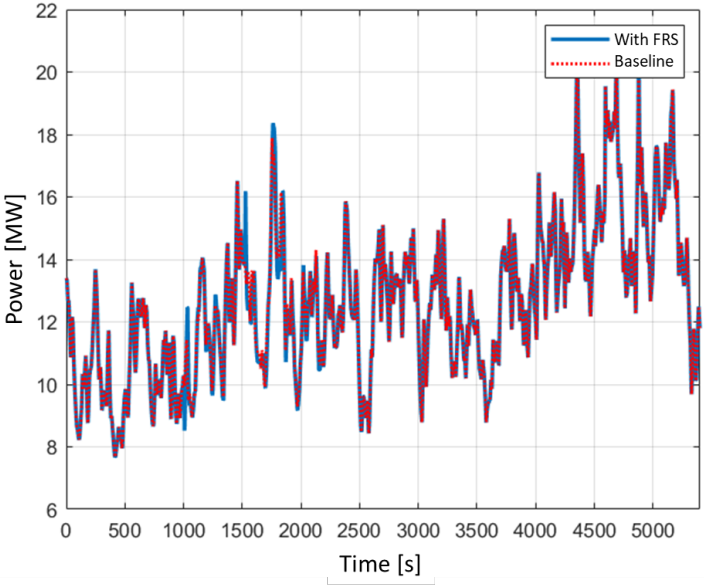

Figure 5.16: Withdrawal profiles example.

With the plausible frequency profile, same conclusion can be made by observing the FRU power output in Figure 5.17 and the batteries SoC, along with the wind turbines speed, in Figure 5.18. The FRU successfully provides the desired power profile when the service is active with contribution from both the BESS system and the wind farm and apply the energy management strategy during Stage 1 which leads to the differences between the desired power profile and the actual power profile within the band of 1 MW, accordingly to FRS specifications.

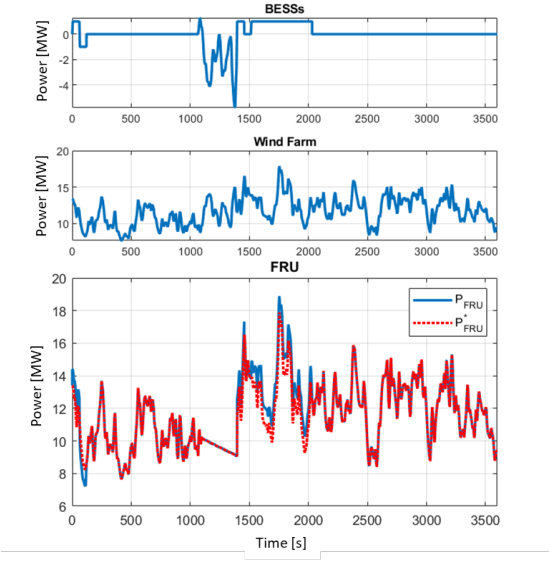

Figure 5.17: FRUs power profile.

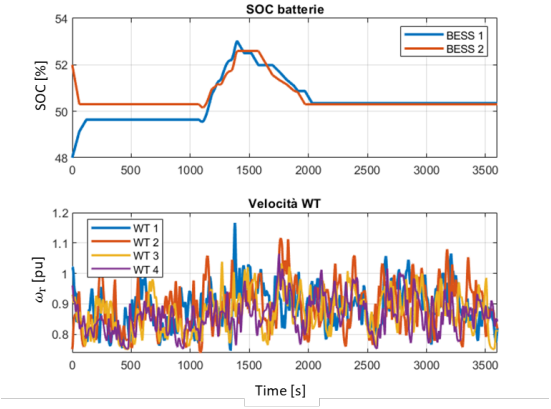

Figure 5.18: BESS state of charge and WTs speed.

5.3 Validation through hardware in the Loop simulations

After validating the algorithm with simulations, the activity continued towards Hardware In the Loop (HIL) tests. The control process has been implemented on hardware and real time simulations have been performed to validate the algorithm time response which have to be fast enough to satisfy the FRS requirements despite the time delay that the communication system introduces.

Algorithm has been tested through Raspberry Pi drive in OPAL-RT environment for real time simulation. In this step, this simulation, namely Control Hardware In the Loop (CHIL), validates the algorithm performance according to the FRS pilot project implemented in physical components. Also, to identify the contribution of FRS to frequency regulation, a new CHIL simulation where five equivalent FRUs, distributed in a transmission system and driven the Master FRU controlled with Raspberry Pi, is carried out.

Finally, experimental tests of Power Control Hardware In the Loop (PCHIL) are realized; the RaspBerry Pi remotely controls a real BESS installed in a test facility of University of Genoa whose measurement are used in real time simulated network.

The Cigrè transmission network [106] has been implemented in Matlab and Simulink environment. It is made of 13 nodes and operates with a voltage level of $220\,\mathrm{kV}/380\,\mathrm{kV}$. In Figure 5.19, three areas are identified, Area 3 hosts the Master FRU.

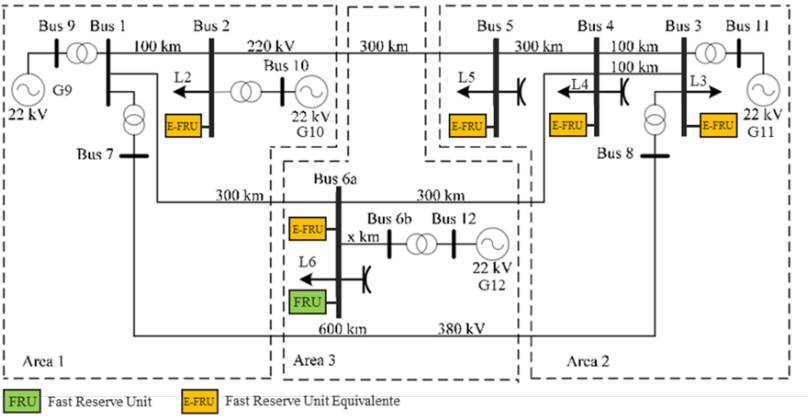

Figure 5.19: Cigrè network implemented in Simulink to realize HILs simulations [106].

Generators and loads information are given in Tables 5.9 and 5.10; other parameters are collected in the reference document [106].

Table 5.9: Transmission network generator parameters.

Generator	Node	S_{rated} [MVA]	P_{out} [MW]	V_{out} [p.u.]
G10	10	700	500	1.03
G11	11	500	500	1.03
G12	12	500	500	1.03
G9	9	slack	slack	1.03

Table 5.10: Transmission network load parameters.

Load	Node	P [MW]	Q [MVar]
L2	2	285	200
L3	3	325	244
L4	4	326	244
L5	5	103	62
L6	6a	435	296

The FRU is connected to the system at node 6 through a $220\,\mathrm{kV}/22\,\mathrm{kV}$ transformer. It consists of two BESSs and a WTs whose parameters are reported in Tables 5.11 and 5.12.

Table 5.11: FRU BESSs parameters.

–	Parameter	Value	Unit
Nominal voltage	$V_{b,i}$	10^3	[V]
Battery capacity	$C_{b,i}$	$6 \cdot 10^3$	[Ah]
Nominal power	$P_{b,i}^{max}$	$6 \cdot 10^6$	[W]
Charge performance	η_i^{ch}	0.98	–
Discharge performance	η_i^{dsc}	0.98	–

Table 5.12: FRU single WTs parameters.

Load	Node	P	Q
Nominal active power	P_w^{nom}	$2 \cdot 10^6$	[W]
Power factor	pf	0.9	–
Inertia constant	H	5.04	[s]
Generator performance	η_w	1	–
Base wind speed	w_b	12	–
Minimum speed	$\bar{w}_i^{cut-in}$	0.71	[p.u.]
Maxium speed	$\bar{w}_i^{cut-off}$	1.2	[p.u.]

The WF consists of four groups, each made of ten WTs, for a total power of 80 MW. In light of this, the FRU total power installed is equal to 92 MW; the qualified power P_Q is set to 8 MW, much lower than the generators nominal power. As said before, the FRS from the FRU alone can't have a significant impact on frequency. For this reason to show relevant effects of FRS on frequency regulation, other five equivalent FRUs, each with qualified power equal to 25 MW, the maximum value set by the TSO in [57], have been implemented in the system, one at each node 5.19. The total qualified power in this case becomes 132 MW, including the first FRU. The simulated event is the deactivation and reactivation of load L6 of 435 MW.

In the real time simulator OPAL-RT [107], the network model, along with the MPC based algorithm, installed on Raspberry Pi, is implemented to realized CHIL simulations. The base architecture is illustrated in Figure 5.20.

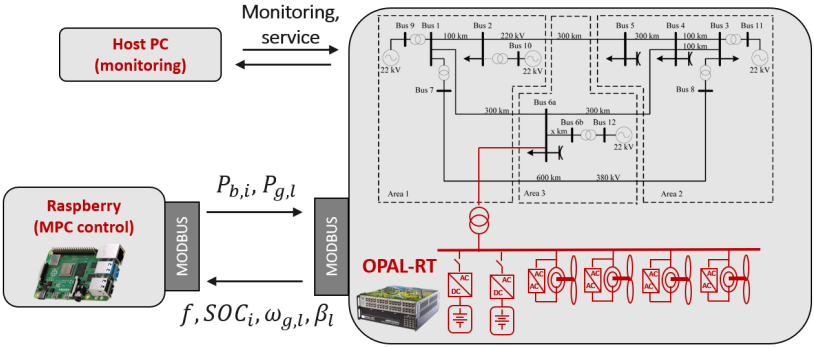

Figure 5.20

Communication between the Raspberry Pi and the real time simulator follows the MODBUS protocol. To give an idea of the data required, Figure 5.21 shows the data exchange during CHIL simulations.

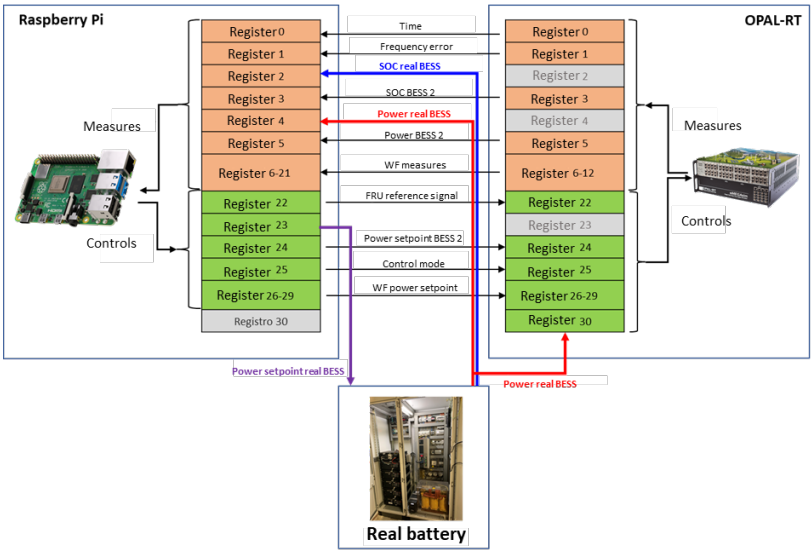

Figure 5.21: MODBUS communication data transfer in CHIL setup.

Register 30 is designed to interface with the real BESS and is deactivated at this stage. During the activity, it has been confirmed that the TSO prescription in [57] of maximum time delay of power response from controlled devices less than $300\,\mathrm{ms}$ is satisfied. This is highlighted because it is worth noting that even communication systems have to meet strict requirements depending on the process dynamic, which is extremely fast for regulation services.

Given the frequency profile in Figure 5.22, CHIL simulation results shows in Figures 5.23 and 5.24 that MPC algorithm works properly despite the delay introduced with the communication system.

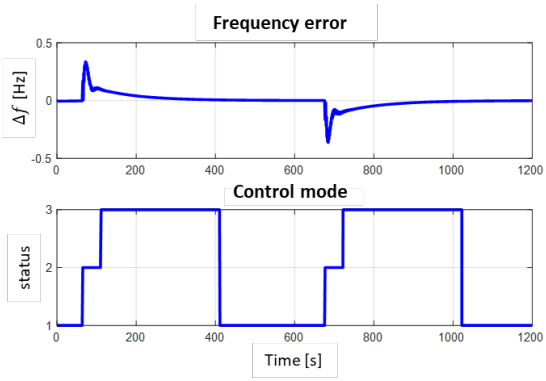

Figure 5.22: Frequency profile used in CHIL simulations.

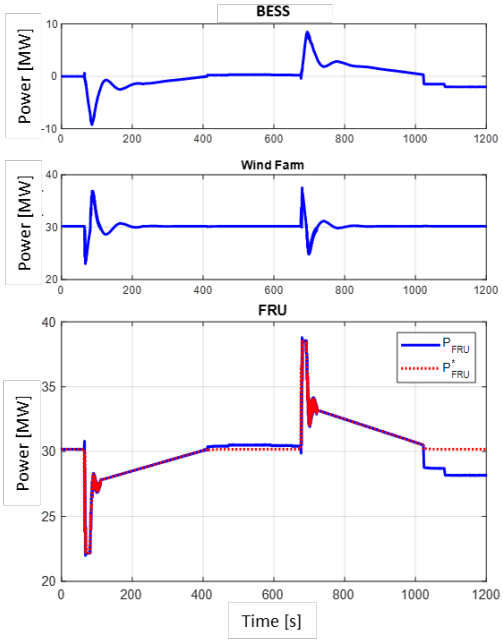

Figure 5.23: Power profiles during CHIL simulations.

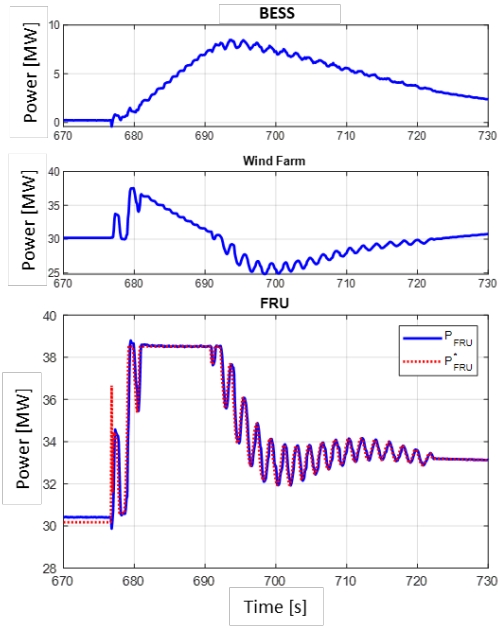

Figure 5.24: Detail of power profiles CHIL simulations.

With the equivalent FRUs activated, the same simulation is carried out to show the impact of FRS on frequency error in Figure 5.25.

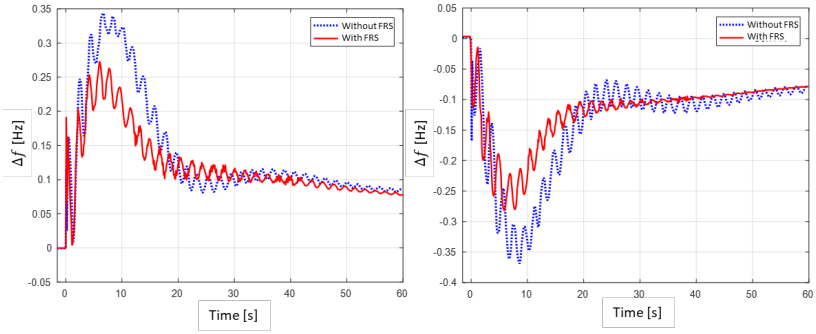

Figure 5.25: Differences in frequency error signal with and without FRS.

In conclusion, the FRS reduces the maximum transient frequency deviation by 20% (69 mHz) when load L6 is deactivated and 24% (88 mHz) when load L6 is reactivated in case the total qualified power is 31% of load variation (133 MW/435 MW.)

After having the algorithm validated in CHIL simulation, PCHIL configuration is realized by replacing one of the simulated BESSs with an equivalent one which reproduces the power exhcange realized by the real BESS. The latter has a nominal power of 9.5 kW and capacity equal to 11 kWh [108].

Base architecture of PCHIL is similar to Figure 5.20 with the introduction of the real BESS (Figure 5.26), as well as the communication of data in Figure 5.27, similar to Figure 5.21 where register 30 takes the place of register 23 to redirect power set-points signal to the equivalent BESS instead of the simulated one.

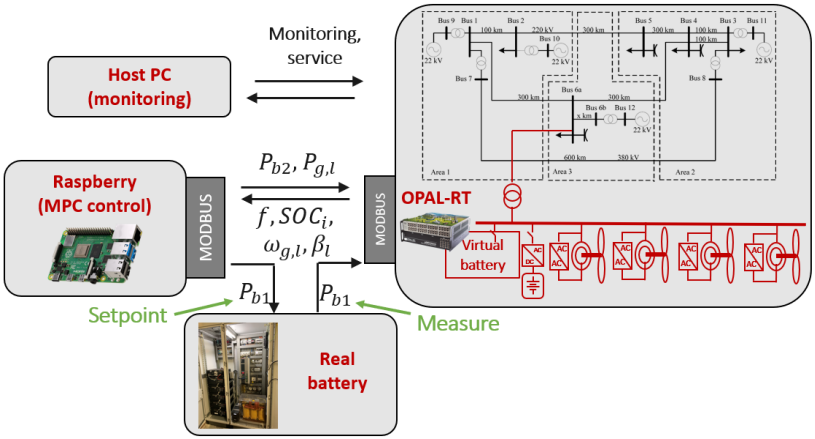

Figure 5.26: PCHIL simulation setup.

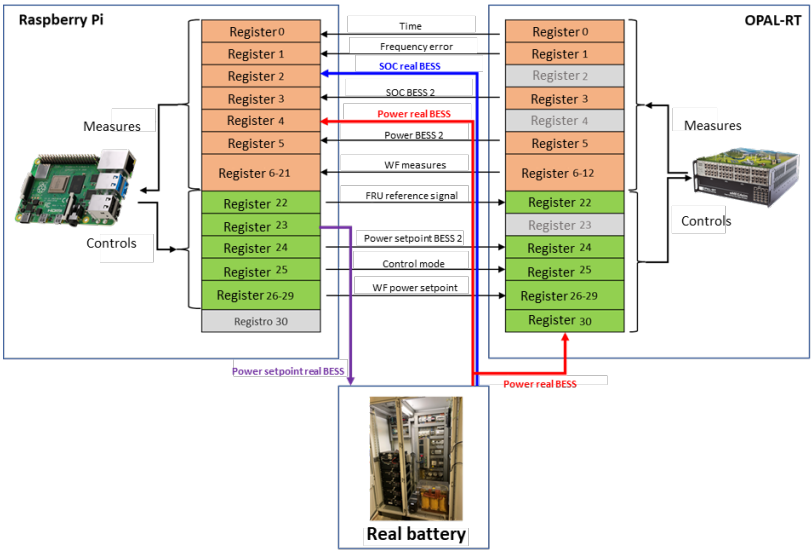

Figure 5.27: MODBUS communication data transfer in PCHIL setup.

In this configuration, the simulation is repeated and results are shown in Figures 5.28 and 5.29 giving evidence of BESS, but also of WFs, to provide FRS according to the pilot project specifications.

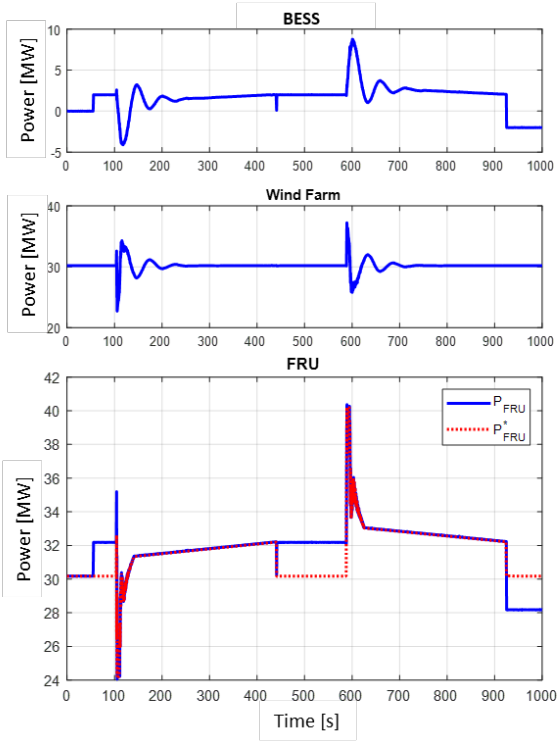

Figure 5.28: Power profiles during PCHIL simulations.

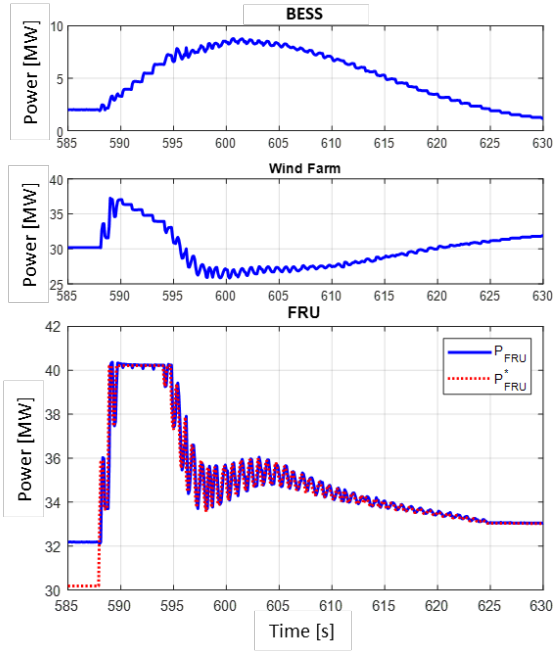

Figure 5.29: Detail of power profiles PCHIL simulations.

5.4 Study of methods to provide service with PVs

The research activity continued moving the focus on the capability of PV systems to provide flexibility services without coordination with BESSs.

The approach shall be similar to the one adopted for BESSs and WFs, based on MPC algorithm and validated with real time simulations with similar architectures of CHIL and PCHIL tests (Figures 5.20 and 5.26). MPC based strategies proves to be suiable for RESs regulation since, with less power reserve, optimal control actions are needed.

In order to provide regulation services, a power reserve must be set up to permit any power variation that can help restore the frequency to its nominal value. Traditionally, PVs are controlled such that they generate the maximum power depending on weather conditions, through Maximum Power Point Tracking (MPPT) algorithms [109].

However, is it possible from TSO rules [110, 111] that PVs and WTs can operate keeping a reserve from the maximum power point which can be used when required from the TSO to deal with perturbation events.

Basically, to have PVs provide regulation services is to change its normal operating point from Maximum Power Point (MPP), corresponding to P_{max} to a lower power generation condition P_0 and control the PV voltage to increase power output when needed using the power reserve P_r (Figure 5.30).

$$P_r = P_{max} - P_0 \tag{5.33}$$

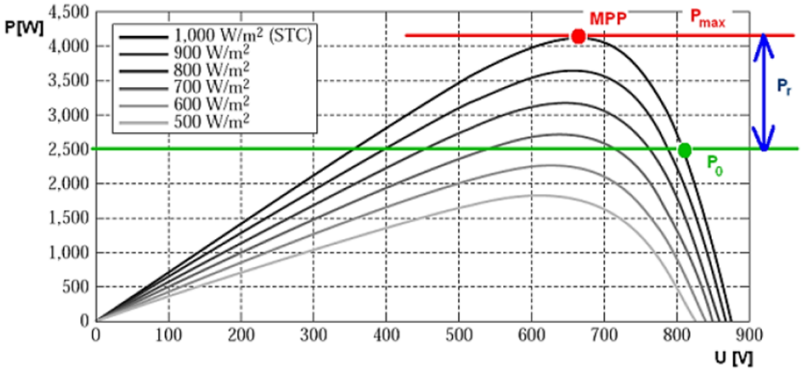

Figure 5.30: Power reserve from PV [112].

Several control methods are already formulated in [112–118], but all of them start from reducing the PV steady state power generation to provide power reserve by moving the operating point away from the MPP following the PV characteristic: [117] refers to this approach with Flexible Power Point (FPP).

To realize simulations, a model of PV and of the interface with the external grid is to be implemented with an architecture similar to Figure 5.31.

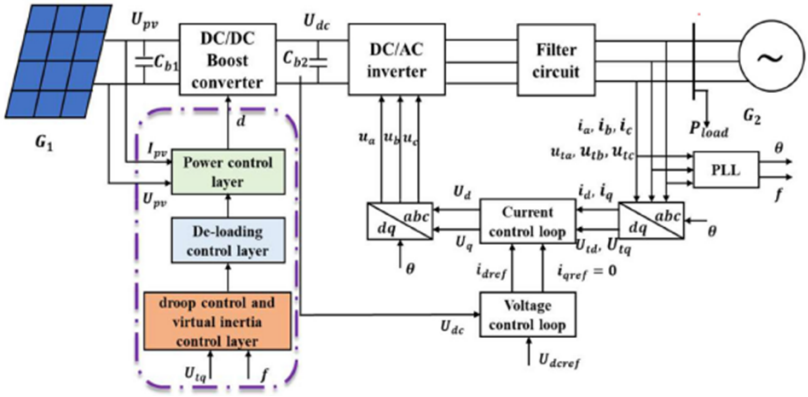

Figure 5.31: PV system and frequency control [116].

With such configuration, external grid frequency and AC voltage are measured and used to compute the desired PV voltage U_{pv} so that the system generates reduced power to prepare the reserve in normal conditions and increases it when a frequency deviation is detected.

Similar approach shall be used to realize CHIL and PCHIL tests in order to validate the MPC based algorithm in real time simulation and confirm that the TSO requirements for the service provision and the communication systems are met.

5.5 Final considerations

The theme of flexibility has been explored with tests and analysis of the potential capability of RESs to vary their power output when requested. All units proved to be able to participate to electric markets by supporting the grid through service provision. Given the innovative technologies and their large application throughout the electrical network, new control methods need to be implemented, along with a suitable communication systems, to keep maintaining the power system reliability and security constraints.

CHAPTER 6

Conclusions

During the three years of Ph.D., this research activity covered themes concerning different areas of interest, but all of them take part in the framework of energy transition. In particular, three main aspects have been identified as the major requirements that the electric power system has to meet in order to deal with the extremely large RES penetration:

- network infrastructure development;
- flexibility resources;
- improvement of communication systems.

The target of the thesis is to describe the importance to pursue each of the three challenges together and show how they are related one another. While most of the activities carried out can be applied to a general network, some of them directly refer to the particular case of Sicily which is definitely one of the most interesting areas in Italy in terms of installation of RESs, given its ideal weather conditions and its limited export capacity.

Putting together all the studies regarding the Sicily framework, issues of network development, regulation services and communication among systems are explored and their correlation one to each other is proven.

A network development complex process is introduced and a glimpse of what is the near future of transmission and distribution networks in Sicily is shown. With enough data to perform load flow analysis, stressed areas are identified in order to optimize the authorization and installation steps of new RESs and feeders.

Data acquired have been used to apply the VoltVar control and optimal BESS allocation to the study case of Sicily. The methodology can lead to perform analysis on real or future networks and help the TSO find the best solution to improve the grid operating conditions.

With the increased need of regulation services, new manners of providing flexibility resources are sought, especially from loads, RES and BESSs; considering that, such aspect should be included in the network planning processes.

Flexibility analysis of thermal load in the Italian framework have been carried out. In order to study the contribution of thermal loads to power system flexibility, a Monte-Carlo approach was performed to simulate stochastic hot water demand of aggregates of thermal loads.

A clear definition of flexibility was given to better understand its key role in terms of frequency regulation. Such theme was explored deeper durings tests of BESSs and WTs for FRS provision. System model has been implemented in OPAL-RT to perform real time simulations and MODBUS protocol is used for communication with real objects.

In this context, MPC proved to be a valuable tool to control new generation units to provide regulation services, but it requires data from the network model and needs to be matched with a properly fast communication system.

Bibliography

[1] "https://www.un.org/sustainabledevelopment/blog/tag/193-member-states/,"

[2] T. Källqvist, "The Sustainable Development Goals in the EU budget," *Directorate-General for Internal Policies*, 2021.

[3] United Nations, "Paris agreement," 2016.

[4] Ministero dello Sviluppo Economico and Ministero dell'Ambiente e della Tutela del Territorio e del Mare and Ministero delle Infrastrutture e dei Trasporti, "Piano nazionale integrato per l'energia e il clima," 2019.

[5] Commissione Europea, "Il Green Deal Europeo," *Comunicazione della commissione al Parlamento europeo, al Consiglio, al Comitato economico e sociale europeo e al Comitato delle regioni*, 2019.

[6] Constanze Fetting ESDN Office , "The European Green Deal," *ESDN Report*, 2020.

[7] European Parliament, "European Climate Law," *European Parliament legislative resolution of 24 June 2021 on the proposal for a regulation*

of the European Parliament and of the Council establishing the framework for achieving climate neutrality and amending Regulation (EU), 2021.

[8] European Parliament, "Regulation (EU) 2021/1119 of the European Parliament and of the Council of 30 June 2021 establishing the framework for achieving climate neutrality and amending regulations (EC) no 401/2009 and (EU) 2018/1999 ('European Climate Law')," *Official Journal of the European Union*, 2021.

[9] ARERA, "Prima apertura del mercato per il servizio di dispacciamento (msd) alla domanda elettrica e alle unità di produzione anche da fonti rinnovabili non già abilitate nonché ai sistemi di accumulo. istituzione di progetti pilota in vista della costituzione del testo integrato dispacciamento elettrico (tide) coerente con il balancing code europeo," *Delibera 300/2017/R/eel*, no. 300, 05 maggio 2017.

[10] Terna S.p.A., "Piano di Sviluppo 2021," 2021.

[11] ENTSO-E, "TYNDP 2022," *Scenario report*, 2022.

[12] Terna S.p.A., "Metodologia per l'individuazione di aree e linee critiche sulla rete in alta e altissima tensione ai sensi della delibera ARG/elt 125/10,"

[13] Terna S.p.A., "Aree e linee critiche delibera 99/08," 2021.

[14] "Decreto legislativo 79/99," no. 79, 16 marzo 1999.

[15] Parlamento Europeo e del Consiglio, "Direttiva 96/92/ce," 19 dicembre 1996.

[16] TERNA S.P.A., "Individuazione zone della rete rilevante," *Allegato A.24 al codice di rete*, 2021.

[17] Terna S.P.A. e Gruppo Terna , "Contesto ed Evoluzione del Sistema Elettrico," 2019.

[18] E. Hirst and B. Kirby, "Electric-power ancillary services," *Oak Ridge, TN, USA: Oak Ridge National Laboratory*, 1996.

[19] "Documentation from "Ricerca di Sistema"," 2011.

[20] Terna S.p.A., "The Transmission, Dispatching, Development and Grid Security Code," 2005.

[21] H. Chabok, J. Aghaei, M. Sheikh, M. Roustaei, M. Zare, T. Niknam, M. Lehtonen, M. Shafi-khah, and J. P. Catalão, "Transmission-constrained optimal allocation of price-maker wind-storage units in electricity markets," *Applied Energy*, vol. 310, 2022.

[22] A. Soroudi, "Energy storage planning for resiliency enhancement against renewable energy curtailment," in *IET International Conference on Resilience of Transmission and Distribution Networks*, 2017.

[23] A. M. Alshamrani, "A mixed-integer quasi-convex optimization model for joint transmission network and wind power investment problem," *Electric Power Systems Research*, vol. 217, 2023.

[24] Ahmad, Ahmad, and R. Sirjani, "Optimal planning and operational strategy of energy storage systems in power transmission networks: An analysis of wind farms," *International Journal of Energy Research*, vol. 45, 2021.

[25] C. Zhang, H. Cheng, L. Liu, H. Zhang, X. Zhang, and G. Li, "Coordination planning of wind farm, energy storage and transmission network with high-penetration renewable energy," *International Journal of Electrical Power & Energy Systems*, vol. 120, p. 105944, 2020.

[26] J. Aguado, S. de la Torre, and A. Triviño, "Battery energy storage systems in transmission network expansion planning," *Electric Power Systems Research*, vol. 145, pp. 63–72, 2017.

[27] Y. Dean, Tejada-Arango, D. A., and W. Sonja, "Storage allocation and investment optimisation for transmission-constrained networks considering losses and high renewable penetration," *IET Renewable Power Generation*, vol. 12, no. 16, pp. 1949–1956, 2018.

[28] Z. Hu, *Integration of Large-Scale Energy Storage System into the Transmission Network*, ch. 8. John Wiley & Sons, Ltd, 2020.

[29] M. Padhee, A. Pal, C. Mishra, and K. Vance, "A fixed-flexible bess allocation scheme for transmission networks considering uncertainties," *IEEE Transactions on Sustainable Energy*, vol. 11, no. 3, pp. 1883–1897, 2020.

[30] M. Motalleb, E. Reihani, and R. Ghorbani, "Optimal placement and sizing of the storage supporting transmission and distribution networks," *Renewable Energy*, vol. 94, pp. 651–659, 2016.

[31] L. Fiorini, M. Aiello, D. Poli, and P. Pelacchi, "Topological considerations on the use of batteries to enhance the reliability of hv-grids," *Journal of Energy Storage*, vol. 18, 2018.

[32] S. Massucco, G. Mosaico, P. Pongiglione, M. Saviozzi, and F. Silvestro, "Probabilistic planning for distribution networks including optimal der regulation and storage allocation," in *2020 IEEE Power & Energy Society General Meeting*, 2020.

[33] M. Crosa, F. D'Agostino, S. Massucco, P. Pongiglione, M. Saviozzi, and F. Silvestro, "The podcast project: An application of volt/var optimization to the electric distribution network of sanremo (italy)," in *1st International Conference on Energy Transition in the Mediterranean Area*, 2019.

[34] F. D'Agostino, S. Massucco, P. Pongiglione, M. Saviozzi, and F. Silvestro, "Optimal der regulation and storage allocation in distribution networks: Volt/var optimization and congestion relief," in *2019 IEEE Milan PowerTech*, 2019.

[35] Terna S.p.A., "The national electricity transmission grid development plan," 2021.

[36] GAMS Software GmbH, "Gams documentation center."

[37] R. Zimmerman and C. Murillo-Sanchez, "Matpower 7.1," 2020.

[38] F. Conte, F. D'Agostino, S. Massucco, G. Palombo, F. Silvestro, C. Bossi, and M. Cabiati, "Dynamic equivalent modelling of active distribution networks for tso-dso interactions," in *2017 IEEE PES Innovative Smart Grid Technologies Conference Europe*, 2017.

[39] F. Conte, F. D'Agostino, S. Massucco, F. Silvestro, C. Bossi, and M. Cabiati, "Experimental validation of a dynamic equivalent model for microgrids," *IEEE Transactions on Industry Applications*, vol. 57, no. 3, pp. 2202–2211, 2021.

[40] NASA Langley Research Center (LaRC), "Prediction of worldwide energy resource (POWER) project."

[41] Autorità per l'energia elettrica il gas e il sistema idrico (AEEGSI), "Stato di utilizzo e di integrazione degli impianti di produzione alimentati dalle fonti rinnovabili e degli impianti di cogenerazione ad alto rendimento - anno 2016," *Relazione 464/2017/I/EFR*, 2017.

[42] Autorità per l'energia elettrica il gas e il sistema idrico (AEEGSI), "Mercato dell'energia elettrica. revisione delle regole per il dispacciamento – orientamenti finali," *Documento per la consultazione, 557/2013/R/EEL*, 2013.

[43] RSE, Politecnico di Milano, "Partecipazione della domanda flessibile al mercato del servizio di dispacciamento," *Best practices internazionali. Scenario attuale di mercato e prospettive evolutive. Il ruolo della Domanda e la figura dell'Aggregatore. Analisi Costi-Benefici*, 2018.

[44] European Commission, "Commission regulation (eu) 2017/2195 of 23 november 2017 establishing a guideline on electricity balancing (text with eea relevance),"

[45] "https://www.arera.it/it/index.htm,"

[46] European Commission, "European commission regulation 2017/1485 of 2 august 2017 establishing a guideline on electricity transmission system operation," 2017.

[47] European Commission, "European commission regulation 2017/2195 of 23 november 2017 establishing a guideline on electricity balancing," 2017.

[48] TERNA S.p.A., "Regolamento UVAM MSD," 2018.

[49] European Commission, "Commission regulation (eu) 2016/1388 of 17 august 2016 establishing a network code on demand connection," 2016.

[50] Enerdata *World Energy Council*, 2010.

[51] SEDC, "Explicit demand response in europe mapping the markets 2017," 2017.

[52] C. Latour, "Lessons learnt from the french experience -challenges and opportunities in the context of energy transitions," *Markets Department*.

[53] IndustRE, "Regulatory and market framework analysis: A working document assessing the impact of the regulatory and market framework on the industre business models," *IndustRE Deliverable 2.2*, 2015.

[54] Smart energy collective, "An introduction to the universal smart energy framework,"

[55] SEDC, "Demand response status in eu member states - jrc science for policy report," *Empowering Residential and SME Consumers*.

[56] "Demand response activation by independent aggregators as proposed in the draft electricity,"

[57] Terna S.p.A., "Requisiti tecnici dei dispositivi inclusi in fast reseve unit," *pilot project pursuant the Deliberation 300/2017/R/eel of the Regulatory Authority for Energy, Networks and Environment*, vol. 3, 2017.

[58] TERNA S.p.A., "Regolamento uvac msd," 2017.

[59] E. Vrettos, S. Koch, and G. Andersson, "Load frequency control by aggregations of thermally stratified electric water heaters," *3rd IEEE PES Innovative Smart Grid Technologies Europe*, vol. 141, no. pp. 137-146, 2012.

[60] F. Conte, S. Massucco, and F. Silvestro, "Frequency control services by a building cooling system aggregate," *Electric Power Systems Research*, vol. 141, no. pp. 137-146, 2016.

[61] H. Hao, B. M. Sanandaji, K. Poolla, and T. L. Vincent, "Aggregate flexibility of thermostatically controlled loads," *IEEE Transactions on Power Systems*, vol. 30, no. 1, pp. 189-198, 2015.

[62] P. Kepplinger, G. Huber, and J. Petrasch, "Field testing of demand side management via autonomous optimal control of a domestic hot water heater," *Energy and Buildings*, vol. 127, no. pp. 730-735, 2016.

[63] M. Liu, S. Peeters, D. S. Callaway, and B. J. Claessens, "Trajectory tracking with an aggregation of domestic hot water heaters: Combining model-based and model-free control in a commercial deployment," *IEEE Transactions on Smart Grid*, vol. 10, no. 5 pp. 5686-5695, 2019.

[64] L. Zhang, N. Good, and P. Mancarella, "Building-to-grid flexibility: Modelling and assessment metrics for residential demand response from heat pump aggregations," *Applied Energy*, vol. 233–234, no. pp. 709-723, 2019.

[65] TERNA S.p.A., "Regolamento UVAM MSD," *Allegato 6*, 2018.

[66] LuceeGas, "https://luceegasitalia.it/2020/01/22/le-zone-climatiche-italiane-e-i-periodi-di-accensione-degli-impianti-di-riscaldamento/,"

[67] RSE, "DPR 26 Agosto 1993, n. 412," *Regolamento recante norme per la progettazione, l'installazione, l'esercizio e la manutenzione degli impianti termici degli edifici ai fini del contenimento dei consumi di energia, in attuazione dell'ART. 4, comma 4, della Legge 9 Gennaio 1991, N. 10*, 1993.

[68] UNI Ente Italiano di Normazione , "UNI EN ISO 15927-6," *Prestazione termoigrometrica degli edifici - Calcolo e presentazione dei dati climatici - Parte 6: Differenze di temperatura cumulate (gradi giorno)*, 2008.

[69] ASHRAE, "Hvac application handbook," Atlanta, 2003.

[70] Ente Italiano di Normazione, "Prestazioni energetiche degli edifici. parte 2: Determinazione del fabbisogno di energia primaria e dei rendimenti per la climatizzazione invernale, per la produzione di acqua calda sanitaria, per la ventilazione e per l'illuminazione," *UNI TS 11300-2 2014*, Ottobre 2014.

[71] ISTAT, "Indagine "aspetti della vita quotidiana," *condotta su un campione di circa 20.000 famiglie e 50.000 individui*, 2020.

[72] F. Conte, S. Massucco, F. Silvestro, E. Ciapessoni, and D. Cirio, "Studi modellistici e sperimentali sull'interazione tra pompe di calore geotermiche e il terreno," *Tech. Rep. RSE 12000316*, 2012.

[73] RSE, "https://www.rse-web.it," *RSE Climatic Database*, 2012.

[74] F. Conte, S. Massucco, F. Silvestro, E. Ciapessoni, and D. Cirio, "Demand side response for frequency control in a regional power system," *5th International Conference on Clean Electrical Power: Renewable Energy Resources Impact (ICCEP)*, no. 7177633, pp. 258-264, 2015.

[75] P. Fern´andez-Bustamante, O. Barambones, I. Calvo, C. Napole, and M. Derbeli, "Provision of frequency response from wind farms: A review," *Energies*, vol. 14, no. 20, 2021.

[76] S. M. M. Dreidy, H. Mokhlis, "Inertia response and frequency control techniques for renewable energy sources: A review," *Renew. Sustain. Energy Reviews*, vol. 69, 2017.

[77] F. D´ıaz-Gonz´alez, A. S. M. Hau, and O. Gomis-Bellmunt, "Participation of wind power plants in system frequency control: Review of grid code requirements and control methods," *Renew. Sustain. Energy Reviews*, vol. 34, no. pp. 551-564, 2014.

[78] H. Karbouj, Z. H. Rather, D. Flynn, and H. W. Qazi, "Non-synchronous fast frequency reserves in renewable energy integrated power systems: A critical review," *Int. J. Electr. Power Energy Syst*, vol. 106, no. pp. 488-501, 2019.

[79] N. R. Ullah, T. Thiringer, and D. Karlsson, "Temporary primary frequency control support by variable speed wind turbines - potential and applications," *IEEE Trans. Power Syst*, vol. 23, no. 2, 2008.

[80] I. Erlich and M. Wilch, "Primary frequency control by wind turbines," *IEEE PES General Meeting*, 2010.

[81] F. Baccino, F. Conte, S. Grillo, S. Massucco, and F. Silvestro, "An optimal model-based control technique to improve wind farm participation to frequency regulation," *IEEE Trans. Sustain. Energy*, vol. 6, no. 3, 2015.

[82] F. Bignucolo, A. Cervi, and R. Stecca, "Network frequency regulation with dfig wind turbines compliant with italian standards," *in IEEE EEEIC/I&CPS Europe*, 2019.

[83] ENTSO-E, "Commission regulation (eu) 2016/631 of 14 april 2016 establishing a network code on requirements for grid connection of generators,," *Official J. of the EU*, no. 14, 2016.

[84] A. Zertek, G. Verbic, and M. Pantos, "A novel strategy for variable-speed wind turbines' participation in primary frequency control," *IEEE Trans. Sustain. Energy*, vol. 3, no. 4, 2012.

[85] Z. S. Zhang, Y. Z. Sun, J. Lin, and G. J. Li, "Coordinated frequency regulation by doubly fed induction generator-based wind power plants," *IET Renew. Power Gener*, vol. 6, no. 1, 2012.

[86] K. V. Vidyanandan and N. Senroy, "Primary frequency regulation by deloaded wind turbines using variable droop," *IEEE Trans. Power Syst.*, vol. 28, no. 2, 2013.

[87] J. Boyle, T. Littler, S. M. Muyeen, and A. M. Foley, "An alternative frequency-droop scheme for wind turbines that provide primary frequency regulation via rotor speed control," *Int. J. Electr. Power Energy Syst.*, vol. 133, 2021.

[88] A. S. Alsharafi, A. H. Besheer, and H. M. Emara, "Primary frequency response enhancement for future low inertia power systems using hybrid control technique," *Energies*, vol. 11, no. 4, 2018.

[89] X. Zhao, B. F. Z. Lin, and S. Gong, "Research on frequency control method for micro-grid with a hybrid approach of ffr-oppt and pitch angle of wind turbine," *Int. J. Electr. Power Energy Syst.*, vol. 127, 2021.

[90] H. Luo, H. Z. Z. Hu, and H. Chen, "Coordinated active power control strategy for deloaded wind turbines to improve regulation performance in agc," *IEEE Trans. Power Syst.*, vol. 34, no. 1, 2019.

[91] P. Yang, B. He, B. Wang, X. Dong, W. Y. Liu, J. Zhang, Z. K. Wu, J. X. Liu, and Z. Qin, "Coordinated control of rotor kinetic energy and pitch angle for large-scale doubly fed induction generators participating in system primary frequency regulation," *IET Renew. Power Gener.*, vol. 15, no. 8, 2021.

[92] Z. Dong, Z. Li, Y. Dong, S. Jiang, and Z. Ding, "Fully-distributed deloading operation of dfig-based wind farm for load sharing," *IEEE Trans. Sustain. Energy*, vol. 12, no. 1, 2021.

[93] T. Liu, W. Pan, R. Quan, and M. Liu, "A variable droop frequency control strategy for wind farms that considers optimal rotor kinetic energy," *IEEE Access*, vol. 7, no. pp. 68636–68645, 2019.

[94] W. Bao, Q. Wu, L. Ding, S. Huang, F. Teng, and V. Terzija, "Synthetic inertial control of wind farm with bess based on model predictive control," *IET Renew. Power Gener.*, vol. 14, 2020.

[95] F. Conte, S. Massucco, G.-P. Schiapparelli, and F. Silvestro, "Frequency regulation services by a bess-generator system using predictive control," *IEEE Milan PowerTech*, no. pp. 1-6, 2019.

[96] J. Liu, J. Wen, W. Yao, and Y. Long, "Solution to short-term frequency response of wind farms by using energy storage systems," *IET Renew. Power Gener.*, vol. 10, no. 5, 2016.

[97] F. Conte, S. Massucco, G.-P. Schiapparelli, , and F. Silvestro, "Day-ahead and intra-day planning of integrated bess-pv systems providing frequency regulation," *IEEE Transactions on Sustainable Energy*, vol. 11, no. 3 pp. 1797–1806, 2020.

[98] S. Zhang, Y. Mishra, and M. Shahidehpour, "Fuzzy-logic based frequency controller for wind farms augmented with energy storage systems," *IEEE Trans. Power Syst.*, vol. 31, no. 2 pp. 1595–1603, 2016.

[99] A. M. Howlader, Y. Izumi, A. Uehara, N. Urasaki, T. Senjyu, and A. Y. Saber, "A robust h controller based frequency control approach using the wind-battery coordination strategy in a small power system," *Int. J. Electr. Power Energy Syst.*, vol. 58, no. pp. 190–198, 2014.

[100] J. Tan and Y. Zhang, "Coordinated control strategy of a battery energy storage system to support a wind power plant providing multi-timescale frequency ancillary services," *IEEE Trans. Sustain. Energy*, vol. 8, no. 3 pp. 1140–1153, 2017.

[101] M. Morari, C. E. Garcia, and D. M. Prett, "Model predictive control: Theory and practice," *IFAC Proceedings Volumes*, vol. 21, no. 4 pp. 1-12, 1988.

[102] N. Atic, "Model predictive control design for load frequency control problem," *Master thesis, West Virginia University*, 2003.

[103] S. C. e. G. A. A. Ulbig, T. Rinke, "Predictive control for real-time frequency regulation and rotational inertia provision in power systems," *52nd IEEE Conference on Decision and Control*, no. pp. 2946-2953, 2013.

[104] AMPL Optimization inc., "A mathematical programming language." [Online]. Available: https://ampl.com/.

[105] MathWorks, "https://it.mathworks.com/help/physmod/sps/ug/wind-farm-dfig-phasor-model.html,"

[106] CIGRE Task Force C6.04.02, "Benchmark Systems for Network Integration of Renewable and Distributed Energy Resources," *Cigre technical brochure*, Apr 2012.

[107] S. Heier, "https://www.opal-rt.com," *[Online; accessed 05-Sep-2022].*

[108] F. Conte, F. D'Agostino, P. Pongiglione, M. Saviozzi, and F. Silvestro, "Mixed-integer algorithm for optimal dispatch of integrated pv-storage systems," *IEEE Transactions on Industry Applications*, vol. 55, no. 1, pp. 238–247, 2019.

[109] Y. T. Tan and D. S. K. e N. Jenkins, "A model of pv generation suitable for stability analysis," *IEEE Transactions on Energy Conversion*, vol. 19, no. 4, 2004.

[110] Terna S.p.A., "Centrali fotovoltaiche: Condizioni generali di connessione alle reti at. sistemi di protezione regolazione e controllo," *Guida Tecnica*, vol. Allegato A.68, 2018.

[111] Terna S.p.A., "Centrali eoliche: Condizioni generali di connessione alle reti at. sistemi di protezione regolazione e controllo," *Guida Tecnica*, vol. Allegato A.17, 2018.

[112] E. Dvorský, L. Raková, and P. Hejtmánková, "Primary and secondary frequency regulation with photovoltaic generators," *16th International Scientific Conference on Electric Power Engineering (EPE)*, 2015.

[113] Y. Liu, L. Zhan, J. R. Gracia, T. J. King, and Y. Liu, "Active power control of solar pv generation for large interconnection frequency regulation and oscillation damping," *International Journal of Energy Research*, 2015.

[114] P. Zarina, S. Mishra, and P. Sekhar, "Exploring frequency control capability of a pv system in a hybrid pv-rotating machine-without storage system," *International Journal of Electrical Power & Energy System*, 2014.

[115] X. Huanhai, L. Yun, W. Zhen, G. Deqjang, and Y. Taicheng, "A new frequency regulation strategy for photovoltaic systems without energy storage," *IEEE Transactions on Sustainable Energy*, vol. 4, no. 4 pp. 985-993, 2013.

[116] Z. Jianhua, Z. Bin, L. Qian, Z. Guiping, W. Lei, L. Bin, and L. Kang, "Fast frequency regulation method for power system with two-stage photovoltaic plants," *IEEE Transactions on Sustainable Energy*, 2022.

[117] H. D. Tafti, G. Konstantinou, J. E. Fletcher, L. Callegaro, G. G. Farivar, and J. Pou, "Control of distributed photovoltaic inverters for frequency support and system recovery," *IEEE Transactions on Power Electronics*, vol. 27, no. 4, 2021.

[118] L. Xingshuo, W. Huiqing, Z. Yinxiao, J. Lin, H. Yihua, and X. Weidong, "A novel sensorless photovoltaic power reserve control with simple real-time mpp estimation," *IEEE Transactions on Power Electronics*, vol. 34, no. 8 pp. 7521-7531, 2018.

List of publications originated during the Ph.D. work

- **Journal paper**

  [1] F. Conte, F. D'Agostino, B. Gabriele, G. -P. Schiapparelli and F. Silvestro, "Fault Detection and Localization in Active Distribution Networks Using Optimally Placed Phasor Measurements Units," in IEEE Transactions on Power Systems, vol. 38, no. 1, pp. 714-727, 2023.

  [2] F. Conte, F. D'Agostino, B. Gabriele, G. -P. Schiapparelli and F. Silvestro, "Fast Frequency Regulation from a Wind Farm-BESS Unit by Model Predictive Control Method and Hardaware-In-the-Loop Validation", in IEEE Transactions on Software Engineering, under review.

- **Conference papers**

  [3] F. Conte, B. Gabriele and G. -P. Schiapparelli, "Assessment of State Estimation Methods for Power Systems with Uncertain Parameters", 55th International Universities Power Engineering Conference (UPEC),pp. 1-6, 2020.

  [4] F. Conte, B. Gabriele, S. Massucco, F. Silvestro, D. Cirio and L. Croci, "Domestic Heat-Pump Water Heater Aggregates a Contribution to Demand Flexibility", 2021 AEIT International Annual Conference (AEIT), pp. 1-5, 2021.

[5] F. Conte, B. Gabriele, G. -P. Schiapparelli, F. Silvestro, C. Bossi and M. Cabiati, "Optimal Positioning of PMUs for Fault Detection and Localization in Active Distribution Networks," 2021 IEEE Madrid PowerTech, pp. 1-6, 2021.

[6] F. Conte, B. Gabriele, S. Massucco, F. Silvestro, D. Cirio and L. Croci, "Flexibility Evaluation of Domestic Electric Water Heater Aggregates," 2021 IEEE Madrid PowerTech, pp. 1-6, 2021.

- **Submitted papers**

[7] Optimal Storage Allocation for Transmission Network Development Planning Study Case of Sicily, submitted to PowerTech 2023.

[8] Investigation on the contribution to system inertia of dual fuel two-stroke engines in isolated grid system: a case study, submitted to SUPEHR23 (Sustainable PolyEnergy generation and HaRvesting).

Projects into which I have been involved during my Ph.D. work

1. **Assessments of Battery Energy Storage Systems Potential in Improving the Working Condition of the Grid of Sicily**, year: 2022.
2. **Assessment of the curtailment risk in the Italian market**, year: 2022-2023.
3. **Optimal Storage Allocation for Transmission Network Development Planning: Study Case of Sicily**, year: 2023.
4. **Investigation on the contribution to system inertia of dual fuel two-stroke engines in isolated grid system: a case study**, year: 2022.
5. **Modelling and simulation of network regulation services provided by control of heat pumps meant for the production of domestic hot water**, with "Ricerca di Sistema", year: 2019-2022.
6. **e-SCALE (Energy and services connected to the aggregate management)**, financed by POR FESR LAZIO ID: A0206-2018-17604, year: 2020.
7. **Model and control techniques to flexibility service provision from RES and load**, with "Ricerca di Sistema", year: 2020-2023.
8. **Distribution network protection through measurements from Phasor Measurement Units**, with "Ricerca di Sistema", year: 2019-2022.

Attended post-graduation courses and foreign experiences during the Ph.D.

1. Participation in the doctoral course ”Non linear system dynamics” - Prof. Marco Storace, DITEN, January 2020 (20 hours).
2. Participation in the doctoral course ”Model and applications of predictive control” - Mauro Gaggero - DIBRIS, March 2020 (20 hours)
3. Participation in the doctoral course ”Advanced Programming In Matlab And Simulink” - Prof. Matteo Lodi, DITEN, May 2020 (20 hours).
4. Virtual conference UPEC 2020 “Verifying the Targets” - Septemper 2020 (40 hours).
5. Participation in the doctoral course ”Open Science and Research Data Management” - Prof. Anna Maria Pastorini e Prof. Valentina Pasquale, DITEN, February 2021 (6 hours).
6. Participation in the doctoral online course ”Agenda 2030 and Sustainable Development Goals to provide cross-cutting training on sustainable development” - Aulaweb, March 2021 (3 hours).
7. Participation as speaker in the webinar ”Power systems regulation services: Markets evolution and new actors in the E-SCALE project” - March 2021 (4 hours).

8. Participation in the course ”Pes Pav (Pei): electrical works (CEI 11-27:2014 e CEI EN 50110-2014)” ” - organized by AltaFormazione, March 2021 (16 hours).

9. Virtual conference PowerTech ”Power for the Sustainable Development Goals” - July 2021 (40 hours).

10. Participation in the European PhD School organized by University of Cassino in cooperation with ECPE in Gaeta (Italy) - July 12-16, 2021 (40 hours).

11. AEIT International Annual Conference - October 2021 (30 hours).

12. International conference IEEE PES ISGT Europe 2022 “Together Towards Digitized, Decarbonised, and Distributed Smart Grids” in Novi Sad (Serbia) - October 2022 (40 hours).

13. Participation in the course to DIgSILENT introduction - Prof. Gianluca Pasini, STREL, October 2022 (16 hours).

14. Participation in the online course to DIgSILENT ”Unit Commitment and Dispatch Optimisation” - July 2022 (8 hours).

15. Participation in the online course to OPAL-RT introduction - November 2021 (16 hours).

16. Activity as didactic tutor to support students of Electrical Engineering Bachelor’s degree course at University of Genoa (50 hours).